

UCLA

UCLA Electronic Theses and Dissertations

Title

Degradable Hydrogels and Nanogels for the Delivery of Cells and Therapeutics

Permalink

<https://escholarship.org/uc/item/1t9969gq>

Author

Boehnke, Natalie

Publication Date

2017

Peer reviewed|Thesis/dissertation

UNIVERSITY OF CALIFORNIA

Los Angeles

Degradable Hydrogels and Nanogels for the
Delivery of Cells and Therapeutics

A dissertation submitted in partial satisfaction of the
requirements for the degree Doctor of Philosophy
in Chemistry

by

Natalie Boehnke

2017

ABSTRACT OF THE DISSERTATION

Degradable Hydrogels and Nanogels for the
Delivery of Cells and Therapeutics

by

Natalie Boehnke

Doctor of Philosophy in Chemistry

University of California, Los Angeles, 2017

Professor Heather D. Maynard, Chair

Degradable polymeric materials such as hydrogels are extensively utilized as delivery vehicles due to their biocompatibility and tunable properties. Encapsulating therapeutic agents inside hydrogels stabilizes the cargo by preventing degradation, extending circulation time, and also allows for targeted release and delivery. Due to their small size and tunable properties, nano-scale hydrogels, or nanogels, are frequently utilized to deliver therapeutics to areas difficult to reach, such as tumors and the cytoplasm, through traditional means. To control hydro- and nanogel function, degradable cross-links can be installed, allowing for cargo release in response to specific stimuli, such as hydrolysis or reduction. This dissertation offers three degradable strategies that

can be applied to synthesize hydrogels and nanogels for the stabilization and release of therapeutic cargo.

In the first example, mixed imine cross-linking chemistry was applied to synthesize poly(ethylene glycol) (PEG)-based hydrogels with tunable degradability to encapsulate and deliver cells (**Chapter 2**). Time to degradation of the gels could be controlled from 24 hours to more than 7 days by varying the hydrazone structure and the ratio of hydrazone and oxime cross-links. Encapsulated cells exhibited high viability up to at least 7 days, suggesting this system may be useful for cell delivery applications.

In the second example, disulfide cross-links were utilized to form redox-responsive nanogels comprised of trehalose copolymers (**Chapter 3**). The synthesis of a methacrylate trehalose monomer (TrMA) was optimized, improving the overall yield from 14% to 42%. TrMA was subsequently copolymerized with pyridyl disulfide ethyl methacrylate (PDSMA) using free radical polymerization conditions to form copolymers with two monomer ratios (1:1 and 2:1) which were cross-linked with 1 kDa PEG-dithiol via disulfide exchange to form uniform nanogels approximately 9 nm in diameter. The addition of a cross-linker eliminated the need to add reducing agent to facilitate cross-linking and nanogel formation, making this approach ideal for the encapsulation of sensitive therapeutic agents.

Next, PDSMA-*co*-TrMA nanogels were utilized to encapsulate, stabilize, and release glucagon, an unstable peptide hormone used to treat hypoglycemia (**Chapter 4**). The amines on glucagon were modified with thiol groups while retaining their positive charges for reversible conjugation and cross-linking. Glucagon-nanogel conjugates were synthesized with >80% conjugation yield, and the reversible disulfide linkage between peptide and polymer allowed for efficient cargo release under mild reducing conditions. The nanogels stabilized glucagon against

aggregation in solution up to five days as well as solubilized the peptide at neutral pH. *In vitro* bioactivity of the modified peptide was found to be comparable to native glucagon, suggesting this may be a promising formulation strategy for further *in vivo* study.

Finally, a series of dual-enzyme responsive peptides was synthesized by masking the ϵ -amine of lysine with protease substrates (**Chapter 5**). After unmasking the amine by enzymatic cleavage, a second enzyme was able to cleave at the C terminus of lysine, which was monitored colorimetrically. Three different dual-enzyme responsive peptides were prepared, (AcAAF)K-pNA, (AcFG)K-pNA, and (AcDEVD)K-pNA, for chymotrypsin, papain, and caspase 3 sensitivity, respectively, followed by trypsin sensitivity after cleavage by the first enzyme. This modular peptide design could be useful for selective drug delivery, studies on dual enzyme activity, as well as for diagnostic enzyme screening.

The dissertation of Natalie Boehnke is approved.

Dino Di Carlo

Kendall N. Houk

Heather D. Maynard, Committee Chair

University of California, Los Angeles

2017

*This dissertation is dedicated to my family,
especially my parents, Helmut and Ursula Boehnke,
and my best friend, Brice Curtin.*

Table of Contents

Abstract of the Dissertation.....	ii
Table of Contents.....	vii
List of Figures.....	x
List of Tables.....	xix
List of Schemes.....	xx
List of Abbreviations.....	xxi
Acknowledgements.....	xxiv
Vita.....	xxvii
Chapter 1. General Introduction: Degradable Hydrogels and Nanogels for the Delivery of Cells and Therapeutics.....	1
1. 1. Overview of Hydrogels for Therapeutics Delivery.....	2
1. 1. 1. Click Chemistry for Hydrogel Cross-Linking.....	5
1. 1. 2. Degradable Cross-Linking Strategies for Hydrogels.....	10
1. 2. Overview of Nanogels for Therapeutics Delivery.....	13
1. 2. 1. Degradable Nanogel Cross-linking Strategies.....	16
1. 3. Summary.....	23
1. 4. References.....	24
Chapter 2. Imine Hydrogels with Tunable Degradability.....	35
2. 1. Introduction.....	36
2. 2. Results and Discussion.....	39
2. 3. Conclusions.....	53
2. 4. Experimental.....	53

2. 4. 1. Materials and Analytical Techniques.....	54
2. 4. 2. Methods.....	54
2. 5. References.....	77
Chapter 3. Synthesis of Redox-Responsive Trehalose Glycopolymer Nanogels.....	81
3.1. Introduction.....	82
3. 2. Results and Discussion.....	84
3. 2. 1. Monomer and Polymer Synthesis.....	84
3. 2. 2. Nanogel Synthesis and Characterization.....	89
3. 2. 3. Protein Encapsulation.....	91
3. 3. Conclusions.....	93
3. 4. Experimental.....	94
3. 4. 1. Materials and Analytical Techniques.....	94
3. 4. 2. Methods.....	95
3. 5. References.....	113
Chapter 4. Trehalose Glycopolymer Nanogels for the Stabilization and Release of a Peptide Hormone.....	117
4. 1. Introduction.....	118
4. 2. Results and Discussion.....	121
4. 2. 1. Glucagon Modification.....	121
4. 2. 2. Nanogel Synthesis and Characterization.....	125
4. 2. 3. Nanogel Solubility.....	130
4. 2. 4. Nanogel Stability.....	130
4. 2. 5. Bioactivity Studies.....	134

4. 3. Conclusions.....	136
4. 4. Experimental.....	137
4. 4. 1. Materials and Analytical Techniques.....	137
4. 4. 2. Methods.....	137
4. 5. References.....	147
Chapter 5. Design of Modular Dual-Enzyme Responsive Peptides.....	152
5. 1. Introduction.....	153
5. 2. Results and Discussion.....	154
5. 3. Conclusions.....	163
5. 4. Experimental.....	163
5. 4. 1. Materials and Analytical Techniques.....	163
5. 4. 2. Methods.....	164
5. 5. References.....	180

List of Figures

- Figure 2.1.** Hydrogels can be formed through the incorporation of two types of imine cross-links: hydrazones and oximes.....38
- Figure 2.2.** PEG-CHO can react with PEG-ADH and PEG-CDH to form degradable hydrogels via reversible hydrazone cross-links and can also react with PEG-AO to form nonreversible oxime bonds to stabilize the hydrazone gels.....40
- Figure 2.3.** 5.0 wt.% PEG hydrazone hydrogels (40 μ L, approximately 1 cm in diameter and 1 mm in height) dyed with food coloring shown during self-healing. PEG-ADH hydrogels formed within one minute (A) and were cut in half (B). The opposite halves were placed next to each other (C), and after ten minutes, bonds re-formed (D). After fifteen minutes, the two pieces formed one complete gel that can readily be handled (E).....42
- Figure 2.4.** Swelling of 5.0 wt.% PEG-ADH (A) and 5.0 wt.% PEG-CDH (B) based hydrogels. 40 μ L gels were placed in respective solutions, and PEG-ADH gels degraded after five days in DMEM (-) FBS and after two days in DMEM (+) FBS. PEG-CDH gels retained constant masses throughout the experiment for all conditions, including cell conditioned DMEM.....44
- Figure 2.5.** ^1H NMR of CDH hydrazone (A) after adding one equivalent of hydroxylamine per hydrazone bond (B), and ^1H NMR of ADH hydrazone (C) after adding one equivalent hydroxylamine per hydrazone bond (D).....45
- Figure 2.6.** Rheological characterization of hydrazone and oxime hydrogels. Storage modulus can be controlled by changing total polymer concentration and amounts of hydrazone and oxime cross-links. Data is displayed as the average and standard deviation of three independent hydrogels for each condition.....48

Figure 2.7. Live/dead staining of encapsulated mMSCs. 100:0 hydrazone: oxime gels showed good viability at day 1 (A) but degraded before imaging at day 7. 75:25 hydrazone: oxime gels at day 1 (C) and day 7 (D); 50:50 gels at day 1 (E) and day 7 (F); 25:75 gels at day 1 (G) and day 7 (H); 0:100 gels at day 1 (I) and day 7 (J). Scale bar = 100 μm . Cell viability of all gel conditions at day 1 and day 7 (B) represented as % live cells per gel (y axis).....50

Figure 2.8. DAPI/Phalloidin staining for cell spreading at day 2. mMSCs were encapsulated in 5 wt.% 100:0 hydrazone: oxime (A), 75:25 hydrazone: oxime (B), 50:50 hydrazone: oxime (C), and 0:100 hydrazone: oxime (D) gels containing 0.5 mM AO-RGD. Scale bars = 50 μm for both 10x and 40x magnification.....52

Figure 2.9. ^1H NMR spectrum of PEG-adipohydrazide in D_2O55

Figure 2.10. ^1H NMR spectrum of PEG-CDH taken in D_2O56

Figure 2.11. ^1H NMR spectrum of PEG-acetal in CDCl_357

Figure 2.12. ^1H NMR spectrum of PEG-aldehyde in CDCl_358

Figure 2.13. ^1H NMR spectrum of PEG-hydroxyphthalimide in CDCl_359

Figure 2.14. ^1H NMR spectrum of PEG-aminoxy in CDCl_360

Figure 2.15. Cytotoxicity assays of PEGs with mMSCs with $p > 0.05$ for all conditions relative to the control. Experiments were repeated six times, and the results are represented as the average with standard deviation relative to the control with no PEG added.....65

Figure 2.16. Rheological measurements of PEG-ADH based gels. 5.0 wt.% gels have a higher storage modulus than the more dilute 3.5 wt.% gels. Changing the ratio of aldehyde to hydrazide (r value) also decreases the storage modulus.....65

Figure 2.17. ^1H NMR (A) and ^{13}C NMR (B) of ADH-hydrazone in DMSO-d_666

Figure 2.18. ESI-MS spectrum of purified aminoxy-GRGDSL-OH.....68

Figure 2.19. Rheological characterization of 3.5 wt.% PEG-CDH based hydrogels containing 1, 0.1, and 0 mM RGD. Statistical difference ($p < 0.05$) observed between 1-0.1 and 1-0 mM RGD containing gels.....69

Figure 2.20. Light microscope images of 5.0 wt.% hydrazone (PEG-CDH) and mixed hydrazone/oxime gels containing mMSCs (5,000 cells/ μ L, 0.5 mM AO-RGD). Wells containing 100:0 hydrazone: oxime gels were imaged at day 1 (A) and day 6 (B) even though gels had degraded on day 5. Wells containing 75:25 hydrazone: oxime at day 1 (C) and day 6 (D), 50:50 hydrazone: oxime at day 1 (E) and day 6 (F), 0:100 hydrazone: oxime at day 1 (G) and day 6 (H) were also imaged. Scale bar = 100 μ m.....70

Figure 2.21. ^1H NMR of CDH hydrazone in MeOD.....72

Figure 2.22. ^1H NMR of reaction of CDH hydrazone with hydroxylamine in D_2O73

Figure 2.23. ^1H NMR of reaction of ADH hydrazone with hydroxylamine in D_2O74

Figure 2.24. DAPI/Phalloidin staining for cell spreading at day 5. mMSCs were encapsulated in 5.0 wt.% 100:0 hydrazone: oxime (not shown due to gel degradation), 75:25 hydrazone: oxime (A), 50:50 hydrazone: oxime (B), and 0:100 hydrazone: oxime (C) gels containing 0.1 mM AO-RGD. Experiments were repeated using HDFs, encapsulated in 100:0 hydrazone: oxime (not shown due to gel degradation), 75:25 hydrazone: oxime (D), 50:50 hydrazone: oxime (E), and 0:100 hydrazone: oxime (F) gels also containing 0.1 mM AO-RGD. 40x magnification is shown for all images. Scale bar = 50 μ m.....75

Figure 2.25. Light microscope images of 5 wt.% hydrazone (PEG-CDH) gels containing mMSCs (5,000 cells/ μ L) with (A) 0.1 mM AO-RGD and (B) 1 mM RGD on day 1 after encapsulation. Scale bar = 100 μ m.....76

Figure 3.1. ^1H NMR spectra of PDSMA _{1-co} -TrMA _{0.8} (A) and PDSMA _{1-co} -TrMA _{1.7} (B) acquired in DMSO-d ₆	87
Figure 3.2. PDSMA _{1-co} -TrMA _{0.8} nanogels were formed using PEG-dithiol as a cross-linker (A) and characterized using DLS (B) and TEM (C).....	90
Figure 3.3. SDS PAGE of Lyz and BSA encapsulation attempt using PDSMA-co-TrMA nanogels cross-linked with PEG-dithiol. Lane 1: protein ladder; lane 2: lyz; lane 3: PDSMA-co-TrMA (3 wt. eq. PDSMA _{1-co} -TrMA _{0.8}) nanogels + Lyz; lane 4: PDSMA-co-TrMA (4 wt. eq. PDSMA _{1-co} -TrMA _{1.7}) nanogels + Lyz; lane 5: BSA; lane 6: PDSMA-co-TrMA (4 wt. eq. PDSMA _{1-co} -TrMA _{1.7}) nanogels + BSA. Non-reducing conditions.....	92
Figure 3.4. Cytotoxicity studies of PDSMA _{1-co} -TrMA _{1.7} (A) and nanogels (B) with HDFs.....	93
Figure 3.5. ^1H NMR spectrum of PDSOH in CDCl ₃	96
Figure 3.6. ^{13}C NMR spectrum of PDSOH in CDCl ₃	97
Figure 3.7. ^1H NMR spectrum of PDSMA in CDCl ₃	98
Figure 3.8. ^{13}C NMR spectrum of PDSMA in CDCl ₃	99
Figure 3.9. HPLC traces of TrMA at 1:1 (A), 2:1 (B), and 5:1 (C) trehalose to methacrylic anhydride. Unreacted trehalose elutes first, at 4 min, followed by the other TrMA regioisomers between 7 and 10 min. C6 TrMA regioisomer elutes at 14 min, as indicated by an asterisk.....	101
Figure 3.10. ^1H NMR spectrum of TrMA (C6) in D ₂ O.....	102
Figure 3.11. ^{13}C NMR Spectrum of TrMA (C6) in DMSO-d ₆	103
Figure 3.12. HSQC NMR spectrum of TrMA in DMSO-d ₆	104
Figure 3.13. ^1H NMR spectra of C6 regioisomer of TrMA prepared from previously reported method (A) and method described in this manuscript (B) in D ₂ O.....	105

Figure 3.14. ^1H NMR spectrum of PDSMA _{1-co} -TrMA _{0.8} (1:1 feed ratio) acquired in DMSO- d ₆	107
Figure 3.15. ^1H NMR spectrum of PDSMA _{1-co} -TrMA _{1.7} (1:3 feed ratio) acquired in DMSO- d ₆	108
Figure 3.16. TEM Images of PDSMA _{1-co} -TrMA _{0.8} only (A) and of PDSMA _{1-co} -TrMA _{0.8} (+) TCEP.....	109
Figure 3.17. TEM image of PDSMA- <i>co</i> -TrMA nanogels formed at 10 mg/ml PDSMA _{1-co} - TrMA _{0.8} using PEG-dithiol as the cross-linker.....	110
Figure 3.18. Characteristic fluorescence microscopy images of HDFs incubated with 1.0 (A), 2.5 (B) and 5.0 (C) mg/mL PDSMA _{1-co} -TrMA _{1.7} using LIVE/DEAD staining.....	112
Figure 3.19. Characteristic fluorescence microscopy images of HDFs incubated with 0.5 (A) and 1.0 (B) mg/mL PDSMA _{1-co} -TrMA _{1.7} nanogels cross-linked with PEG-dithiol using LIVE/DEAD staining.....	112
Figure 4.1. General glucagon nanogel formation and release (A) and representative structure of glucagon cross-linked PDSMA- <i>co</i> -TrMA (B).....	124
Figure 4.2. Glucagon conjugation to PDSMA _{1-co} -TrMA _{0.8} was monitored via HPLC at 280 nm (A) and SDS-PAGE (B). Lane 1: protein ladder; lane 2: thiolated glucagon; lane 3: PDSMA _{1-co} - TrMA _{0.8} ; lane 4: crude nanogel; lane 5: purified nanogel; lane 6: nanogel from lane 5 reduced with TCEP (10 mg/mL).....	125
Figure 4.3. TEM images of glucagon nanogels formed at 2 mg/mL PDSMA _{1-co} -TrMA _{0.8} (A) and 0.65 mg/mL PDSMA _{1-co} -TrMA _{0.8} (B).....	127
Figure 4.4. DLS data of glucagon and PDSMA _{1-co} -TrMA _{0.8} nanogels at acidic and neutral pH.....	128

Figure 4.5. Volume (A) and number (B) DLS measurements of glucagon nanogels formed with PDSMA_{1-co}-TrMA_{1.7} at 0 and 5 days in solution.....128

Figure 4.6. TEM images of PDSMA_{1-co}-TrMA_{0.8} glucagon nanogels in solution (A), immediately after reduction (B), and 24h after reduction (C).....131

Figure 4.7. TEM images of PDSMA_{1-co}-TrMA_{1.7} glucagon nanogels on day 0 (A) and day 5 (B). In addition to nanogels, small glucagon aggregates were observed in solution after 5 days (C)....132

Figure 4.8. Native PAGE of glucagon and nanogels. Lane 1: glucagon; lane 2: thiolated glucagon; lane 3: PDSMA_{1-co}-TrMA_{1.7}; lane 4: glucagon- PDSMA_{1-co}-TrMA_{1.7} nanogel; lane 5: glucagon- PDSMA_{1-co}-TrMA_{1.7} nanogel aged 5 days; lane 6: glucagon- PDSMA_{1-co}-TrMA_{1.7} nanogel after lyophilization; lane 7: glucagon- PDSMA_{1-co}-TrMA_{1.7} nanogel from lane 5 reduced with TCEP (10 mg/mL).....133

Figure 4.9. Dose response curves of glucagon (A) and thiolated glucagon (B) using Chem-1 cells expressing human glucagon receptor. A signal in response to PDSMA_{1-co}-TrMA_{1.7} glucagon nanogels was also measured (C). Calculated EC₅₀ values of 113 ± 1 nM ($R^2 = 0.99$) and 126 ± 10 nM ($R^2 = 0.98$) for native glucagon and thiolated glucagon, respectively, were obtained.....135

Figure 4.10. ESI-MS of glucagon thiolated with Traut's reagent. $m/z = 1161.5$ corresponds to glucagon and $m/z = 1189.8$ corresponds to the byproduct of singly thiolated glucagon ($z = 3$).....138

Figure 4.11. Ellman's assay results of glucagon thiolated with 2-IT trapped with PDS or PDSMA-*co*-TrMA.....138

Figure 4.12. Ellman's assay results of thiolated glucagon and wash solution.....140

Figure 4.13. LC trace after TCEP reduction of glucagon thiolated with DTBP (peak at 8.3 min) (A) and ESI-MS data of thiolated glucagon after TCEP reduction (B). $m/z = 1191.2$ corresponds

to singly thiolated glucagon and $m/z = 1219.6$ corresponds to doubly thiolated glucagon ($z = 3$).....141

Figure 4.14. TEM images of nanogels formed using 5:1 (A) and 10:1 (B) PDSMA_{1-co}-TrMA_{0.8} and 5:1 (C) and 10:1 PDSMA_{1-co}-TrMA_{1.7} to thiolated glucagon. Scale bars = 200 nm.....144

Figure 4.15. TEM images of fresh PDSMA_{1-co}-TrMA_{1.7} glucagon nanogels in solution (A), aged (2 days) nanogels imaged immediately after TCEP reduction (B), and three days after reduction (C).....145

Figure 4.16. TEM images of PDSMA_{1-co}-TrMA_{1.7} glucagon nanogels in solution (A). However, after lyophilization and reconstitution a mixture of nanogels (B) and micron sized aggregates was observed after lyophilization (C).....145

Figure 5.1. Structures of dual-enzyme responsive peptides. Structures of chymotrypsin/trypsin sensitive peptide (AcAAF)K-pNA (A), papain/trypsin sensitive peptide (AcFG)K-pNA (B), caspase 8/trypsin sensitive peptide (AcIEPD)K-pNA (C), and caspase 3/trypsin sensitive peptide (AcDEV)K-pNA (D).....155

Figure 5.2. (Ac-AAF)K-pNA digestion with trypsin and chymotrypsin resulted in an absorbance increase, corresponding to pNA release. Digestion with trypsin or chymotrypsin only did not result in a significant absorbance increase. Absorbance measurements were taken for first 60 minutes and at the five-hour mark to confirm absorbance values had reached their maxima. Average and standard deviation of three repeats are shown.....157

Figure 5.3. Papain and trypsin digestion of (AcFG)K-pNA at varying substrate concentrations released pNA, resulting in proportional absorbance increases. Incubating the substrate with papain

or trypsin only resulted in no absorbance increase. Average and standard deviation of three repeats are shown.....	158
Figure 5.4. Digestion of (AcDEVD)K-pNA with trypsin and caspase 3 results in p-nitroaniline release. No release is observed when only trypsin or caspase 3 is used or when the caspase 3 recognition sequence was scrambled. Average and standard deviation of four repeats are shown.....	160
Figure 5.5. ¹ H NMR spectrum of <i>t</i> -butyl (<i>S</i>)-(5-acetamido-6-((4-nitrophenyl)amino)-6-oxohexyl)carbamate (2) in (CD ₃) ₂ SO.....	166
Figure 5.6. ¹³ C NMR spectrum of <i>t</i> -butyl (<i>S</i>)-(5-acetamido-6-((4-nitrophenyl)amino)-6-oxohexyl)carbamate (2) in (CD ₃) ₂ SO.....	167
Figure 5.7. ¹ H NMR spectrum of (<i>S</i>)-2-acetamido-6-amino- <i>N</i> -(4-nitrophenyl)hexanamide (A) as the TFA salt in (CD ₃) ₂ SO.....	168
Figure 5.8. ¹³ C NMR spectrum of (<i>S</i>)-2-acetamido-6-amino- <i>N</i> -(4-nitrophenyl)hexanamide (A) as the TFA salt in (CD ₃) ₂ SO.....	169
Figure 5.9. Structure of (AcAAF)K-pNA.....	170
Figure 5.10. Structure of (AcFG)K-pNA.....	171
Figure 5.11. Structure of (AcDEVD)K-pNA.....	171
Figure 5.12. Structure of (AcDVED)K-pNA.....	172
Figure 5.13. Structure of (AcIEPD)K-pNA.....	173
Figure 5.14. UV absorption spectra of dual-enzyme responsive peptides before digestion and of the colorimetric compound <i>p</i> -nitroaniline that is released after enzyme digestion of the peptides.....	174

Figure 5.15. Standard curve of trypsin digestion of **A**. Each measurement was carried out in triplicate, and a linear trend line was generated from average absorbance values plotted against concentration.....177

Figure 5.16. 500 μ M (AcDEVd)K-pNA and (AcIEPD)K-pNA was incubated with caspase 8 for 24 hours before adding trypsin, which did not result in a significant absorbance increase. Average and standard deviation of three repeats are shown.....178

Figure 5.17. Incubating caspase 8 with commercially available AcDEVd-pNA and AcIEPD-pNA resulted in a significant absorbance increase over time. Average and standard deviation of three repeats are shown.....178

Figure 5.18. Caspase 3 digestion of commercial Ac-DEVd-pNA. Each measurement was carried out in triplicate, and a linear trend line was generated from average absorbance values plotted against concentration.....179

List of Tables

Table 1.1. Commonly used click reactions to form hydrogels.....	6
Table 1.2. Examples of degradable hydrogel cross-linking strategies.....	10
Table 1.3 Examples of degradable nanogel cross-linking strategies.....	17
Table 3.1. GPC characterization of PDSMA- <i>co</i> -TrMA polymers.....	88
Table 3.2. Reagent amounts for TrMA syntheses.....	100
Table 4.1. Conjugation yields of nanogels made from PDSMA ₁ - <i>co</i> -TrMA _{0.8} and PDSMA ₁ - <i>co</i> -TrMA _{1.7} at two different ratios.....	143
Table 5.1. Kinetic parameters of Phe-Gly substrates.....	162

List of Schemes

Scheme 3.1. Syntheses of PDSMA (A) and TrMA (B) monomers. The copolymer containing PDS and trehalose side chains, PDSMA- <i>co</i> -TrMA, was synthesized using free radical polymerization conditions (C).....	86
Scheme 4.1. Thiolation with 2-IT (A) and DTBP (B).....	123
Scheme 5.1. Dual enzyme responsive systems were designed with a protease substrate coupled to the ϵ -amino group of lysine. When the protease substrate is cleaved off by one of three model enzymes, the lysine is unmasked, allowing for subsequent trypsin digestion. Upon digestion, a colorimetric compound, nitroaniline, is released. The release of nitroaniline does not occur if only one enzyme is present.....	154
Scheme 5.2. Synthesis of nitroanilide peptides using method 1.....	164
Scheme 5.3. Synthesis of (<i>S</i>)-2-acetomido-6-amino- <i>N</i> -(4-nitrophenyl)hexanamide.....	165

List of Abbreviations

2-IT	2-Iminothiolane
ADH	Adipodihydrazide
AGET	Activator Generated by Electron Transfer
AIBN	2,2'-Azobis(2-methylpropionitrile)
AO	Aminooxy
ATRP	Atom Transfer Radical Polymerization
BOC	<i>tert</i> -Butyloxycarbonyl
BSA	Bovine Serum Albumin
CDH	Carbodihydrazide
CTA	Chain Transfer Agent
CuAAC	Copper(I)-Catalyzed Alkyne-Azide Cycloaddition
D-PBS	Dulbecco's Phosphate Buffered Saline
DCM	Dichloromethane
Dex	Dexamethasone
DIEA	Diisopropylethylamine
DLS	Dynamic Light Scattering
DMEM	Dulbecco's Modified Eagle's Medium
DMF	Dimethylformamide
DMSO	Dimethylsulfoxide
DTBP	Dimethyl-3,3'-dithio-bis(propionimidate)
DTNB	5,5'-dithiobis-(2-nitrobenzoic acid)
DTT	Dithiothreitol

ECM	Extracellular Matrix
EDC	1-Ethyl-3-(3-dimethylaminopropyl)carbodiimide
EDTA	Ethylenediaminetetraacetic acid
EPR	Enhanced Permeability and Retention
ESI	Electron Spray Ionization
FBS	Fetal Bovine Serum
Fmoc	Fluorenylmethyloxycarbonyl
FRET	Fluorescence Resonance Energy Transfer
FRP	Free Radical Polymerization
GFP	Green Fluorescent Protein
GPC	Gel Permeation Chromatography
GSH	Glutathione
HBSS	Hank's Balanced Salt Solution
HDAC	Histone Deacetylase
HDF	Human Dermal Fibroblast
HEPES	4-(2-hydroxyethyl)-1-piperazineethanesulfonic acid
HMPA	N-(2-hydroxypropyl)methacrylamide
HNE	Human Neutrophil Elastase
HPLC	High-Performance Liquid Chromatography
LCST	Lower Critical Solution Temperature
Lyz	Lysozyme
MMP	Matrix Metalloproteinase
mMSC	Mouse Mesenchymal Stem Cells

MS	Mass Spectrometry
NMR	Nuclear Magnetic Resonance
PAGE	Poly(acrylamide) Gel Electrophoresis
PDS	Pyridyl Disulfide
PDSMA	Pyridyl Disulfide Ethyl Methacrylate
PEG	Poly(ethylene glycol)
PEGMA	Poly(ethylene glycol) Methacrylate
PEO	Poly(ethylene) Oxide
pHEMA	Poly(hydroxymethylacrylate)
PMMA	Poly(methyl methacrylate)
pNA	Para-nitroaniline
pNIPAAm	Poly(N-isopropylacrylamide)
PVA	Poly(vinyl alcohol)
PVBA	Poly(vinylbenzaldehyde)
RAFT	Reversible Addition-Fragmentation Chain-Transfer
RGD	Arginine-Glycine-Aspartic Acid
RI	Refractive Index
SDS	Sodium Dodecyl Sulfate
SEC	Size Exclusion Chromatography
SPAAC	Strain Promoted Alkyne-Azide Cycloaddition
TCEP	Tris(2-carboxyethyl)phosphine
TEA	Triethylamine
TEM	Transmission Electron Microscopy

TFA	Trifluoroacetic Acid
TIPS	Triisopropylsilane
TrMA	Methacrylate Functionalized Trehalose
VEGF	Vascular Endothelial Growth Factor

Acknowledgements

In writing this dissertation, I have come to reflect on just how many people have helped me over the years to get to this point. While writing a dissertation is a singular task, it truly takes a village, as they say, to raise a scientist. I would not be the scientist, or person, I am today without the help and guidance I received from my professors, peers, friends, and family, and I am happy to take the time to highlight their contributions below.

I would like to begin by thanking my advisor, Professor Heather Maynard, for her continued guidance and support over the past five years. I am especially grateful for her creative and fearless approach to science, which taught me that failed experiments (and there were many!) simply open the door to new opportunities. I also want to thank her for the chance to work with many incredible scientists during my time in the Maynard lab. Of note is Dr. Erhan Bat, the very first person I worked with in the lab, who was my mentor during my first and second years. I certainly would not have been able to finish my first project without his help, and I am grateful for his support and for setting a very high standard in research and beyond. I also would like to thank all other Maynard lab members past and present, for their help and support, especially my office mates, Uland, Jacquelin, Kyle, and Doug, who have shared in my successes and failures. Thank you for making the past five years a lot of fun.

I also would like to thank the members of my doctoral committee, Professors Houk and Di Carlo, for their support over the years. They continue to open my eyes to new perspectives and have taught me that there are many different ways to look at and solve a problem. Additionally, I would like to acknowledge my collaborators at UCLA. Thank you to Professor Tatiana Segura and her lab for getting me up to speed on all things hydrogels. And thank you to Dr. Robert Damoiseaux

in the MSSR facility in CNSI for his guidance on a very time sensitive project. I also want to acknowledge the NIH Biotechnology Training Program run by Professor Yi Tang for helping fund my research.

And finally, I would like to thank my family. A huge thank you goes to Brice for his unwavering support during our time in grad school together. Thank you for telling me “you can do it” every time I said I couldn’t. After overcoming every obstacle that has come our way, we can finally say we did it! I also want to thank my brother, Patrick, for his support and for always leading the way. Most importantly, I want to thank my parents for their help and guidance. I never would have made it this far without them. Thank you for believing in me even when I did not, and for encouraging and supporting all my dreams no matter what.

Vita

Education:

University of California, Los Angeles, Department of Chemistry, Los Angeles, CA

Ph. D. in Chemistry, Summer 2017 (expected)

Purdue University, College of Science, West Lafayette, IN

Bachelor of Science in Chemistry, May 2012

Publications:

Boehnke, N.; Kammeyer, J. K.; Damoiseaux, R.; Maynard, H. D. Stabilization of Glucagon by Trehalose Glycopolymer Nanogels. Manuscript in preparation, **2017**.

Boehnke, N.; Maynard, H. D. Design of Modular Dual-Enzyme Responsive Peptides. *Peptide Science* **2017**, in press.

Boehnke, N.; Cam, C.; Bat, E.; Segura, T.; Maynard, H. D. Imine Hydrogels with Tunable Degradability for Tissue Engineering. *Biomacromolecules*, **2015**, *16*, 2101-2108.

Lin, E.-W.; Boehnke, N.; Maynard, H.D. Protein-Polymer Conjugation via Ligand Affinity and Photoactivation of Glutathione S-Transferase. *Bioconjugate Chemistry*, **2014**, *25*, 1902-1909.

Presentations:

Boehnke, N.; Maynard, H.D. Redox-Responsive Trehalose Nanogels. Poster presented at: Seaborg Symposium at UCLA; November 12, 2016; Los Angeles, CA.

Boehnke, N.; Maynard, H.D. Hydrogels and Nanogels for Protein and Cell Delivery. Poster presented at: Warwick 2016 Polymer Conference at the University of Warwick; July 13, 2016; United Kingdom.

Boehnke, N.; Maynard, H.D. Hydrogels and Nanogels for Protein and Cell Delivery. Oral Presentation at: Warwick 2016 Polymer Conference at the University of Warwick; July 12, 2016; United Kingdom.

Boehnke, N.; Cam, C.; Bat, E.; Segura, T.; Maynard, H.D. Mixed Imine Hydrogels with Tunable Degradability. Poster presented at: 2016 International Symposium on Nanobiotechnology at UCLA; February 4, 2016; Los Angeles, CA.

Boehnke, N.; Cam, C.; Bat, E.; Segura, T.; Maynard, H.D. Self-Healing Hydrazone Hydrogels for Multicellular Tissue Engineering. Poster presented at: Sigman Symposium at UCLA; February 21, 2014; Los Angeles, CA.

Boehnke, N.; Segura, T.; Maynard, H.D. Multicellular Self-Healing Hydrogels. Oral Presentation at: Annual NIH Biotechnology Symposium; June 13, 2013; Los Angeles, CA.

Honors and Awards:

University of California, Los Angeles

Best Poster Prize, International Symposium on Nanobiotechnology (2016)

NIH Biotechnology Training Grant Fellowship (2013-2015)

Purdue University

Trustees Scholar (2008-2012)

Semester Honors (2009-2012)

Stine Summer Research Award (2010)

Chapter 1

General Introduction: Degradable Hydrogels and Nanogels for the Delivery of Cells and Therapeutics

1.1 Overview of Hydrogels for Therapeutics Delivery

Hydrogels are three-dimensional polymeric networks that are physically or chemically cross-linked and are capable of absorbing large amounts of water. The polymeric networks used to create hydrogels can be formed from either natural or synthetic materials.¹ Naturally derived hydrogels, such as those made from collagen or chitosan, have been used for numerous applications in tissue engineering.² These materials have shown promise but do not enable fine tuning of properties, have batch-to-batch variability, and can elicit a host-immune response.² Synthetically derived hydrogels are typically more tunable and do not exhibit the variability that is traditionally associated with natural materials.³ Wichterle and Lim reported the first example of synthetically derived hydrogels in 1960 wherein cross-linked glycolmethacrylate was proposed for biological use.⁴ Since then, synthetically derived hydrogels have been used for many biomedical applications, including drug delivery systems, scaffolds to act as structural supports for cell culture and tissue engineering, and to encapsulate and deliver cells.

Synthetic hydrogels can be prepared by polymerizing and cross-linking monomers via a chain-growth mechanism, by cross-linking multi-functional polymers with mutual reactivity via a step-growth mechanism, or by a combination of the two.⁵ Chain-growth gelation typically requires radicals to initiate the polymerization. In order to prepare hydrogels via a biocompatible radical based chain-growth mechanism, photo-initiators are often used, which circumvents the need to use elevated temperatures to initiate polymerization and gelation; however, the radicals needed to initiate the polymerizations can still elicit a cytotoxic response.⁶ Additionally, unless full monomer conversion is

achieved, unreacted monomers may induce an inflammatory or immune response when applied *in vivo*.⁷ On the other hand, step-growth gelation conditions are typically milder, often requiring no additional reagents, and result in gels that are more ordered than those prepared through chain-growth.^{5, 8-9} For both gelation mechanisms, gel characteristics can be controlled by changing polymer size, concentration, or cross-linker stoichiometry. However, many monomers used in step-growth gelation are available that are nontoxic and can be used to further functionalize the gel with proteins or targeting ligands.¹⁰

Hydrogels in biomedicine often need to be degradable to allow for cargo release and prevent bioaccumulation. Therefore hydrogels and their degradation products must be biocompatible, nontoxic, and non-immunogenic.¹¹ Moreover, the degradation products should either be metabolized into harmless byproducts or cleared efficiently via renal filtration.¹² A variety of biocompatible polymers have been utilized to create synthetic hydrogels, including poly(hydroxymethylacrylate) (pHEMA), poly(*N*-isopropylacrylamide) (pNIPAAm), poly(vinyl alcohol) (PVA), and poly(ethylene glycol) (PEG).¹³⁻¹⁴ PEG is one of the most common polymers used to create synthetic hydrogels for biomedical applications due to its biocompatibility, amphiphilicity, ease of functionalization, and commercial availability,¹⁵⁻¹⁶ making it an ideal choice to create hydrogels for therapeutic delivery applications.

Hydrogels are frequently used as delivery systems, particularly to deliver sensitive therapeutic cargo. Many therapeutic agents suffer from enzymatic degradation upon administration, rapid clearance *in vivo*, and nonspecific uptake, ultimately resulting in reduced efficacy, high costs, and off-target effects. Packaging therapeutics into hydrogels

can mitigate these issues.¹⁷ For example, systemic delivery of vascular endothelial growth factor (VEGF), which is used to promote angiogenesis, can lead to plaque formation and tumor growth as a result of off targets effects.¹⁸ Researchers have shown that when VEGF was encapsulated inside alginate hydrogel delivery vehicles and implanted into femoral artery ligation sites in mice, it was able to promote favorable angiogenesis in while mitigating unfavorable side effects.¹⁹⁻²⁰ While an initial burst release of the growth factor was observed, release eventually slowed to a constant rate for up to three weeks in rat models, leading to improved vascularization in the animals. Additionally, Hubbell and coworkers developed PEG-based hydrogels for protein delivery applications via step-growth mechanism through a Michael-type addition of PEG-dithiol or dithiothreitol (DTT) to PEG-acrylates.²¹⁻²² They further expanded their work to create protein-PEG hydrogels containing cell adhesion and enzymatically degradable peptides using PEG-divinylsulfone as cross-linker, demonstrating the versatility of PEG-based hydrogels as delivery systems and extracellular matrix (ECM) mimics.^{10, 23}

Another common use of synthetic hydrogels is to promote cellular function, adhesion, and proliferation when used as a cell culture support. Since cells do not typically adhere to polymeric systems, hydrogels are often functionalized with peptides and biomolecules to effectively mimic the ECM and facilitate cell adhesion.²⁴ The tripeptide Arg-Gly-Asp (RGD) is most commonly used to install cell adhesive properties due to its recognition by fibronectin, which mediates adhesion of cells to the ECM.²⁵ RGD has been used extensively to functionalize PEG hydrogels, and has shown to improve cell adhesion and migration.²⁶⁻²⁸ Other strategies to create cell adhesive surfaces include incorporating

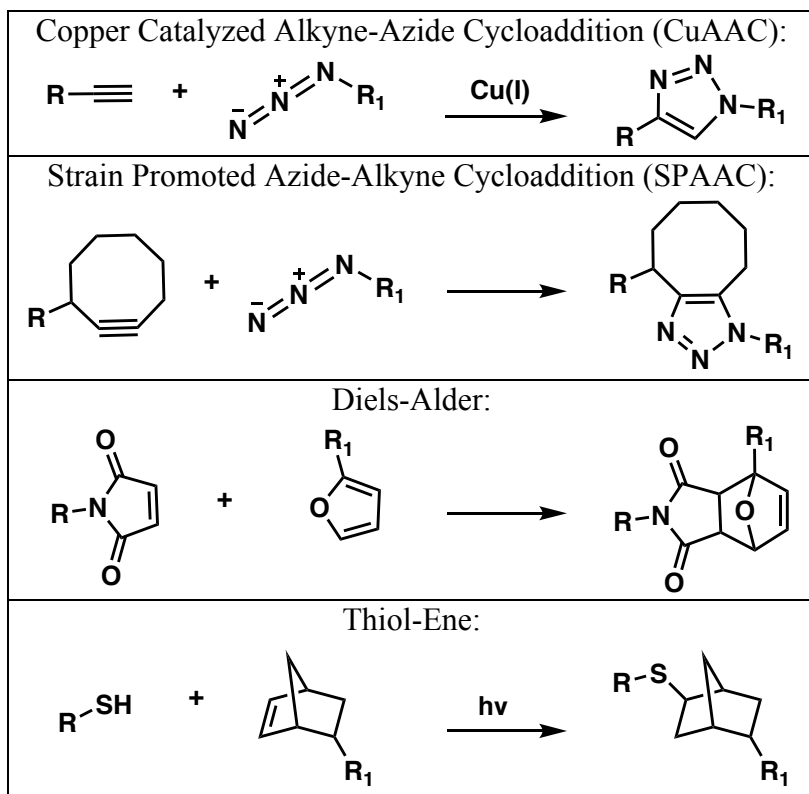
ECM proteins²⁹ or peptide fragments^{2, 30-32} in the hydrogel. Moreover, growth factors can also be encapsulated inside hydrogels to aid in cell migration, interaction, and proliferation.^{2, 33-35}

For these applications, the physical properties of hydrogels must be carefully controlled. For example, it has been shown that gel swelling is directly controlled through cross-linking density and polymer size. Specifically, increasing the size of the polymer repeat unit between cross-links reduces cross-linking density, improving the swelling behavior of the gel.³⁶ Varying the cross-linking chemistry also allows for control over hydrogel properties. The efficiency of the ligation strategy must also be taken into account as reactions that do not go to completion can form loosely or inconsistently cross-linked gels.³⁷ Herein, different types of cross-linking strategies will be discussed with a focus on how the selection of cross-linking strategy relates to the hydrogel function.

1. 1. 1. Click Chemistry for Hydrogel Cross-Linking

The types of chemistries used in the cross-linking of polymers to form hydrogels are important to the function of the gel. Reactions should be biocompatible and high yielding in order to create materials with uniform and predictable properties. Therefore, hydrogels prepared using click chemistry have become popular due to the ease with which these reactions can be carried out (Table 1.1). The term ‘click chemistry’ was coined by Sharpless in 2001 to describe reactions that are specific yet wide in scope, high yielding, simple to perform, and can be carried out in benign and/or easy to remove solvents.³⁸

Table 1.1. Commonly used click reactions to form hydrogels.



The most common click reaction is the copper catalyzed 1,3-dipolar cycloaddition between an alkyne and an azide (CuAAC), which has been used extensively to create hydrogel networks. For example, the Hawker group cross-linked linear alkyne-functionalized PEG with tetraazide-functionalized tetraethylene glycol to create well-defined PEG hydrogels.⁸ They observed that their click hydrogels exhibited superior physical properties, such as increased tensile stress and strain, when compared to photochemically cross-linked hydrogels, likely due to the controlled nature and high efficiency of the CuAAC cross-linking. They additionally noted that unreacted azide or alkyne groups could be used for further functionalization of the hydrogel. CuAAC cross-

linking has also been utilized to create biodegradable PEG hydrogels for cell delivery applications by incorporating azide-functionalized RGD peptides into the gel to promote cell adhesion and proliferation.³⁹ While high cell viability and proliferation were observed, it is important to note that cells were only seeded on top of hydrogel surfaces and were not encapsulated inside the hydrogel matrix. This may be due to the cytotoxic copper catalyst that is required for CuAAC reactions, making this cross-linking approach incompatible with most biological applications.⁴⁰

As an alternative to CuAAC, the Bertozzi group has developed copper free, strain-promoted alkyne-azide cycloadditions (SPAAC).⁴¹ They found that cyclooctynes were able to react efficiently with azides in the absence of catalyst as a result of ring strain. The addition of electron withdrawing substituents, such as fluorine, can further accelerate the reaction.⁴² Because SPAAC exhibits the same orthogonality as CuAAC without the associated cytotoxicity, it has rapidly grown in popularity and is frequently used for biomedical applications including hydrogel cross-linking. To create biodegradable hydrogels via SPAAC, the Anseth group cross-linked multi-arm azide-functionalized PEG with a difluorinated cyclooctyne enzyme-sensitive peptide cross-linker.⁴³ Additionally, the peptide cross-linker was modified with alkenes to allow for site-specific and orthogonal photopatterning via thiol-ene, and fluorescein was photopatterned onto the gel using a collagenase-sensitive linker. Fluorescent signal was observed upon enzymatic cleavage of the linker, whereas fluorophore quenching was observed in the absence of collagenase, indicating no fluorophore was cleaved.⁴³ The physical properties of this gel system can be tuned by changing polymer size and cross-linker ratio.⁴⁴ The Anseth group expanded their

work further by incorporating *o*-nitrobenzyl ether groups into their peptide cross-linkers that cleave upon exposure to UV light.⁴³ Using this approach, RGD peptides were incorporated into the gel to promote adhesion of encapsulated cells. Upon UV irradiation, cell detachment was observed, indicating that the RGD had cleaved from the polymer matrix. Similarly, Becker and coworkers reported the synthesis of SPAAC cross-linked PEG hydrogels using a 4-dibenzocyclooctyne functionalized PEG cross-linker for cell culture applications and showed that encapsulated mesenchymal stem cells retained up to 89% viability after 24 hours.⁴⁵ More recently, degradable PEG-based hydrogels cross-linked via SPAAC were shown to have tunable properties with good cytocompatibility.⁴⁶ Ester linkages were incorporated into the polymer backbone, and it was found that time to degradation could be varied from 1 to 35 days by changing polymer composition.

Diels-Alder reactions have also been employed to create biocompatible hydrogels. Anseth and Bowman reported a mixed hydrogel system consisting of thiol and maleimide-functionalized PEG cross-linked via Michael addition. Excess maleimide-PEG was functionalized with peptides containing furan moieties via reversible Diels-Alder reactions to study peptide release in response to temperature increase.⁴⁷ Moreover, they covalently bound dexamethasone (dex) into their hydrogel using Diels-Alder chemistry.⁴⁸ Since Diels-Alder reactants and products exist in equilibrium, time-dependent release of dex was observed, which was utilized to induce osteogenic differentiation of encapsulated human mesenchymal stem cells. Kirchhof et al. have cross-linked maleimide and furan functionalized multi-arm PEGs to form degradable hydrogels useful for protein and antibody delivery applications.⁴⁹⁻⁵¹ The gelation rate, physical properties, and time to

degradation were controlled by changing polymer content, branching, and size. They additionally observed that, depending on the conditions, either a reverse Diels-Alder or base catalyzed ring-opening hydrolysis of cross-linked maleimides was responsible for gel degradation.⁵²

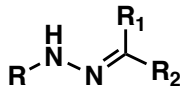
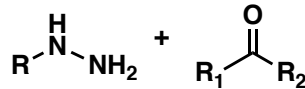
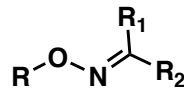
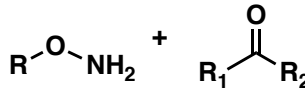


Thiol-ene is one of the most commonly utilized click chemistries to form hydrogels.⁵³ This is due to the high reaction rate and efficiency of the reaction under physiological conditions, as well as the ease with which alkenes and thiols can be installed into hydrogel systems. Additionally, thiol-ene cross-linking occurs via a radical mechanism that can be initiated thermally, photochemically, or via oxidation-reduction,⁵⁴ but, unlike other radically initiated reactions, thiol-ene reactions do not require oxygen-free environments to reach quantitative conversion.⁵⁵ For biomedical applications, photochemical initiation is preferred because this offers control over where, when, and how fast gelation occurs, and low doses of UV light are not damaging to biological cargo such as cells and proteins.⁵⁶ To demonstrate the usefulness of thiol-ene chemistry to create hydrogels for protein delivery, Anseth and coworkers encapsulated various proteins in enzyme sensitive hydrogels by cross-linking 4-arm PEG functionalized with norbornene groups with a human neutrophil elastase (HNE) sensitive peptide containing cysteine residues at the N- and C- termini.⁵⁷ Degradation rates were controlled by changing enzyme and peptide concentrations as well as the peptide cross-linker structure. In the presence of HNE, protein release with high retention of activity was observed, whereas in the absence of HNE no protein release occurred. Degradability has also been incorporated into thiol-ene cross-linked gels by installing hydrolytically sensitive esters⁵⁸ as well as

photodegradable linkages.⁵⁹ Thiol-ene cross-linking has also been used to create hydrogels for cell culture applications.⁶⁰ Biochemical cues can be photopatterned into the gel and changing polymer concentration can create scaffolds that mimic a range of soft tissue environments.⁶¹

1. 1. 2. Degradable Cross-Linking Strategies for Hydrogels

For biomedical applications, degradability is often incorporated into hydrogels for delivery applications to create dynamic scaffolds, and prevent bioaccumulation. A variety of different methods can be used to install degradability (Table 1.2).

Table 1.2. Examples of degradable hydrogel cross-linking strategies.

Hydrolytically Degradable:	
Hydrazones	
	\rightleftharpoons 
Oximes	
	\rightleftharpoons 
Enzymatically Degradable:	
	$\xrightarrow{\text{Enzyme}}$ 

Incorporating reversible hydrazone bonds, which form from the reaction of a hydrazine or hydrazide with an aldehyde or ketone, results in hydrogels that can degrade

under physiological conditions. Anseth and coworkers have reported the design and synthesis of hydrazone cross-linked PEG hydrogels for cell culture, wherein the structure of the aldehyde group was studied as a way to control the physical properties of their gels.⁶²⁻
⁶⁴ Hydrazone chemistry has also been utilized by Patenaude et al. to create hydrogels by cross-linking pNIPAAm and carbohydrate polymers. Hydrazone groups were installed by copolymerizing NIPAAm with acrylic acid and functionalizing the side chains with adipic acid dihydrazide. Aldehyde groups were installed by oxidizing polysaccharides using sodium periodate. They demonstrated that hydrazones were the weakest points in their hydrogels, indicating that degradation would most likely occur at those bonds.⁶⁵⁻⁶⁷ The effect of hydrazone structure on stability has also been studied. Varghese and coworkers have found that resonance stabilized hydrazones, such as those derived from carbodihydrazide, are more stable and less susceptible to degradation compared to hydrazones without resonance stabilization, such as those made from adipodihydrazide.⁶⁸ Aromatic hydrazones are considered even more stable, and Deng and coworkers created poly(ethylene oxide) (PEO) based hydrazone hydrogels by cross-linking aromatic hydrazide and aldehyde groups. They observed that gel degradation did not occur until pH 4, and their gels exhibited self-healing behavior but at a much slower rate (15 hours) than aliphatic hydrazone cross-linked gels.⁶⁹ It has also been reported that, in addition to acidic conditions, cells are also able to degrade and even prevent the formation of hydrazone bonds in hyaluronic acid and alginate-based hydrogels, which could be useful for creating cell delivery constructs where such degradation may be desired.⁷⁰

Analogous to hydrazone bonds, oximes form from the reaction of aminoxy groups with aldehydes or ketones. Maynard and coworkers reported the use of oxime cross-linking to form PEG-based hydrogels to create stable and biocompatible scaffolds for cell culture.⁷¹ To form the hydrogels, 8-arm PEG functionalized with aminoxy groups was cross-linked with glutaraldehyde, a small molecule di-aldehyde, in the presence of RGD. Cells cultured on top of these gels were able to spread out and exhibited high viability, although encapsulated cells were alive but retained rounded morphology, most likely due to the non-degradable environment of the hydrogel. It has also been shown by Christman and coworkers that 4-arm PEG-aminoxy could be cross-linked with ketone-functionalized 4-arm PEG to form injectable hydrogels for catheter delivery.⁷² While not reversible under physiological conditions, oximes are reversible at acidic pH, and Mukherjee et al. have shown that oxime hydrogels can exhibit sol-gel transitions and self-healing behavior upon the addition of trifluoroacetic acid.⁷³ Additionally, the Becker group reported multi-functional oxime cross-linked hydrogels with dangling azide and alkene groups to pattern peptides into the gel via click chemistry.⁷⁴

Enzyme degradation sites are commonly incorporated into hydrogels to form biodegradable materials responsive to specific stimuli. This is commonly achieved through the installation of short peptides that act as cleavage sites for certain proteases. Such biodegradable hydrogels can either be used for delivery applications or as dynamic ECM mimics where proteases excreted by cells are able to degrade their surroundings. The enzymatic cleavage site should be chosen carefully depending on the application. For example, hydrogels used as ECM mimics can contain degradation sites for specific

enzymes secreted by cells during migration, including matrix metalloproteinases (MMPs) and plasmin.^{33,75} These enzymes are of particular importance due to their ability to break down structural proteins and allow cells to move and spread out in their environment. To demonstrate the potential for using PEG hydrogels as ECM mimics, Hubbell and West utilized two peptides, Ala-Pro-Gly-Leu and Val-Arg-Asn, to install MMP I and plasmin sensitivity, respectively, and observed that hydrogels degraded in the presence of enzyme but were stable indefinitely to passive hydrolysis.⁷⁶ The addition of cell adhesive peptides resulted in biocompatible hydrogels that supported cell proliferation and migration.²⁷ Another example of the tunability of enzymatic degradation for specific applications was carried out by the West group where the incorporation of cathepsin K-sensitive peptides into PEG hydrogels allowed degradation in response to bone resorption after bone graft procedures.⁷⁷ Moreover, protease sensitive hydrogels have been created for potential drug delivery applications by cross-linking 4- and 8-arm PEG-alkyne with an azide-functionalized plasmin and trypsin substrate D-Ala-Phe-Lys.⁷⁸ Hydrogel degradation was measured through swelling studies, and the authors found that only trypsin was able to degrade the gels. The larger size of plasmin could prevent it from accessing the hydrogel and modification of the peptide substrate with azide groups could prevent interactions with the active site of plasmin, potentially explaining the lack of degradation by plasmin.

1.2 Overview of Nanogels for Therapeutics Delivery

Nanogels are defined as three-dimensional, physically or chemically cross-linked polymeric networks less than one micron in diameter.⁷⁹⁻⁸⁰ Main fabrication strategies

include self-assembly, polymerization, polymer cross-linking, and template-assisted fabrication where cross-linking can occur intermolecularly or intramolecularly.⁸¹⁻⁸² Similar to hydrogels, nanogels used for biomedical applications should be biocompatible with tunable physical and chemical properties. While hydrogels are often used as effective delivery vehicles, nanogels are gaining popularity because of their small size, which allows for either active or passive targeting of specific sites, including cells or tumors via the enhanced permeability and retention (EPR) effect.⁸³ Sunamoto and Akiyoshi first described nanogels in 1993 when they observed particle formation after physical cross-linking of cholesterol-functionalized polysaccharides⁸⁴, although the term was not officially coined until 1999 by Kabanov and coworkers.⁸⁵

Nanogels are commonly used for the delivery of therapeutics, such as proteins, where cargo can be retained inside the nanogel either covalently or noncovalently or by attachment to the nanogel surface.^{81, 86} Therapeutic proteins are increasingly used for clinical applications, though their full potential has not yet been realized due to their instability. Proteins have limited shelf lives and, upon administration, are degraded or cleared rapidly from the body, limiting their efficacy.⁸⁷ One strategy to overcome these problems is the covalent attachment, or conjugation, of polymers to proteins, which has been shown to improve pharmacokinetic properties.¹⁶ Abuchowski and co-workers first reported the conjugation of PEG to a protein, also known as PEGylation, in 1977 and demonstrated that PEG-protein conjugates exhibit lower immunogenicity as well as increased circulation times *in vivo*.⁸⁸⁻⁸⁹ PEGylation creates a steric shield around the protein

and increases the biomolecule's diameter, therefore reducing clearance from the blood and lowering the required dosage amount and frequency.¹⁶

One drawback to protein conjugation is the loss of activity that can occur, which can be circumvented by encapsulating proteins non-covalently or reversibly into polymeric nanogels.⁹⁰⁻⁹¹ Two main strategies have been developed to encapsulate biomacromolecules inside nanogels. Proteins can either be encapsulated during nanogel formation⁹² or after nanogel formation by diffusion into the nanogel.⁹³ The first method typically results in even distribution of biomolecule cargo and encapsulation efficiency can be tuned by controlling the extent of cross-linking. The second method allows for nanogel formation without the presence of the cargo, which could potentially affect physical characteristics of the nanogels, but diffusion limitations may result in reduced encapsulation. Shea and coworkers reported the synthesis of polymeric nanoparticles consisting of acrylic acid and *N-tert*-butylacrylamide copolymers for the encapsulation of lysozyme.⁹⁴ They found that positively charged and hydrophobic lysozyme interacted favorably with their particles due to the charge-based interactions between enzyme and acrylic acid groups and the hydrophobic interactions between enzyme and their polymer. They were able to selectively encapsulate the protein by raising the temperature above the lower critical solution temperature (LCST) of the polymers comprising the nanoparticles. Cooling the solution below the LCST caused lysozyme to be released, restoring enzyme activity. After three LCST cycles, 79% of lysozyme activity was retained. Alternatively, Averick et al. prepared protein-nanogel hybrids via activator generated by electron transfer atom transfer radical polymerization (AGET ATRP) by using genetically modified green fluorescent protein

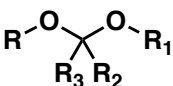
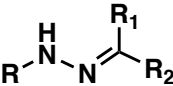
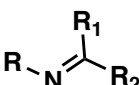
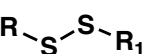
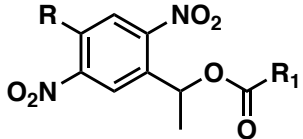
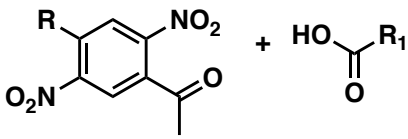


(GFP) functionalized with an ATRP initiator.⁹⁵ They found that the protein retained its tertiary structure and fluorescent properties during polymerization and simultaneous nanogel formation, but no fluorescence was observed in the nanogels when wild type GFP, lacking the initiator functionality, was encapsulated non-covalently, indicating that it was not retained and that covalent attachment may be required for high encapsulation efficiency.

Incorporating degradable characteristics into nanogels allows for selective cargo release in response to specific stimuli, such as pH changes or reducing conditions. Additionally, nano-sized materials, upon administration *in vivo*, are known to accumulate in the liver and spleen.⁹⁶ Incorporating degradable units allows the nanogels to be broken into smaller units that can be cleared from the body more easily. Commonly utilized strategies to create biodegradable nanogels will be discussed below.

1. 2. 1. Degradable Nanogel Cross-linking Strategies

To allow for cargo release, degradable units are often incorporated into nanogels either in the polymer backbone⁹⁷⁻⁹⁹ or at the cross-linking site¹⁰⁰, though the latter approach is more versatile since a broader range of functional groups can be incorporated without having to withstand polymerization and purification conditions. Additionally, physical properties can easily be controlled by varying the cross-linking extent and chemistry, and multi-stimuli responsive gels can be created by incorporating multiple orthogonal cross-linking chemistries in the same system. Degradable nanogels can be categorized by their degradation mechanism, which can occur through hydrolysis, reduction, enzymatic cleavage, or photolysis (Table 1.3).¹⁰¹⁻¹⁰²

Table 1.3 Examples of degradable nanogel cross-linking strategies.

Acid Degradable:	
Acetals	
 $\xrightarrow{\hspace{1cm}}$	$R-OH + HO-R_1$
Hydrazones	
 \rightleftharpoons	$R-NH-NH_2 + R_1-C(=O)-R_2$
Imines	
 \rightleftharpoons	$R-NH_2 + R_1-C(=O)-R_2$
Redox-Responsive:	
Disulfides	
 \rightleftharpoons	$R-SH + HS-R_1$
Photolytically Degradable:	
 $\xrightarrow{h\nu}$	
Enzymatically Degradable:	
 $\xrightarrow{\text{Enzyme}}$	

A common degradation mechanism is through the hydrolysis of pH labile cross-linkers due to the acidic environment of endosomes and some tumors.⁸³ For example, the Fréchet group has used cross-linkers containing pH labile acetal units to create hydrolytically degradable nanogels for the delivery of protein-based vaccines. Inversion emulsion polymerizations were used to encapsulate ovalbumin for delivery to the mildly acidic environment of the phagosomes of antigen presenting cells, allowing for 80% release

within 5 hours at pH 5.0, but only 10% release at pH 7.4.¹⁰³ The addition of a cationic cross-linker to their degradable particles increased antigen presentation even further.¹⁰⁴⁻¹⁰⁵ They expanded their work by encapsulating plasmid DNA for vaccine development and demonstrated that their particles increased immunostimulatory activity and protected DNA against enzymatic degradation.¹⁰⁶ Haag and coworkers have also utilized acetal cross-linking to create biodegradable nanogels for the delivery of biomolecules.¹⁰⁷ Benzacetal bonds were introduced to cross-link polyglycerol nanogels that degraded at acidic pH but remained stable at neutral pH. Encapsulation of lysozyme and asparaginase was reported to be 100% with full retention of activity.

An alternative approach to creating pH sensitive biodegradable nanogels is the incorporation of hydrazone bonds, resulting from the reaction of an aldehyde or ketone with a hydrazine or hydrazide moiety. The Fulton group synthesized poly(vinylbenzaldehyde) (PVBA) polymers that were cross-linked via bis-hydrazide cross-linkers to create single chain nanoparticles. Gel permeation chromatography (GPC) was utilized to characterize these nanogels and demonstrate that intramolecular cross-linking had occurred, as evidenced by a decrease in M_n and M_w .¹⁰⁸ Additionally, they reported the formation of single chain nanoparticles from oligoethyleneglycol and p-(2-methacryloxyethoxy)benzaldehyde polymers exhibiting LCST behavior.¹⁰⁹⁻¹¹⁰ Hydrazone bonds have also been used to reversibly anchor cargo, such as doxorubicin, into nanogels for selective delivery to the acidic environment of certain tumor tissues.¹¹¹

Similar to hydrazones, imine bonds have also been utilized for the formation of degradable nanogels. The Fulton group has formed imine cross-linked nanogels by mixing

aldehyde- and amine-functionalized styrene and methacrylate polymers, and they found that the nanogels undergo structural reorganization in the presence of small molecule amines that disrupt the imine cross-links via trans-amination.¹¹² Tan et al. utilized aldehyde-functionalized PEG to cross-link urokinase via imine formation with the lysine side chains to create protein-polymer nanogels. They observed that their nanogels degraded within three hours at pH 5.0 but were stable at pH 7.4. Additionally, the encapsulated protein exhibited improved stability against proteinases, and protein activity could be controlled by changing the molecular weight of the PEG cross-linker.¹¹³

Biodegradability can also be introduced into nanogels via redox-responsive disulfide bonds. Unlike hydrolytically degradable linkages, disulfides allow for more selective delivery, making them an attractive choice for therapeutic delivery vehicles. Since these cross-links degrade only in reducing environments, such as the inside of cells where millimolar levels of the natural reducing agent glutathione (GSH) are present, disulfides are often incorporated when intracellular delivery is desired.¹¹⁴ Additionally GSH levels are elevated in many types of tumors, making redox-responsive delivery vehicles useful for anti-cancer therapy applications.¹¹⁵ Matyjaszewski and coworkers have utilized ATRP of water-soluble monomers and a disulfide-functionalized dimethacrylate cross-linker in an inverse miniemulsion to synthesize nanogels with narrow molecular weight distributions that degrade into individual polymer chains upon addition of reducing agents.¹¹⁶ Matyjaszewski and coworkers continued their work to demonstrate biocompatibility of their nanogels and degradability in the presence of GSH. Additionally, hydroxyl-functionalized nanogels were prepared by introducing 2-hydroxyethyl acrylate

during nanogel formation for subsequent modification with biotin and formation of avidin-nanogel conjugates.¹¹⁷

Redox-responsive nanogels have also been developed by the Thayumanavan group from polymers prepared by reversible addition-fragmentation chain transfer (RAFT) polymerization of pyridyl disulfide ethylmethacrylate (PDSMA) and various comonomers, such as *N*-hydroxysuccinimide methacrylate¹¹⁸ and polyethyleneglycol methacrylate (PEGMA).¹¹⁹ To create nanogels, PDSMA-*co*-PEGMA, which exhibited LCST behavior, was cross-linked via disulfide exchange in the presence of stoichiometric reducing agent. UV-vis spectroscopy was utilized to monitor the cross-linking reaction by measuring the absorbance of the reaction byproduct, pyridinethione, over time. To demonstrate that the interior of the resulting nanogels is hydrophobic, the researchers chose to encapsulate a hydrophobic dye, Nile Red, which exhibits a higher emission intensity when in a hydrophobic environment. They found that upon degradation, a decrease in the spectral emission intensity of Nile red was detected, signifying the dye was successfully released from the nanogel. Additionally, the exterior of the nanogels was functionalized with small molecule thiols, including a modified cell-penetrating peptide, Tat-SH. Confocal microscopy was utilized to show that Tat-functionalized nanogels were internalized by cells much more readily than the control nanogels without Tat peptide.¹¹⁹ Thayumanavan and coworkers continued their work to show that these nanogels can be used to deliver doxorubicin to cells since the disulfide cross-links are reduced upon internalization, and they controlled the release rate from the nanogels by varying monomer ratio and cross-linking density.¹²⁰⁻¹²¹ In collaboration with the Maynard group, they

synthesized protein-nanogel conjugates by conjugating the same nanogel system, PDSMA-co-PEGMA, to thiolated bovine serum albumin.¹²² The nanogel conjugates were characterized using dynamic light scattering (DLS) and gel electrophoresis. An increase in size was observed when comparing nanogel conjugates unfunctionalized nanogels, indicating the conjugation was successful. Further, Thayumanavan and coworkers demonstrated that their nanogels can be used to encapsulate and deliver caspase 3 with retention of activity.¹²³

Nanogels with sensitivity to multiple stimuli have been developed to increase target specificity and control. For example, nanogels containing both disulfide and hydrazone cross-links have been developed for combined redox and pH responsiveness.¹²⁴ Polyacrylamide polymers containing benzaldehyde and pyridyl disulfide side chains were cross-linked with polymers containing pyridyl disulfide and amine side chains. Through the addition of reducing agent, disulfide exchanged occurred, whereas at pH 8 imine formation occurred. It was shown that both acidic and reducing environments are required for cargo release due to the high cross-linking density between both functionalities. The Boyer and Davis groups reported the synthesis of nanogels cross-linked with pH sensitive ketal groups to encapsulate small molecule cargo via redox-responsive disulfide linkages.¹²⁵ Hydrolysis of the ketal cross-linker was observed within 24 hours at pH 5. To test the dual stimuli responsiveness, both Nile Red and FITC dyes were loaded into the nanogels via disulfide bond formation. Addition of dithiothreitol (DTT) did not result in Nile Red release due to the hydrophobic nature of the dye. FITC, which is more hydrophilic and therefore can be released into aqueous environments more easily, did release under the

same conditions, indicating that the disulfide bonds had been cleaved while the nanogel remained intact.

Photodegradable nanogels have been developed in order to allow for user-controlled degradation in a spatiotemporally defined manner. The *ortho*-nitrobenzyl group is commonly used for biomedical applications because of its cytocompatibility, lack of cross-reactivity with biomolecules both before and after degradation, and absorbance at longer wavelengths.¹²⁶ A methoxy-nitrobenzyl ether derivative has been utilized as a cross-linker to synthesize photodegradable nanogels for on-demand release of proteins.¹²⁷ The cross-linker was copolymerized with hydroxyethyl acrylate in the presence of alkaline phosphatase to create protein-laden nanogels with 50% loading efficiency. A size increase from 50 to 200 nm was observed upon encapsulation, and enzyme activity of the encapsulated protein was regained after degradation of the nanogels by exposure to UV light. *O*-nitrobenzyl groups have also been utilized to cross-link poly(2-hydroxyethylmethacrylate-*co*-methacrylic acid) into nanogels with pH-dependent swelling behavior.¹²⁸ This behavior was used to encapsulate positively charged myoglobin using electrostatic interactions with the negatively charged methacrylic acid groups. Irradiation of the gels with UV light triggered rapid release of the cargo within minutes whereas release from the swollen gels at neutral pH took over 24 hours.

In order to install selective degradability, enzyme sensitive nanogels have been developed by incorporating peptides or polysaccharides as cross-linking agents. Landfester and coworkers reported nanogels formed from poly(styrene-*co*-acrylic acid) cross-linked with a trypsin and pepsin cleavable peptide, Gly-Phe-Phe.¹²⁹ They utilized fluorescence

resonance energy transfer (FRET) to monitor enzymatic degradation of the gels and found that the majority of the particles were cleaved within one hour. This work was expanded using polystyrene-peptide triblock polymers to form nanoparticles sensitive to trypsin and pepsin for potential anti-cancer drug delivery applications since these enzymes are overexpressed in early stages of prostate cancer.¹³⁰ Other examples of enzymatically degradable nanogels include dextran methacrylate based nanogels degraded by dextranases¹³¹ and phosphoester based nanogels degraded by phosphatases.¹³²⁻¹³³

1.3. Summary

The properties and functions of biomaterials can be tuned for various applications by selecting appropriate cross-linking strategies. To this end, the dissertation will describe various approaches to create reversibly cross-linked biomaterials. In **Chapter 2**, the combination of hydrazone and oxime cross-links to form selectively degradable hydrogels will be discussed. In **Chapters 3 and 4**, redox-responsive cross-links utilized to create nanogels for protein encapsulation, stabilization, and release are described. Additionally, **Chapter 5** will cover the design and synthesis of dual-enzyme responsive peptides that can be used as degradable cross-linkers or conjugation handles. Overall, selective degradability was incorporated into biomaterials through the use of reversible cross-links, and the potential to use these materials for cell and therapeutics delivery was successfully demonstrated.

1. 4. References

1. Hennink, W. E.; van Nostrum, C. F. *Adv. Drug Del. Rev.* **2002**, *54*, 13-36.
2. Zhu, J. M.; Marchant, R. E. *Expert Rev. Med. Devices* **2011**, *8*, 607-626.
3. Fisher, O. Z.; Khademhosseini, A.; Langer, R.; Peppas, N. A. *Acc. Chem. Res.* **2010**, *43*, 419-428.
4. Wichterle, O.; Lim, D. *Nature* **1960**, *185*, 117-118.
5. Lin, C. C.; Anseth, K. S. *Pharm. Res.* **2009**, *26*, 631-643.
6. Lin, C.; Raza, A.; Shih, H. *Biomaterials* **2011**, *32*, 9685-9695.
7. Fournier, E.; Passirani, C.; Montero-Menei, C. N.; Benoit, J. P. *Biomaterials* **2003**, *24*, 3311-3331.
8. Malkoch, M.; Vestberg, R.; Gupta, N.; Mespouille, L.; Dubois, P.; Mason, A. F.; Hedrick, J. L.; Liao, Q.; Frank, C. W.; Kingsbury, K.; Hawker, C. J. *Chem. Commun.* **2006**, 2774-2776.
9. Metters, A. T.; Anseth, K. S.; Bowman, C. N. *J. Phys. Chem. B* **2001**, *105*, 8069-8076.
10. Rizzi, S. C.; Hubbell, J. A. *Biomacromolecules* **2005**, *6*, 1226-1238.
11. Nicodemus, G. D.; Bryant, S. J. *Tissue Eng. Pt. B. Rev.* **2008**, *14*, 149-165.
12. Prestwich, G. D. *J. Cell. Biochem.* **2007**, *101*, 1370-1383.
13. Ratner, B. D.; Hoffman, A. S. *ACS Symp. Ser.* **1976**, 1-36.
14. Peppas, N. A.; Bures, P.; Leobandung, W.; Ichikawa, H. *Eur. J. Pharm. Biopharm.* **2000**, *50*, 27-46.

15. Slaughter, B. V.; Khurshid, S. S.; Fisher, O. Z.; Khademhosseini, A.; Peppas, N. A. *Adv. Mater.* **2009**, *21*, 3307-3329.
16. Alconcel, S. N. S.; Baas, A. S.; Maynard, H. D. *Polym. Chem.* **2011**, *2*, 1442-1448.
17. Fisher, S. A.; Baker, A. E. G.; Shoichet, M. S. *J. Am. Chem. Soc.* **2017**.
18. Epstein, S. E.; Fuchs, S.; Zhou, Y. F.; Baffour, R.; Kornowski, R. *Cardiovasc. Res.* **2001**, *49*, 532-542.
19. Lee, K. Y.; Peters, M. C.; Anderson, K. W.; Mooney, D. J. *Nature* **2000**, *408*, 998-1000.
20. Elcin, Y. M.; Dixit, V.; Gitnick, T. *Artif. Organs* **2001**, *25*, 558-565.
21. Elbert, D. L.; Pratt, A. B.; Lutolf, M. P.; Halstenberg, S.; Hubbell, J. A. *J. Control. Release* **2001**, *76*, 11-25.
22. van de Wetering, P.; Metters, A. T.; Schoenmakers, R. G.; Hubbell, J. A. *J. Control. Release* **2005**, *102*, 619-627.
23. Rizzi, S. C.; Ehrbar, M.; Halstenberg, S.; Raeber, G. P.; Schmoekel, H. G.; Hagenmuller, H.; Muller, R.; Weber, F. E.; Hubbell, J. A. *Biomacromolecules* **2006**, *7*, 3019-3029.
24. Drury, J. L.; Mooney, D. J. *Biomaterials* **2003**, *24*, 4337-4351.
25. Ruoslahti, E.; Pierschbacher, M. D. *Cell* **1986**, *44*, 517-518.
26. Hern, D. L.; Hubbell, J. A. *J. Biomed. Mater. Res.* **1998**, *39*, 266-276.
27. Mann, B. K.; Gobin, A. S.; Tsai, A. T.; Schmedlen, R. H.; West, J. L. *Biomaterials* **2001**, *22*, 3045-3051.

28. Guarnieri, D.; De Capua, A.; Ventre, M.; Borzacchiello, A.; Pedone, C.; Marasco, D.; Ruvo, M.; Netti, P. A. *Acta Biomater.* **2010**, *6*, 2532-2539.
29. Nuttelman, C. R.; Mortisen, D. J.; Henry, S. M.; Anseth, K. S. *J. Biomed. Mater. Res.* **2001**, *57*, 217-223.
30. Rowley, J. A.; Madlambayan, G.; Mooney, D. J. *Biomaterials* **1999**, *20*, 45-53.
31. Liu, X. H.; Holzwarth, J. M.; Ma, P. X. *Macromol. Biosci.* **2012**, *12*, 911-919.
32. Zhu, J. M. *Biomaterials* **2010**, *31*, 4639-4656.
33. Moon, J. J.; Saik, J. E.; Poche, R. A.; Leslie-Barbick, J. E.; Lee, S. H.; Smith, A. A.; Dickinson, M. E.; West, J. L. *Biomaterials* **2010**, *31*, 3840-3847.
34. Mann, B. K.; Schmedlen, R. H.; West, J. L. *Biomaterials* **2001**, *22*, 439-444.
35. Elisseeff, J.; McIntosh, W.; Fu, K.; Blunk, T.; Langer, R. *J. Orthop. Res.* **2001**, *19*, 1098-1104.
36. Rydholm, A. E.; Reddy, S. K.; Anseth, K. S.; Bowman, C. N. *Polymer* **2007**, *48*, 4589-4600.
37. Jiang, Y. J.; Chen, J.; Deng, C.; Suuronen, E. J.; Zhong, Z. Y. *Biomaterials* **2014**, *35*, 4969-4985.
38. Kolb, H. C.; Finn, M. G.; Sharpless, K. B. *Angew. Chem. Int. Ed.* **2001**, *40*, 2004-2021.
39. Liu, S. Q.; Ee, P. L. R.; Ke, C. Y.; Hedrick, J. L.; Yang, Y. Y. *Biomaterials* **2009**, *30*, 1453-1461.
40. Huisgen, R. *Angew. Chem. Int. Ed.* **1963**, *75*, 742-&.

41. Agard, N. J.; Prescher, J. A.; Bertozzi, C. R. *J. Am. Chem. Soc.* **2004**, *126*, 15046-15047.
42. Baskin, J. M.; Prescher, J. A.; Laughlin, S. T.; Agard, N. J.; Chang, P. V.; Miller, I. A.; Lo, A.; Codelli, J. A.; Bertozzi, C. R. *Proc. Natl. Acad. Sci. U. S. A.* **2007**, *104*, 16793-16797.
43. DeForest, C. A.; Polizzotti, B. D.; Anseth, K. S. *Nat. Mater.* **2009**, *8*, 659-664.
44. DeForest, C. A.; Sims, E. A.; Anseth, K. S. *Chem. Mater.* **2010**, *22*, 4783-4790.
45. Zheng, J. K.; Callahan, L. A. S.; Hao, J. K.; Guo, K.; Wesdemiotis, C.; Weiss, R. A.; Becker, M. L. *ACS Macro Lett.* **2012**, *1*, 1071-1073.
46. Hodgson, S. M.; Bakaic, E.; Stewart, S. A.; Hoare, T.; Adronov, A. *Biomacromolecules* **2016**, *17*, 1093-1100.
47. Koehler, K. C.; Anseth, K. S.; Bowman, C. N. *Biomacromolecules* **2013**, *14*, 538-547.
48. Koehler, K. C.; Alge, D. L.; Anseth, K. S.; Bowman, C. N. *Biomaterials* **2013**, *34*, 4150-4158.
49. Kirchhof, S.; Brandl, F. P.; Hammer, N.; Goepferich, A. M. *J. Mater. Chem. B* **2013**, *1*, 4855-4864.
50. Kirchhof, S.; Gregoritz, M.; Messmann, V.; Hammer, N.; Goepferich, A. M.; Brandl, F. P. *Eur. J. Pharm. Biopharm.* **2015**, *96*, 217-225.
51. Kirchhof, S.; Abrami, M.; Messmann, V.; Hammer, N.; Goepferich, A. M.; Grassi, M.; Brandl, F. P. *Mol. Pharm.* **2015**, *12*, 3358-3368.

52. Kirchhof, S.; Strasser, A.; Wittmann, H. J.; Messmann, V.; Hammer, N.; Goepferich, A. M.; Brandl, F. P. *J. Mater. Chem. B* **2015**, *3*, 449-457.
53. Kharkar, P. M.; Rehmann, M. S.; Skeens, K. M.; Maverakis, E.; Kloxin, A. M. *ACS Biomater. Sci. Eng.* **2016**, *2*, 165-179.
54. Hoyle, C. E.; Lowe, A. B.; Bowman, C. N. *Chem. Soc. Rev.* **2010**, *39*, 1355-1387.
55. Hoyle, C. E.; Bowman, C. N. *Angew. Chem. Int. Ed.* **2010**, *49*, 1540-1573.
56. Nguyen, K. T.; West, J. L. *Biomaterials* **2002**, *23*, 4307-4314.
57. Aimetti, A. A.; Machen, A. J.; Anseth, K. S. *Biomaterials* **2009**, *30*, 6048-6054.
58. Shih, H.; Lin, C. C. *Biomacromolecules* **2012**, *13*, 2003-2012.
59. Kharkar, P. M.; Kiick, K. L.; Kloxin, A. M. *Polym. Chem.* **2015**, *6*, 5565-5574.
60. Lin, C. C.; Ki, C. S.; Shih, H. *J. Appl. Polym. Sci.* **2015**, *132*.
61. Sawicki, L. A.; Kloxin, A. M. *Biomater. Sci.* **2014**, *2*, 1612-1626.
62. McKinnon, D. D.; Domaille, D. W.; Cha, J. N.; Anseth, K. S. *Chem. Mater.* **2014**, *26*, 2382-2387.
63. McKinnon, D. D.; Domaille, D. W.; Brown, T. E.; Kyburz, K. A.; Kiyotake, E.; Cha, J. N.; Anseth, K. S. *Soft Matter* **2014**, *10*, 9230-9236.
64. McKinnon, D. D.; Domaille, D. W.; Cha, J. N.; Anseth, K. S. *Adv. Mater.* **2014**, *26*, 865-872.
65. Patenaude, M.; Hoare, T. *Biomacromolecules* **2012**, *13*, 369-378.
66. Patenaude, M.; Hoare, T. *ACS Macro Lett.* **2012**, *1*, 409-413.
67. Patenaude, M.; Campbell, S.; Kinio, D.; Hoare, T. *Biomacromolecules* **2014**.

68. Oommen, O. P.; Wang, S. J.; Kisiel, M.; Sloff, M.; Hilborn, J.; Varghese, O. P. *Adv. Funct. Mater.* **2013**, *23*, 1273-1280.
69. Deng, G. H.; Tang, C. M.; Li, F. Y.; Jiang, H. F.; Chen, Y. M. *Macromolecules* **2010**, *43*, 1191-1194.
70. Dahlmann, J.; Krause, A.; Moller, L.; Kensah, G.; Mowes, M.; Diekmann, A.; Martin, U.; Kirschning, A.; Gruh, I.; Drager, G. *Biomaterials* **2013**, *34*, 940-951.
71. Grover, G. N.; Lam, J.; Nguyen, T. H.; Segura, T.; Maynard, H. D. *Biomacromolecules* **2012**, *13*, 3013-3017.
72. Grover, G. N.; Braden, R. L.; Christman, K. L. *Adv. Mater.* **2013**, *25*, 2937-2942.
73. Mukherjee, S.; Hill, M. R.; Sumerlin, B. S. *Soft Matter* **2015**, *11*, 6152-6161.
74. Lin, F.; Yu, J.; Tang, W.; Zheng, J.; Defante, A.; Guo, K.; Wesdemiotis, C.; Becker, M. L. *Biomacromolecules* **2013**, *14*, 3749-58.
75. Sershen, S.; West, J. *Adv. Drug Del. Rev.* **2003**, *55*, 439-439.
76. West, J. L.; Hubbell, J. A. *Macromolecules* **1999**, *32*, 241-244.
77. Hsu, C. W.; Olabisi, R. M.; Olmsted-Davis, E. A.; Davis, A. R.; West, J. L. *J. Biomed. Mater. Res. A* **2011**, *98a*, 53-62.
78. van Dijk, M.; van Nostrum, C. F.; Hennink, W. E.; Rijkers, D. T. S.; Liskamp, R. M. J. *Biomacromolecules* **2010**, *11*, 1608-1614.
79. Oh, J. K.; Drumright, R.; Siegwart, D. J.; Matyjaszewski, K. *Prog. Polym. Sci.* **2008**, *33*, 448-477.
80. Kabanov, A. V.; Vinogradov, S. V. *Angew. Chem. Int. Ed.* **2009**, *48*, 5418-5429.

81. Zhang, X. J.; Malhotra, S.; Molina, M.; Haag, R. *Chem. Soc. Rev.* **2015**, *44*, 1948-1973.
82. Mavila, S.; Eivgi, O.; Berkovich, I.; Lemcoff, N. G. *Chem. Rev.* **2016**, *116*, 878-961.
83. Wu, H. Q.; Wang, C. C. *Langmuir* **2016**, *32*, 6211-6225.
84. Akiyoshi, K.; Deguchi, S.; Moriguchi, N.; Yamaguchi, S.; Sunamoto, J. *Macromolecules* **1993**, *26*, 3062-3068.
85. Vinogradov, S.; Batrakova, E.; Kabanov, A. *Colloids Surf., B* **1999**, *16*, 291-304.
86. Oh, J. K.; Lee, D. I.; Park, J. M. *Prog. Polym. Sci.* **2009**, *34*, 1261-1282.
87. Jiskoot, W.; Randolph, T. W.; Volkin, D. B.; Middaugh, C. R.; Schoneich, C.; Winter, G.; Friess, W.; Crommelin, D. J. A.; Carpenter, J. F. *J. Pharm. Sci.* **2012**, *101*, 946-954.
88. Abuchowski, A.; Vanes, T.; Palczuk, N. C.; Davis, F. F. *J. Biol. Chem.* **1977**, *252*, 3578-3581.
89. Abuchowski, A.; Mccoy, J. R.; Palczuk, N. C.; Vanes, T.; Davis, F. F. *J. Biol. Chem.* **1977**, *252*, 3582-3586.
90. Caliceti, P.; Veronese, F. M. *Adv. Drug Del. Rev.* **2003**, *55*, 1261-1277.
91. Haag, R.; Kratz, F. *Angew. Chem. Int. Ed.* **2006**, *45*, 1198-1215.
92. Vermonden, T.; Censi, R.; Hennink, W. E. *Chem. Rev.* **2012**, *112*, 2853-2888.
93. Censi, R.; Di Martino, P.; Vermonden, T.; Hennink, W. E. *J. Control. Release* **2012**, *161*, 680-692.

94. Yoshimatsu, K.; Lesel, B. K.; Yonamine, Y.; Beierle, J. M.; Hoshino, Y.; Shea, K. *J. Angew. Chem. Int. Ed.* **2012**, *51*, 2405-2408.
95. Averick, S. E.; Magenau, A. J. D.; Simakova, A.; Woodman, B. F.; Seong, A.; Mehl, R. A.; Matyjaszewski, K. *Polym. Chem.* **2011**, *2*, 1476-1478.
96. Molina, M.; Asadian-Birjand, M.; Balach, J.; Bergueiro, J.; Miceli, E.; Calderon, M. *Chem. Soc. Rev.* **2015**, *44*, 6161-6186.
97. Nair, L. S.; Laurencin, C. T. *Prog. Polym. Sci.* **2007**, *32*, 762-798.
98. Ulery, B. D.; Nair, L. S.; Laurencin, C. T. *J. Polym. Sci. Part B Polym. Phys.* **2011**, *49*, 832-864.
99. Nicolas, J.; Mura, S.; Brambilla, D.; Mackiewicz, N.; Couvreur, P. *Chem. Soc. Rev.* **2013**, *42*, 1147-1235.
100. Kharkar, P. M.; Kiick, K. L.; Kloxin, A. M. *Chem. Soc. Rev.* **2013**, *42*, 7335-7372.
101. Tomatsu, I.; Peng, K.; Kros, A. *Adv. Drug Del. Rev.* **2011**, *63*, 1257-1266.
102. Kloxin, A. M.; Kasko, A. M.; Salinas, C. N.; Anseth, K. S. *Science* **2009**, *324*, 59-63.
103. Murthy, N.; Xu, M. C.; Schuck, S.; Kunisawa, J.; Shastri, N.; Frechet, J. M. J. *Proc. Natl. Acad. Sci. U. S. A.* **2003**, *100*, 4995-5000.
104. Kwon, Y. J.; Standley, S. M.; Goh, S. L.; Frechet, J. M. J. *J. Control. Release* **2005**, *105*, 199-212.
105. Kwon, Y. J.; Standley, S. M.; Goodwin, A. P.; Gillies, E. R.; Frechet, J. M. J. *Mol. Pharm.* **2005**, *2*, 83-91.

106. Goh, S. L.; Murthy, N.; Xu, M. C.; Frechet, J. M. J. *Bioconjugate Chem.* **2004**, *15*, 467-474.
107. Steinhilber, D.; Witting, M.; Zhang, X. J.; Staegemann, M.; Paulus, F.; Friess, W.; Kuchler, S.; Haag, R. *J. Control. Release* **2013**, *169*, 289-295.
108. Murray, B. S.; Fulton, D. A. *Macromolecules* **2011**, *44*, 7242-7252.
109. Murray, B. S.; Jackson, A. W.; Mahon, C. S.; Fulton, D. A. *Chem. Commun.* **2010**, *46*, 8651-8653.
110. Whitaker, D. E.; Mahon, C. S.; Fulton, D. A. *Angew. Chem. Int. Ed.* **2013**, *52*, 956-959.
111. Zhang, X. J.; Achazi, K.; Steinhilber, D.; Kratz, F.; Dervedde, J.; Haag, R. *J. Control. Release* **2014**, *174*, 209-216.
112. Jackson, A. W.; Stakes, C.; Fulton, D. A. *Polym. Chem.* **2011**, *2*, 2500-2511.
113. Tan, H.; Jin, H. Q.; Mei, H. C.; Zhu, L. J.; Wei, W.; Wang, Q.; Liang, F. X.; Zhang, C. L.; Li, J. L.; Qu, X. Z.; Shanguan, D. H.; Huang, Y. N.; Yang, Z. Z. *Soft Matter* **2012**, *8*, 2644-2650.
114. Cheng, R.; Feng, F.; Meng, F. H.; Deng, C.; Feijen, J.; Zhong, Z. Y. *J. Control. Release* **2011**, *152*, 2-12.
115. Balendiran, G. K.; Dabur, R.; Fraser, D. *Cell Biochem. Funct.* **2004**, *22*, 343-352.
116. Oh, J. K.; Tang, C. B.; Gao, H. F.; Tsarevsky, N. V.; Matyjaszewski, K. *J. Am. Chem. Soc.* **2006**, *128*, 5578-5584.
117. Oh, J. K.; Siegwart, D. J.; Lee, H. I.; Sherwood, G.; Peteanu, L.; Hollinger, J. O.; Kataoka, K.; Matyjaszewski, K. *J. Am. Chem. Soc.* **2007**, *129*, 5939-5945.

118. Ghosh, S.; Basu, S.; Thayumanavan, S. *Macromolecules* **2006**, *39*, 5595-5597.
119. Ryu, J. H.; Jiwanich, S.; Chacko, R.; Bickerton, S.; Thayumanavan, S. *J. Am. Chem. Soc.* **2010**, *132*, 8246-8247.
120. Ryu, J. H.; Chacko, R. T.; Jiwanich, S.; Bickerton, S.; Babu, R. P.; Thayumanavan, S. *J. Am. Chem. Soc.* **2010**, *132*, 17227-17235.
121. Li, L. Y.; Raghupathi, K.; Yuan, C. H.; Thayumanavan, S. *Chem. Sci.* **2013**, *4*, 3654-3660.
122. Matsumoto, N. M.; Gonzalez-Toro, D. C.; Chacko, R. T.; Maynard, H. D.; Thayumanavan, S. *Polym. Chem.* **2013**, *4*, 2464-2469.
123. Ventura, J.; Eron, S. J.; Gonzalez-Toro, D. C.; Raghupathi, K.; Wang, F.; Hardy, J. A.; Thayumanavan, S. *Biomacromolecules* **2015**, *16*, 3161-3171.
124. Jackson, A. W.; Fulton, D. A. *Macromolecules* **2012**, *45*, 2699-2708.
125. Duong, H. T. T.; Marquis, C. P.; Whittaker, M.; Davis, T. P.; Boyer, C. *Macromolecules* **2011**, *44*, 8008-8019.
126. Klan, P.; Solomek, T.; Bochet, C. G.; Blanc, A.; Givens, R.; Rubina, M.; Popik, V.; Kostikov, A.; Wirz, J. *Chem. Rev.* **2013**, *113*, 119-191.
127. Azagarsamy, M. A.; Alge, D. L.; Radhakrishnan, S. J.; Tibbitt, M. W.; Anseth, K. S. *Biomacromolecules* **2012**, *13*, 2219-2224.
128. Klinger, D.; Landfester, K. *Macromolecules* **2011**, *44*, 9758-9772.
129. Maier, M.; Kotman, N.; Friedrichs, C.; Andrieu, J.; Wagner, M.; Graf, R.; Strauss, W. S. L.; Mailander, V.; Weiss, C. K.; Landfester, K. *Macromolecules* **2011**, *44*, 6258-6267.

130. Fuchs, A. V.; Kotman, N.; Andrieu, J.; Mailander, V.; Weiss, C. K.; Landfester, K. *Nanoscale* **2013**, *5*, 4829-4839.
131. Klinger, D.; Aschenbrenner, E. M.; Weiss, C. K.; Landfester, K. *Polym. Chem.* **2012**, *3*, 204-216.
132. Wang, Y. C.; Wu, J.; Li, Y.; Du, J. Z.; Yuan, Y. Y.; Wang, J. *Chem. Commun.* **2010**, *46*, 3520-3522.
133. Xiong, M. H.; Li, Y. J.; Bao, Y.; Yang, X. Z.; Hu, B.; Wang, J. *Adv. Mater.* **2012**, *24*, 6175-6180.

Chapter 2

Imine Hydrogels with Tunable Degradability[†]

2. 1. Introduction

Hydrogels are a common scaffold for tissue engineering due to their biocompatibility and tunable mechanical properties.^{1,2} Scaffolds are commonly prepared from synthetic materials as they allow for more precise control over gel properties and circumvent the problems associated with natural materials such as immune response and batch-to-batch variability.³ Many types of hydrogels have been designed to mimic the extracellular matrix (ECM), which provides a complex environment for cells.⁴⁻⁸ The ECM contains various biofactors that serve as cellular cues and is comprised of glycans and fibrous proteins that provide dynamic structural support.^{9,10} Controlling gel stiffness, elasticity and degradability are therefore important factors in designing synthetic dynamic scaffolds. Cell spreading and mobility, as observed in the ECM, can be achieved in synthetic scaffolds by incorporating integrin-binding peptide sequences, such as RGD, and incorporating hydrolytically degradable cross-links into the hydrogel.^{3,11} Many current hydrogel systems provide cells with a rigid environment that may not allow for cell migration and proper interaction with cellular and biophysical cues.¹² By introducing reversible cross-links that allow for self-healing and selective degradation, synthetic hydrogels can become more dynamic in order to more closely resemble the complex structure of the ECM.

Click chemistry is one of the most widely used methods to easily and rapidly form hydrogels. While numerous click chemistries have been applied to hydrogel formation such as Michael addition, focusing on biocompatible reactions that occur readily at physiological conditions eliminates risks such as cell toxicity and undesirable side

products.¹³⁻¹⁵ Oxime and hydrazone formation are two examples of reversible, biocompatible click reactions. Both reactions are ideal for tissue engineering applications since they occur readily at physiological pH and produce water as the only byproduct.

It has been shown by our group and others that oxime bonds form stable, biocompatible hydrogels *in vitro*.^{16,17} We have previously demonstrated that oxime chemistry can be successfully employed to create stable, bioactive hydrogels using 8-arm aminoxy poly(ethylene glycol) (PEG) and glutaraldehyde. Oxime bond formation was pH dependent, which therefore allowed for control of the time to hydrogel formation by adjusting pH. While oximes are reported to degrade via hydrolysis at decreased pH values, this degradation does not occur readily at pH values compatible with cell culture. Degradability could be incorporated through the use of enzyme-sensitive peptide cross-linkers or polymers, although this can add synthetic complexities, or through the introduction of less stable imine cross-links, such as hydrazone bonds.^{18,19} Imine cross-linked hydrogels are known to exhibit stimuli-responsive and self-healing properties due to bond reversibility,^{20,21} which make them ideal systems for a number of potential clinical applications, such as drug delivery and tissue engineering.²²⁻²⁵

Anseth and coworkers recently reported rapid formation of PEG-based hydrogels via hydrazone bonds for cell culture.^{12,26,27} Hydrazone chemistry has also been applied to other hydrogel systems, such as poly(N-isopropylacrylamide) hydrogels. Patenaude and coworkers determined that hydrazone cross-links were the weakest points in these gels, indicating that this is where degradation would occur most readily.²⁸⁻³⁰ The reversibility of

hydrazone bonds in hydrogels has also been probed by Deng and coworkers, who functionalized poly(ethylene oxide) with a hydrazide group to form hydrazone hydrogels. They observed that gelation can be reversed below pH 4.³¹ In different systems, it has been reported that cells are able to degrade, and even prevent formation of hydrazone-linked hyaluronic acid and alginate-based hydrogels.³²

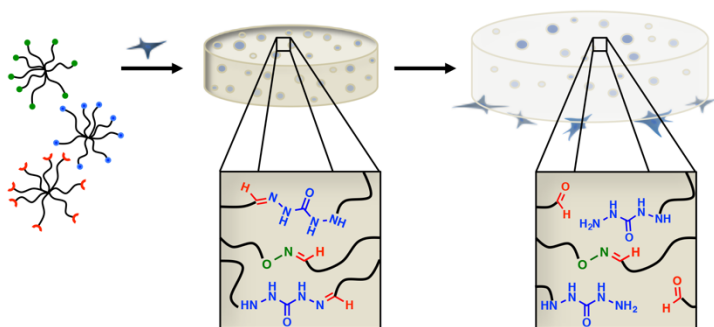


Figure 2.1. Hydrogels can be formed through the incorporation of two types of imine cross-links: hydrazones and oximes.

Oxime and hydrazone bonds form from the reaction between carbonyl groups and an aminoxy or hydrazide group, respectively,^{33,34} and we hypothesized that the mutual reactivity towards carbonyl groups allows these reactions to be used concomitantly to tune degradability in hydrogels. In this paper, we describe a PEG-based hydrogel system that combines oxime and hydrazone chemistries to form hydrogels with tunable degradability and mechanical properties (Figure 2.1). PEG was strategically used as the polymer scaffold due to its biocompatibility and ease of functionalization.³⁵ PEG was functionalized to contain two different hydrazide groups, adipohydrazide and carbodihydrazide, capable of

reacting with aldehyde-functionalized PEG in order to generate hydrazone hydrogels with different degradation rates. Because of the potential of hydrazone bonds to reverse, we chose to use an aldehyde functionalized PEG instead of glutaraldehyde, which is known to be cytotoxic at low millimolar concentrations.³⁶ In addition, PEG was modified with an aminoxy group to incorporate oxime chemistry into the hydrogel to further control gel degradation rates for *in vitro* applications.

2.2. Results and Discussion

Both the aldehyde and amine containing components necessary for imine hydrogel formation were prepared from 8-arm PEG (MW 20,000 Da). Two different hydrazide polymers were synthesized via EDC-coupling of 8-arm PEG-COOH with either adipohydrazide and carbodihydrazide.²⁹ These reactions yielded PEG-adipohydrazide (PEG-ADH) and PEG-carbodihydrazide (PEG-CDH) with 99% and 80% end group conversion, respectively (Figures 2.9-2.10). The 8-arm PEG-aldehyde (PEG-CHO), was made via a Williamson ether synthesis using 8-arm PEG-OH and 2-bromo-1,1-diethoxyethane to yield a protected aldehyde with average end group conversion of 90% in 50% yield (Figure 2.11). The acetal was cleaved by stirring the polymer solution in pH 2 phosphate buffer at 60°C for 18 hours in 60% yield with 85% end group conversion (Figure 2.12).³⁷ The stability of PEG-acetal allowed for prolonged storage of the polymer prior deprotection to PEG-aldehyde. Several direct oxidations were attempted as alternative synthesis routes, including PCC and Moffatt oxidation. These approaches resulted in low conversion rates and resulting aldehydes were more difficult to store.

Aminoxy-functionalized PEG (PEG-AO) was prepared via a Mitsunobu reaction with *N*-hydroxyphthalimide, followed by reaction with hydrazine to yield PEG-AO with 94% end-group conversion in 58% overall isolated yield (Figures 2.13- 2.14).¹⁶

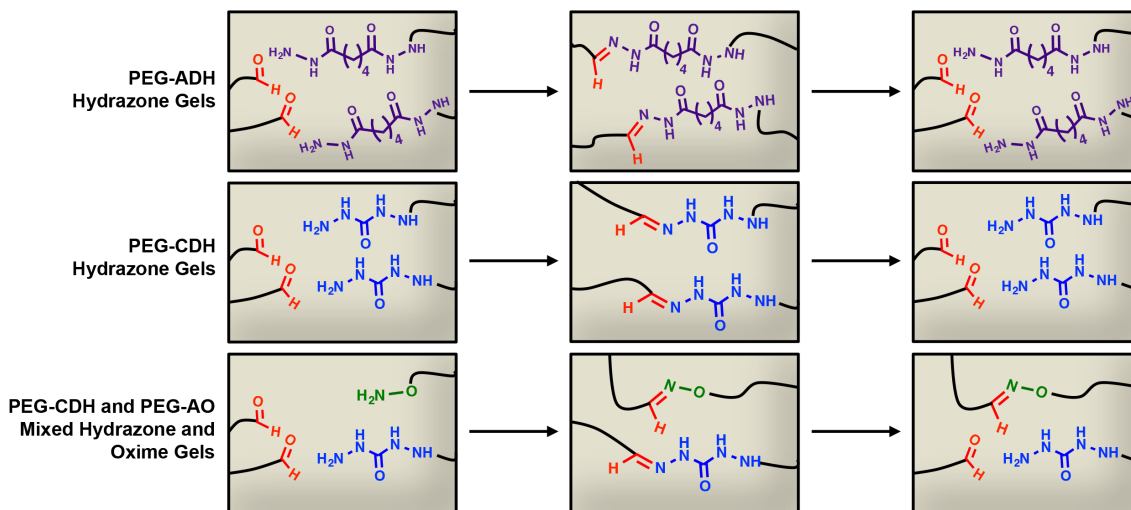


Figure 2.2. PEG-CHO can react with PEG-ADH and PEG-CDH to form degradable hydrogels via reversible hydrazone cross-links and can also react with PEG-AO to form non-reversible oxime bonds to stabilize the hydrazone gels.

We planned to form hydrogels by mixing equal parts hydrazide and/or aminoxy-functionalized PEG in phosphate buffer to form a hydrogel with hydrazone and/or oxime cross-links (Figure 2.2). Because we had previously explored hydrogels formed by oxime chemistry,¹⁶ initial experiments focused on the hydrazide only gels. Hydrogels consisting of PEG-ADH and PEG-CHO components (1:1 ratio) were studied to determine the optimal pH and wt.%. We carried out hydrazone gel formation experiments at increasing pH levels

to determine effects on gelation time. Gel components (5.0 wt.% PEG-ADH and PEG-CHO) were mixed together in phosphate buffer ranging from pH 5-7, and it was observed that all gels formed within five minutes. Since oxime formation slows down significantly around pH 7.0,¹⁶ we chose to continue our experiments with phosphate buffer pH 5.5 to allow for efficient oxime and hydrazone bond formation.³⁸ We tested several different polymer concentrations and chose 3.5 wt.% and 5 wt.% PEG, which had optimal gelation rates and physical properties. At these concentrations, gels formed within 60 seconds at pH 5.5, which allowed for easy pipetting of gel solutions. Rheological characterization of PEG-ADH gels revealed that decreasing the total polymer concentration or changing the ratio of hydrazide to aldehyde groups lowers the storage modulus (Figure 2.16).

To confirm that the hydrogels formed through hydrazone bonds and not as a result of electrostatic interactions, we performed a model study to analyze bond formation by NMR. Adipohydrazide and propionaldehyde were mixed in water, and the resulting product was analyzed by ¹H and ¹³C NMR to monitor hydrazone bond formation (Figure 2.17). Propionaldehyde, which has the same structure as the end group of PEG-CHO, can react with adipohydrazide without cross-linking, allowing for straightforward monitoring of bond formation. The appearance of the hydrazone peaks between 7.43-7.28 ppm (¹H NMR) and 151.4-148.1 ppm (¹³C NMR) indicated hydrazone bond formation. The mechanism is expected to be the same for the PEG-based hydrogel system.

An advantage of utilizing hydrazone chemistry is that the bonds are reversible and can break, then re-form again.³⁹ To test this in our system, two different hydrogels containing different colored dyes were first physically cut in half, and the halves of the two

gels were swapped and placed together. Within ten minutes the dangling hydrazide and aldehyde groups reacted to re-form a single, uniform gel (Figure 2.3). After the gel re-formed, the blue dye took on a green color, indicating the two dyes were able to come into contact and mix throughout the gel, further indicating the two gel halves re-formed into one gel. A higher concentration of yellow dye than blue dye was added to the initial gel solutions in order to create a vivid color, which most likely accounts for the observed color change from blue to a teal in the re-healed gels. Since hydrazone bonds are the weakest link in the gel, it is expected that these bonds are broken most easily upon physical cutting, and this provides evidence that the bonds can re-form.³⁹ It should be noted that gels containing oxime bonds did not show the same re-healing, likely because these bonds are not readily reversible.

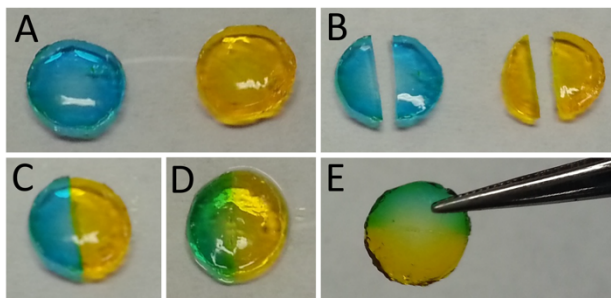


Figure 2.3. 5.0 wt.% PEG hydrazone hydrogels (40 μ L, approximately 1 cm in diameter and 1 mm in height) dyed with food coloring shown during self-healing. PEG-ADH hydrogels formed within one minute (A) and were cut in half (B). The opposite halves were placed next to each other (C), and after ten minutes, bonds re-formed (D). After fifteen minutes, the two pieces formed one complete gel that can readily be handled (E).

Next, hydrogel swelling in various conditions (e.g. buffer, culture medium) was investigated to analyze the differences between PEG-ADH and PEG-CDH gels (Figure 2.4). Both PEG-ADH and PEG-CDH containing gels were stable up to at least six days in pH 5.5 phosphate buffer, indicating that both hydrogels had reached equilibrium and did not swell further in aqueous conditions. In DMEM lacking fetal bovine serum (DMEM (-) FBS), PEG-ADH gels exhibited a significant increase in swelling and fully degraded after five days. However, in DMEM with 10% FBS, PEG-ADH based gels swelled rapidly over two days before dissolving completely (Figure 2.4A). Enzymes present in fetal bovine serum or amines from proteins or peptides could be responsible for the degradation observed for PEG-ADH gels. PEG-CDH based gels, on the other hand, remained intact and exhibited minimal swelling whether in buffer, DMEM (-) FBS, or (+) FBS, indicative of greater bond stability (Figure 2.4). This is expected since it has been shown that changing the structure of the dihydrazide group used as a cross-linker can affect hydrazone bond stability by increasing resonance stabilization by shortening the carbon chain between hydrazide groups.⁴⁰

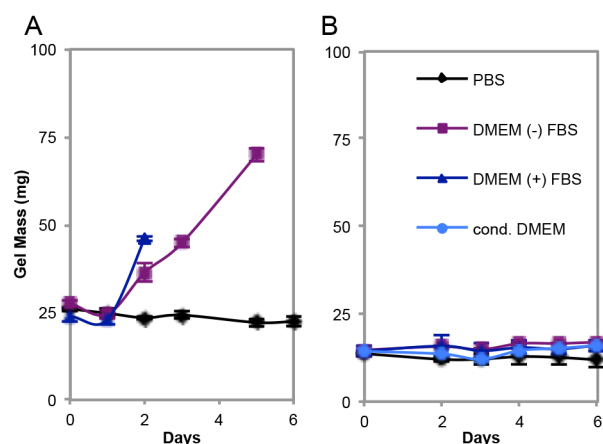


Figure 2.4. Swelling of 5.0 wt.% PEG-ADH (A) and 5.0 wt.% PEG-CDH (B) based hydrogels. 40 μ L gels were placed in respective solutions, and PEG-ADH gels degraded after five days in DMEM (-) FBS and after two days in DMEM (+) FBS. PEG-CDH gels retained constant masses throughout the experiment for all conditions, including cell conditioned DMEM.

To further analyze the difference in time of degradation of our PEG-ADH and PEG-CDH hydrogels, an NMR study was designed to determine the extent to which the two different hydrazone bonds can be reversed in the presence of a nucleophile (Figure 2.5). CDH and ADH hydrazones were formed by reacting each hydrazide group with one equivalent of propionaldehyde. Hydroxylamine was chosen as the nucleophile in this case to match our mixed hydrazone/oxime gel system. After the addition of hydroxylamine to CDH hydrazone, approximately 60% of hydrazone bonds were replaced by oxime bonds after 30 minutes (Figure 2.5A), which can be seen by the appearance of two new imine

peaks at 7.37 and 6.70 ppm corresponding to propionaldehyde oxime (E and Z),⁴¹ and a decrease in peak height corresponding to the hydrazone proton. In comparison, 90% of hydrazone bonds were replaced upon the addition of hydroxylamine to ADH hydrazone (Figure 2.5B) after 30 minutes. In this case, the hydrazone protons at 7.42 and 7.28 ppm are replaced almost entirely by oxime protons at 7.35 and 6.69 ppm. The same ratios of hydrazone to oxime remained constant up to at least 12 hours for both CDH and ADH compounds, suggesting equilibrium is reached. CDH hydrazone was displaced to a lesser extent by hydroxylamine than ADH hydrazone, further indicating that CDH hydrazone bonds are more stable than ADH hydrazones and can help explain why PEG-ADH gels may have degraded in the presence of DMEM, due to amines or other nucleophilic compounds, whereas PEG-CDH gels remained stable.

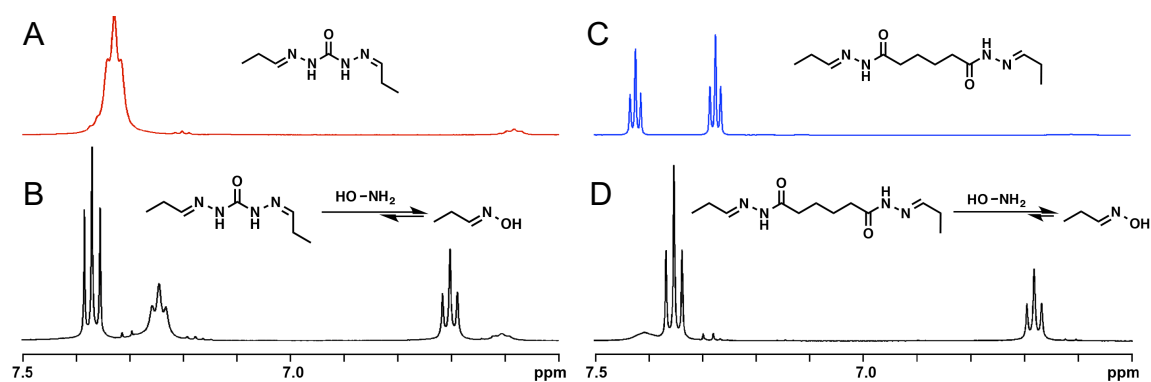


Figure 2.5. ¹H NMR of CDH hydrazone (A) after adding one equivalent of hydroxylamine per hydrazone bond (B), and ¹H NMR of ADH hydrazone (C) after adding one equivalent hydroxylamine per hydrazone bond (D).

Next, the stability of the gels was tested in the presence of mouse mesenchymal stem cells (mMSCs). To anchor cells inside the gel, a commonly used integrin-binding peptide sequence, arginine-glycine-aspartic acid (RGD), was synthesized using standard fmoc solid phase synthesis (Figure 2.18).⁴²⁻⁴⁴ We chose to incorporate a synthetic peptide instead of a natural material, such as collagen, to retain a simple and fully synthetic system. A hydroxylamine, (Boc-aminoxy) acetic acid, was incorporated into the peptide sequence (AO-RGD) at the N-terminus to allow for coupling to PEG-CHO via stable oxime bonds. Covalent attachment of the peptide to PEG-CHO was assessed using rheology to analyze the difference in storage modulus of PEG-CDH gels containing 0, 0.1, or 1 mM AO-RGD (Figure 2.6), which are well within the RGD concentration range (25 μ M – 3.5 mM) reported to support cell spreading in PEG-based hydrogels.⁴⁵⁻⁴⁸ For gels containing 1.0 mM RGD, the ratio of aldehyde functional groups to AO-RGD is 9.96:1. Indeed, it was observed that gels prepared with AO-RGD exhibited lower storage moduli than gels containing no RGD, indicating cross-linking sites of PEG-CHO were taken up by the peptide. We chose to continue with gels containing no more than 1 mM RGD to ensure PEG-CHO would retain enough free aldehyde groups to cross-link after reacting with the peptide and that the resulting hydrogels would be stiff enough to handle. To ensure oxime bond formation between AO-RGD (0.5 mM) and PEG-CHO, the peptide and polymer were incubated at 37 °C for 3 hours prior to use in cell encapsulation studies. Gels (5 μ L total volume) were prepared by mixing PEG components and cells together in sterile pH 5.5 phosphate buffer. The resulting gels were then placed in 100 μ L media in a 96-well plate and incubated at 37 °C. The wells were inspected via light microscope daily. Upon

degradation, gels were no longer observed in the wells and previously encapsulated cells were found spread on the bottom of the well. PEG-ADH gels were observed to degrade more rapidly than without cells, within 24 hours, whether 3,500 or 5,000 cells/ μL initial cells were added. Interestingly, PEG-CDH gels, which were stable in DMEM in the absence of cells, degraded between 4-5 days at 5,000 cells/ μL density, which led us to hypothesize that cells may play a role in the degradation process (Figure 2.20A-B).

To further understand the degradation mechanism, PEG-CDH gels were incubated in cell (mMSC) conditioned DMEM without cells; in this case, the gels were completely stable up to at least 6 days (Figure 2.4B). We believe there are several possible explanations for the observed increased degradation rate in the presence of cells, including that the cells mechanically break the hydrazone bonds or that the mesh size of the gels is altered in the presence of the cells, allowing for more rapid hydrolysis. Because cell-secreted enzyme concentrations are much lower in solution than at the cell-substrate interface,⁴⁹ we cannot entirely rule out that secreted proteins or other molecules do not cause degradation from this experiment, especially since it has been reported that enzymes released from the cells can affect hydrazone bond stability.⁵⁰

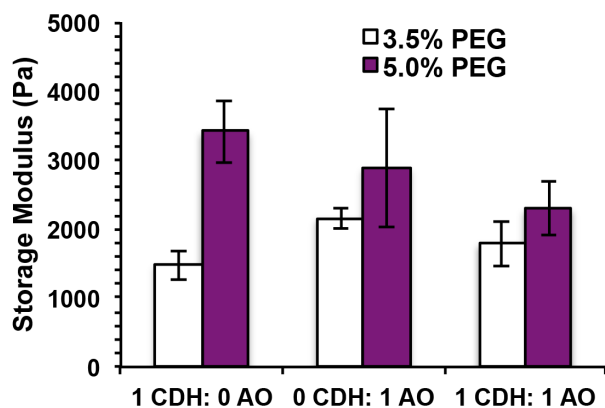


Figure 2.6. Rheological characterization of hydrazone and oxime hydrogels. Storage modulus can be controlled by changing total polymer concentration and amounts of hydrazone and oxime cross-links. Data is displayed as the average and standard deviation of three independent hydrogels for each condition.

In order to tune the degradation rate of our hydrazone gels further, we incorporated oxime chemistry since these bonds do not reverse even when cells are present.¹⁶ Because PEG-ADH gels degraded so quickly, the rest of the experiments were conducted with the more stable PEG-CDH partner only. Gel solutions containing 3:1:4, 2:2:4, and 1:3:4 parts PEG-CDH: PEG-AO: PEG-CHO were mixed and rapidly formed 3.5 wt.% overall PEG hydrogels. When the same solutions were mixed without PEG-CDH (so the gel solutions contained 1:4, 2:4 and 3:4 parts PEG-AO: PEG-CHO) only the 3:4 gel solution resulted in a gel. This indicates that PEG-CDH is participating in cross-linking in the mixed gels. Rheology was used to assess the stiffness of the mixed gels at 3.5 wt.% and 5 wt.% PEG gels (Figure 2.6). For each condition, the combined amount of PEG-AO and PEG-CDH

was equal to the total amount of PEG-CHO, and gels containing only hydrazone bonds, only oxime bonds, or a 1:1 mixture of hydrazone and oxime bonds were formed. All 5 wt.% PEG gels exhibited higher storage moduli than the 3.5 wt.% gels, corresponding to the increase in number of cross-links with increasing polymer concentration.

To explore the stabilizing effects of increasing amounts of oxime cross-links in the presence of cells, gels containing 100:0, 75:25, 50:50 and 0:100 hydrazone: oxime bonds were prepared, placed in wells containing media, and examined under a light microscope daily (Figure 2.20). While we had observed that 100:0 hydrazone: oxime gels degrade fully within 5 days, leaving cells at the bottom of the well, 75:25 hydrazone: oxime gels remained intact at day 6 although a change in gel structure is apparent (Figure 2.20D). The gel edges were no longer as defined as they were on day 1, and cells are starting to be released from the gel, allowing them to spread on the well surface (Figure 2.20C-D). Gels containing 50:50 and 0:100 hydrazone: oxime bonds did not show any degradation and cells remained encapsulated (Figure 2.20E-H).

To study the viability and spreading of cells in the presence of cells, mMSCs were encapsulated in gels containing PEG-CDH and PEG-AO at various ratios. Hydrogels for cell encapsulation studies were formed by adding mMSCs (in DMEM (+) FBS) to the PEG-CHO/AO-RGD (0.1 mM RGD) solution before the addition of PEG-CDH and/or PEG-AO to result in 3.5 and 5 wt.% PEG gels. Live/dead staining of encapsulated cells at days 1 and 7 showed high viability (> 90%) of cells in all gel conditions, indicating that the imine hydrogels at all ratios are biocompatible with cells (Figure 2.7). Cytotoxicity studies of individual PEG components were also carried out to ensure the polymers are not damaging

to the cells upon gel degradation (Figure 2.15). All polymers (PEG-AO, PEG-CHO, PEG-CDH, and PEG-ADH) were non-cytotoxic to mMSCs up to at least 10 mg/mL, which corresponds to twice the amount of each PEG used per gel in the cell studies.

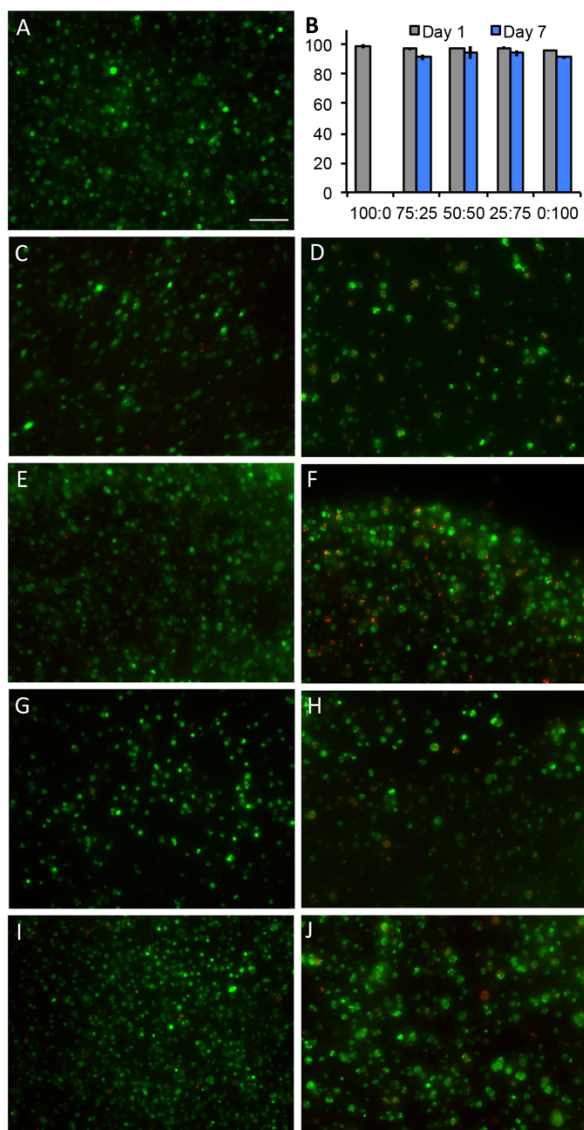


Figure 2.7. Live/dead staining of encapsulated mMSCs. 100:0 hydrazone: oxime gels showed good viability at day 1 (A) but degraded before imaging at day 7. 75:25 hydrazone: oxime gels at day 1 (C) and day 7 (D); 50:50 gels at day 1 (E) and day 7 (F); 25:75 gels at

day 1 (G) and day 7 (H); 0:100 gels at day 1 (I) and day 7 (J). Scale bar = 100 μm . Cell viability of all gel conditions at day 1 and day 7 (B) represented as % live cells per gel (y axis).

Further, the morphology of encapsulated cells in the presence of AO-RGD was investigated. Gels containing 0.1 mM AO-RGD were stained using DAPI/Phalloidin for f-actin after fixing with paraformaldehyde at day 5 (Figure 2.24). mMSCs exhibited rounded morphologies at all hydrazone: oxime ratios, although 100:0 hydrazone: oxime gels were not imaged due to degradation (Figure 2.8A-C). The experiment was repeated using human dermal fibroblasts (HDFs), and again, cells were round with little spreading (Figure 2.24 D-F). In order to image 100:0 hydrazone: oxime gels before degradation, the experiment was repeated and gels were fixed and stained at day 2 (Figure 2.8). This time, AO-RGD concentration was increased to 0.5 mM to determine if increasing RGD affects cell spreading in our gel system. Gels containing 1 mM RGD were also examined (Figure 2.25). Cells maintained similar, rounded morphologies for all tested RGD concentrations. This finding is in contrast to a similar hydrazone cross-linked PEG hydrogel system, but the use of 4-arm PEG instead of 8-arm PEG and hydrazine instead of hydrazide end groups introduce several differences that make cell morphologies in the two systems difficult to compare.²⁷

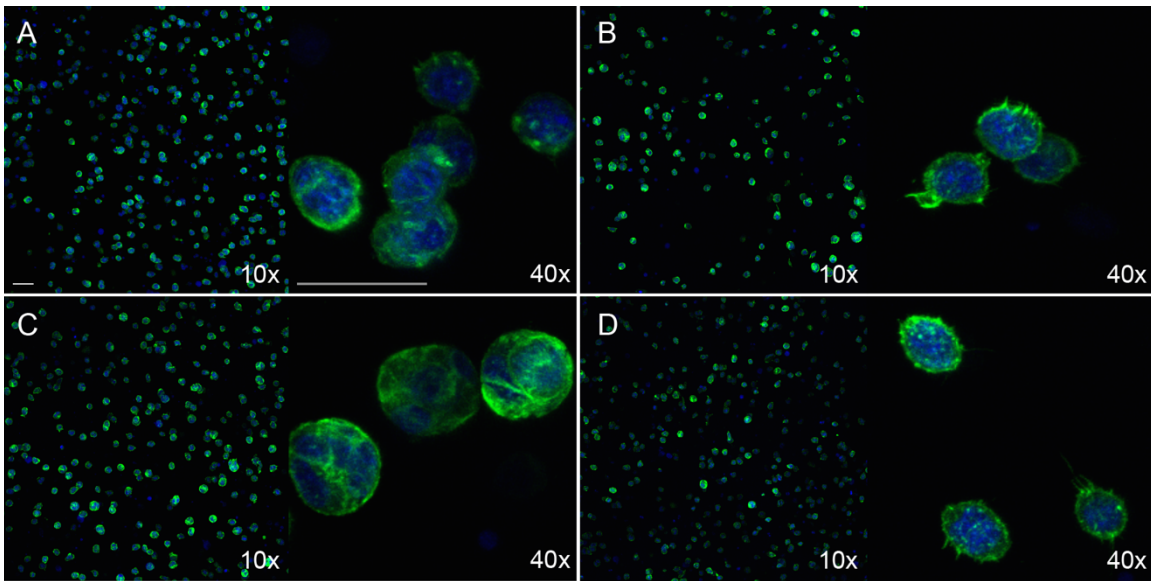


Figure 2.8. DAPI/Phalloidin staining for cell spreading at day 2. mMSCs were encapsulated in 5 wt.% 100:0 hydrazone: oxime (A), 75:25 hydrazone: oxime (B), 50:50 hydrazone: oxime (C), and 0:100 hydrazone: oxime (D) gels containing 0.5 mM AO-RGD. Scale bars = 50 μ m for both 10x and 40x magnification.

With the versatility and tunable design of our imine hydrogels it can be envisioned that the amine component or aldehyde component could be additionally altered to further change the time to degradation in these types of gels. For example, glyoxylamide type carbonyl moieties should degrade more quickly than aldehyde and various hydrazones could be utilized. These gels could then be used in situations where cells or other agents need to be selectively released or, because of the self-healing properties, a mixture of both. In addition, this system could be potentially used not only to encapsulate and deliver cells, but could be used to deliver growth factors or other therapeutic agents. This could be accomplished through simple encapsulation inside the gel or by covalent attachment to the

cross-linked PEG network. Due to the possibility of incorporating such biological compounds and the wide range in stiffness of the hydrogels from 1000-3500 Pa, our current system could potentially be used for vascular or endothelial engineering applications.⁵¹ Since we have shown that increasing the amount of PEG per gel significantly increases gel stiffness, our gel system could be tuned to match the conditions of a wide variety of stiffer tissues, such as muscle, while retaining the ability to tune degradability of the system as needed.

2.3. Conclusions

In this report, a PEG-based imine hydrogel platform that combines the biocompatibility and stability of oxime bonds with the reversibility of hydrazone bonds to create hydrogels with tunable degradation is reported. The ease with which PEG can be functionalized allows for further modification of these gels through modification of hydrazide groups and incorporation of hydroxylamine groups. It was demonstrated that by combining oxime and hydrazone chemistries, the stability of hydrogels could be tuned from less than 24 hours to greater than 7 days. High cell viability in the presence of a covalently bound RGD peptide was observed. The ability to tune the mechanical properties and degradation of these hydrogels as well as to encapsulate cells will allow for this system to be used for research and clinical applications, such as for cell delivery and tissue engineering.

2.4. Experimental

2. 4. 1 Materials and Analytical Techniques

8-arm PEG-OH and 8-arm PEG-COOH were purchased from JenKem Technologies. All other chemicals were purchased from Sigma Aldrich. ^1H NMR and ^{13}C NMR spectroscopy were performed on an Avance DRX 400 MHz or 500 MHz instrument. ESI mass spectra were obtained using a Waters Acquity Premier XE LC-MS.

2. 4. 2 Methods

Synthesis of PEG-Adipohydrazide

8-arm PEG-COOH (400 mg, 0.02 mmol) was dissolved in a minimal amount of pH 5.5 phosphate buffer in a one-neck round bottom flask. Adipohydrazide (1045 mg, 6 mmol) was separately dissolved in a minimal amount of pH 5.5 phosphate buffer before it was added to the PEG-COOH solution. While stirring, EDC (621 mg, 4 mmol) was added to the reaction before adjusting the pH to 4.75 using aqueous HCl. The reaction was stirred 18 hours before neutralizing with aqueous NaOH and dialyzing against water/MeOH for three days. Lyophilization yielded the final, pure PEG-hydrazide product as a white powder (371 mg, 93% yield, 99% conversion). ^1H NMR (400 MHz, D_2O) δ 4.16-4.11 (s, 2H, OCH_2CO), 3.88-3.79 (m, 227H, PEG protons), 2.39-2.21 (t, 4H, $\text{NHCOCH}_2\text{CH}_2$), 1.63-1.49 (t, 4H, $\text{COCH}_2\text{CH}_2\text{CH}_2$) ppm.

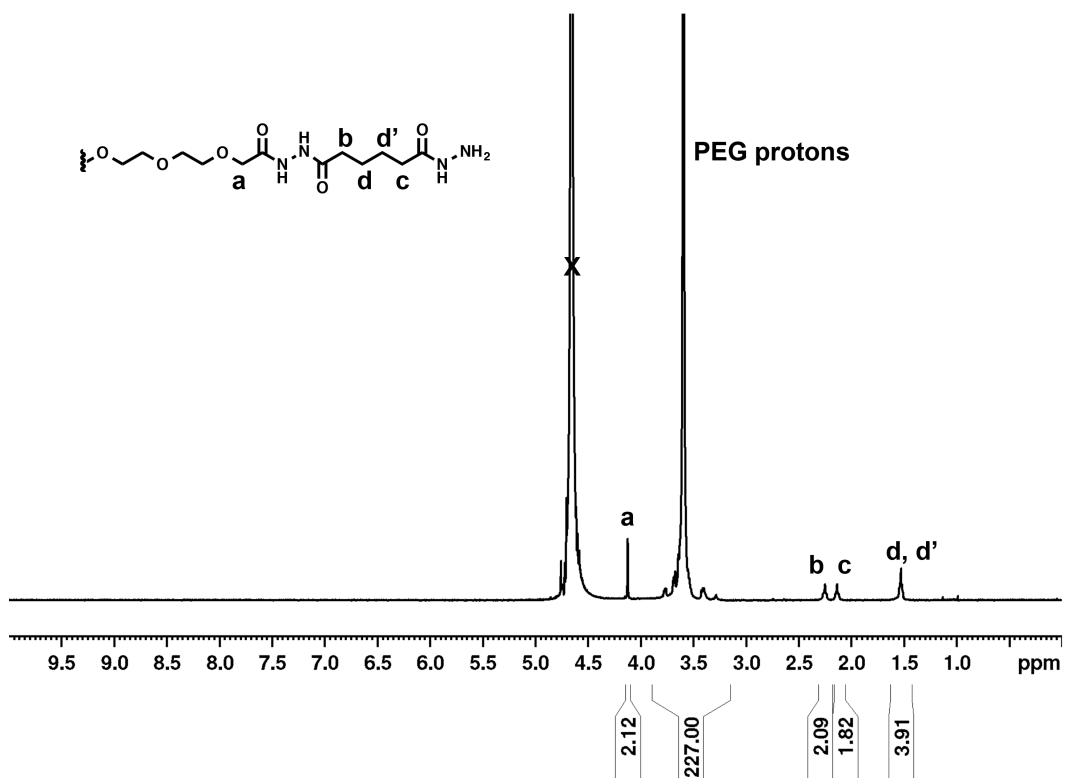


Figure 2.9. ¹H NMR spectrum of PEG-adipohydrazide in D₂O.

Synthesis of PEG-Carbohydrazide

8-arm PEG-COOH (200 mg, 0.01 mmol) was dissolved in pH 5.5 phosphate buffer (10-15 mL) in a one-neck round bottom flask. Carbohydrazide (270 mg, 3 mmol) was separately dissolved in a minimal amount of pH 5.5 phosphate buffer before it was added to the PEG-COOH solution. While stirring, EDC (310 mg, 2 mmol) was added to the reaction before adjusting the pH to 4.75 using aqueous HCl. The reaction was stirred 18 hours before neutralizing with aqueous NaOH and dialyzing against water/MeOH for three days. Lyophilization yielded the final, pure PEG-hydrazide product as a white powder (188 mg,

94% yield, 80% conversion). ^1H NMR (400 MHz, D_2O) δ 4.16-4.11 (s, 2H, OCH_2CO), 3.80-3.77 (m, 227H, PEG protons) ppm.

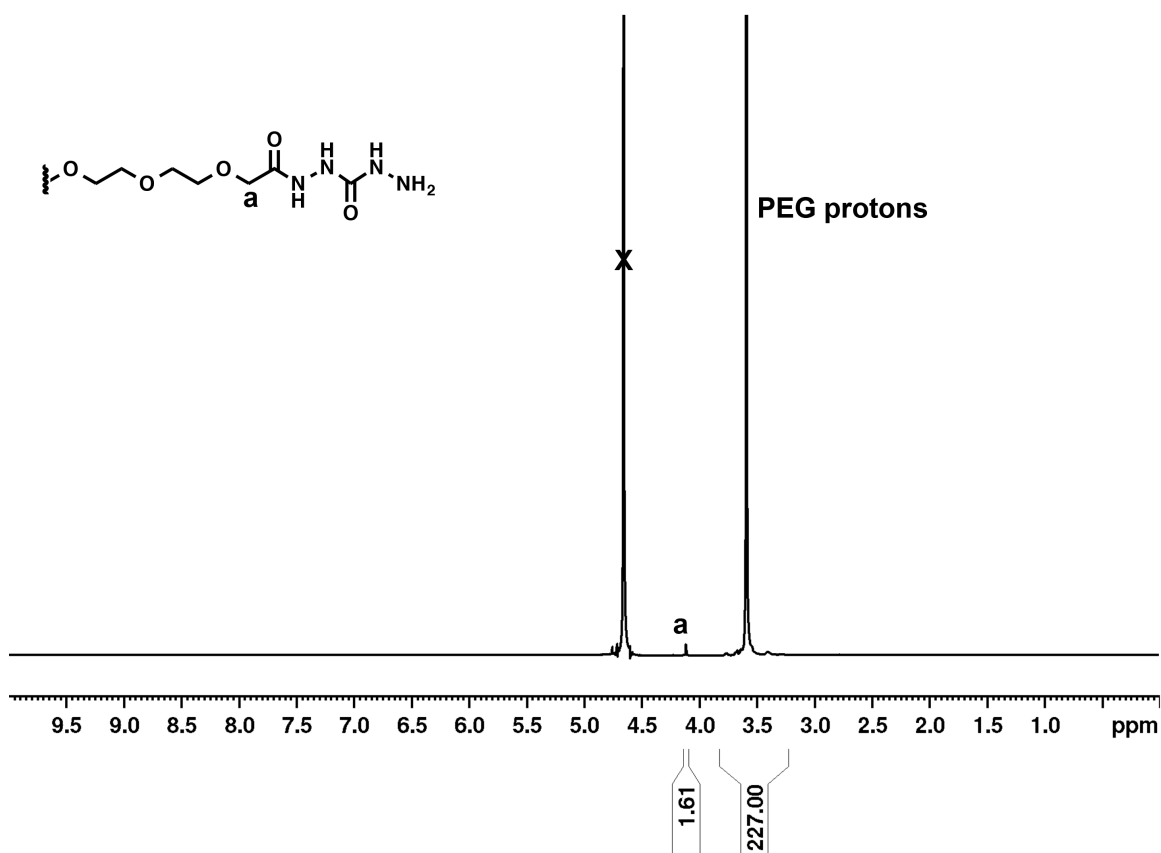


Figure 2.10. ^1H NMR spectrum of PEG-CDH taken in D_2O .

Synthesis of PEG-Acetal

8-arm poly(ethylene glycol) (PEG-OH) (5000 mg, 0.25 mmol) was dissolved in toluene (25 mL) in a two-neck round bottom flask equipped with a Dean Stark trap. After refluxing for twelve hours, the reaction was cooled to 24 °C and NaOH (6733 mg, 120 mmol) and 2-bromo-1,1-diethoxyethane (4600 μL , 30 mmol) were added under argon. The reaction

was refluxed under argon at 130 °C for 48 hours before neutralizing with concentrated HCl. The product was extracted with methylene chloride followed by precipitation into diethyl ether to yield PEG-acetal as a white solid (2010 mg, 41% yield, 96% conversion). ¹H NMR (400 MHz, CDCl₃) δ 4.14-4.12 (t, 1H, CH₂CHO₂), 3.83-3.76 (q, 4H, OCH₂CH₃), 3.75-3.43 (m, 227H, PEG protons), 1.39-1.18 (t, 6H, CH₂CH₃) ppm.

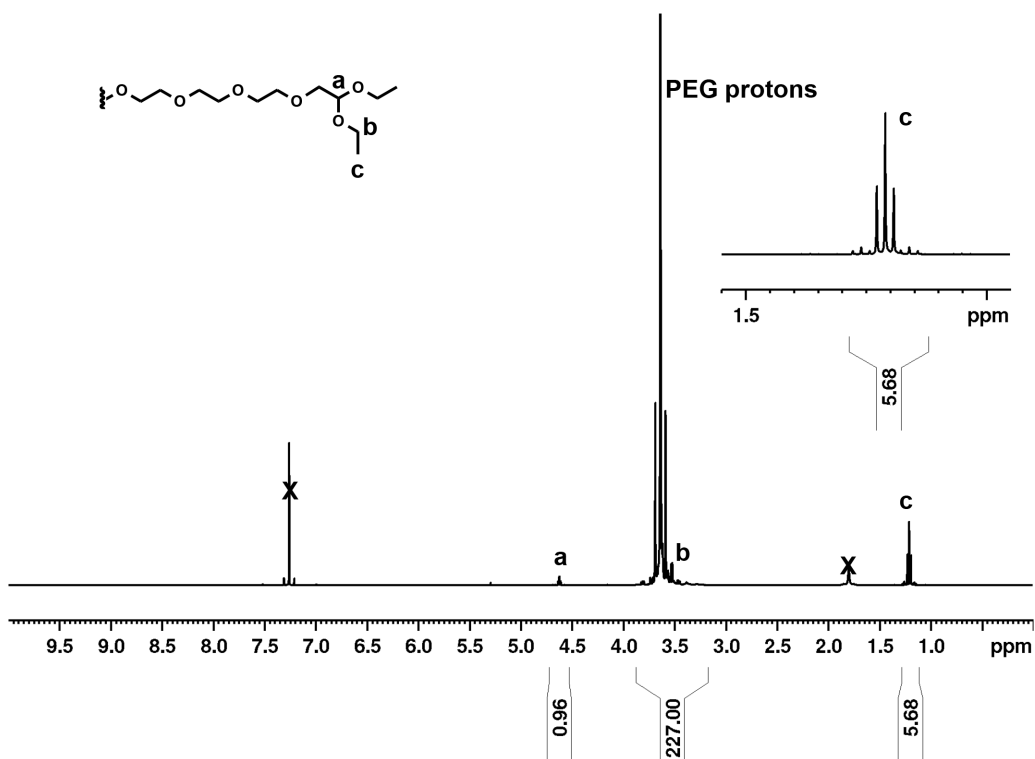


Figure 2.11. ¹H NMR spectrum of PEG-acetal in CDCl₃.

Synthesis of PEG-Aldehyde

Previously synthesized PEG-acetal (122 mg, 0.006 mmol) was dissolved in pH 2 phosphate buffer in a one-neck round bottom flask and stirred at 50 °C for five hours. The polymer

was extracted with methylene chloride after neutralizing with 15% NaHCO₃. Precipitation into ether yielded the desired PEG-aldehyde as a white solid (38.2 mg, 33% yield, 85% conversion). ¹H NMR (400 MHz, CDCl₃) δ 9.76-9.72 (s, 1H, CHO), 4.31-4.22 (s, 2H, CH₂CHO) 3.75-3.61 (m, 227H, PEG protons) ppm.

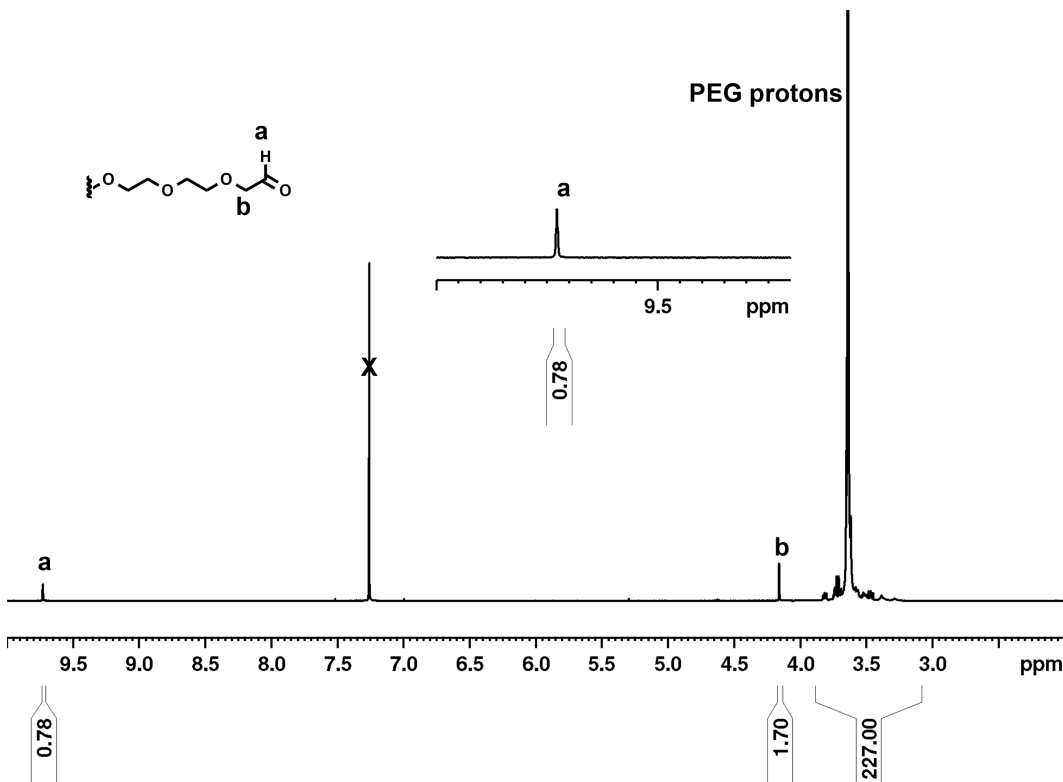


Figure 2.12. ¹H NMR spectrum of PEG-aldehyde in CDCl₃.

Synthesis of PEG-Hydroxyphthalimide

8-arm PEG-OH (500 mg, 0.025 mmol) was dissolved in anhydrous dichloromethane (10 mL) in a two-neck round bottom flask under argon. N-hydroxyphthalimide (65.25 mg, 0.40 mmol) and triphenylphosphine (104.92 mg, 0.40 mmol) were added to the solution. The

reaction was cooled to 0 °C before adding diisopropyl azodicarboxylate (70.88 μL , 0.36 mmol) dropwise. The reaction was warmed to 23 °C and stirred for 18 hours under argon. The resulting PEG-hydroxyphthalimide was purified by precipitating in ether three times to yield the desired product as a white-yellow solid (276 mg, 55% yield, 94% conversion). ^1H NMR (500 MHz, CDCl_3) δ 7.82-7.80 (m, 2H, aromatic Hs, CCHCH), 7.74 (m, 2H, aromatic Hs, CCHCH), 4.37-4.34 (t, 2H, $\text{OCH}_2\text{CH}_2\text{ON}$) 3.86-3.34 (m, 227H, PEG protons) ppm.

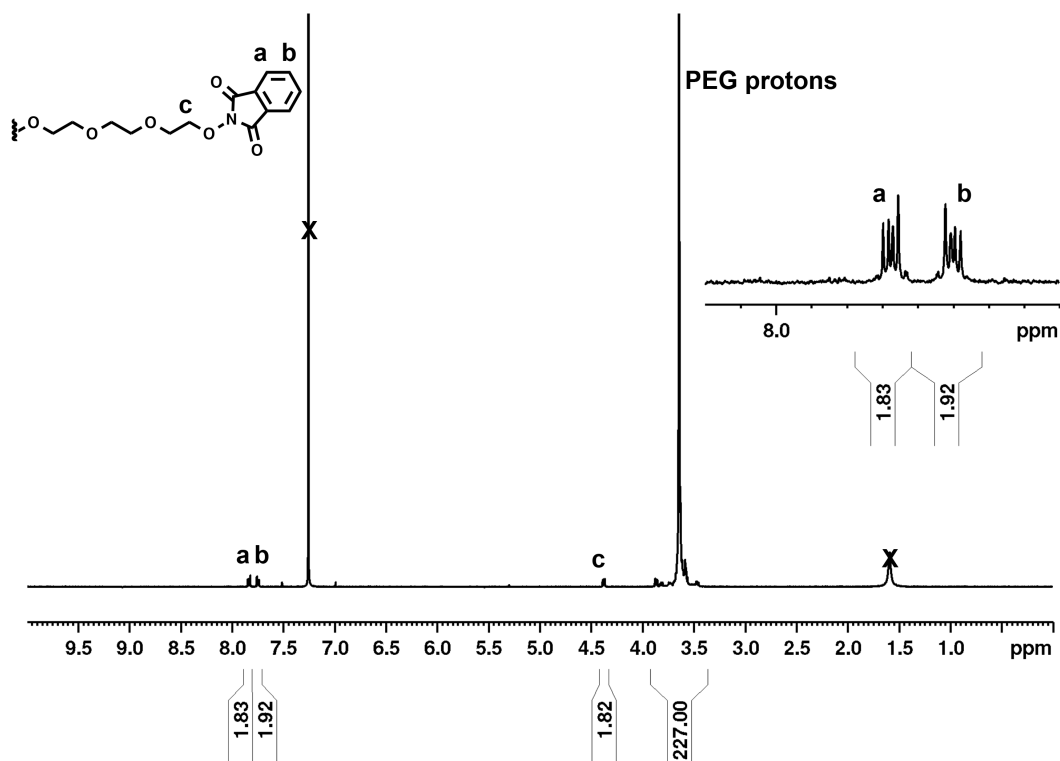


Figure 2.13. ^1H NMR spectrum of PEG-hydroxyphthalimide in CDCl_3 .

Synthesis of PEG-Aminoxy

PEG-hydroxyphthalimide (276 mg, 0.014 mmol) was dissolved in dichloromethane (1 mL) to which hydrazine hydrate (31.4 μ L, 0.52 mmol) was added. The reaction was allowed to stir at 23 $^{\circ}$ C for three hours. The reaction was filtered through glass wool to remove the white precipitate that formed. The organic solvent was removed under vacuum to yield the desired product as a white solid (265 mg, 96% yield, 94% conversion). ^1H NMR (500 MHz, CDCl_3) δ 3.90-3.43 (m, 227H, PEG protons) ppm.

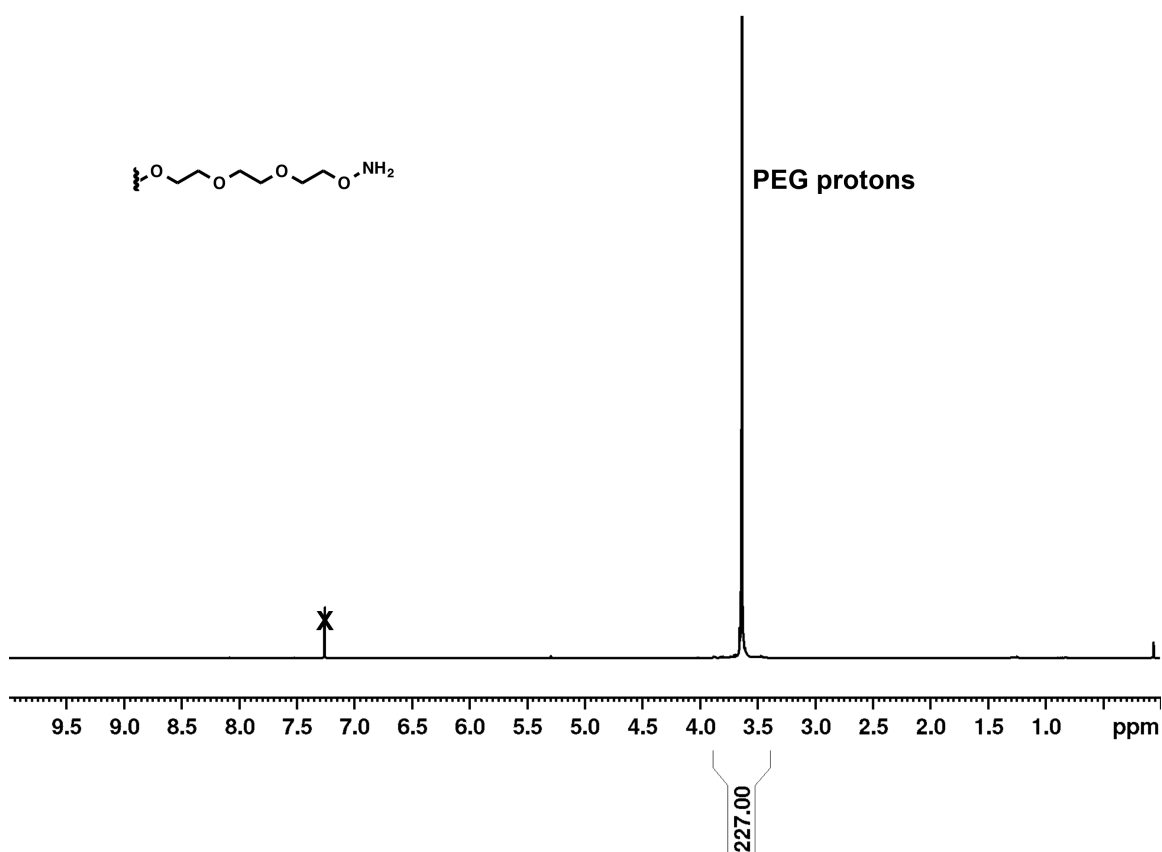


Figure 2.14. ^1H NMR spectrum of PEG-aminoxy in CDCl_3 .

Hydrogel Formation

Equal parts PEG-CHO and PEG-hydrazide/PEG-AO were combined in phosphate buffer for a total polymer concentration of 3.5 or 5.0 wt.%. The polymer solution was vortexed before being pipetted onto a hydrophobic glass slide with 1 mm spacers and sandwiched using a second hydrophobic glass slide. Hydrophobic glass slides were prepared by coating glass slides with a silanization reagent for glass (Sigmacote®) by dipping clean glass slides into the reagent solution for 5-10 minutes. Glass slides were then heated in an oven for 24 hours to allow hydrophobic coating to set before rinsing slides with water.

Rheological Characterization

40 μ L gels containing ratios of PEG-CDH/PEG-ADH, PEG-AO and PEG-CHO were made by adding pH 5.5 phosphate buffer and 20 wt.% PEG-CDH/PEG-ADH/PEG-AO solutions and mixing thoroughly. Then 20 wt.% PEG-CHO was added and the solution was mixed for ten seconds. Gel solutions were sandwiched between two hydrophobic glass slides separated by 1 mm spacers. The newly formed gels were added to buffer or media 10 minutes after gelation. Gels were swollen for 18 hours and liquid was refreshed once before taking measurements. Each gel condition was made and tested in triplicate. The gels were measured on a plate-to-plate Anton Paar rheometer (Physica MCR 301, Anton Paar, Ashland, VA) using an 8 mm plate with an angular frequency range of 0.1 to 10 s^{-1} under a constant strain of 1% at 37°C.

Swelling Studies

Gels were swollen in water for three days before measuring the mass of the swollen hydrogels (m_s). The water was refreshed four times before the measurements were taken.

The gels were lyophilized to remove water and weighed again to determine the dry mass (m_d). Gels were made in triplicate for each condition. The degree of swelling was calculated using $q = 1 + \rho_p \left(\frac{m_s}{m_d \times \rho_s} - \frac{1}{\rho_s} \right)$ where ρ_p is the density of the polymer solution (1.04 g/mL) and ρ_s is the density of the solution, in this case water (1.00 g/mL).

Degradation Studies

5 wt.% gels were swollen in phosphate buffer (pH 5.6) or Dulbecco's modified eagle's medium (DMEM) with or without fetal bovine serum (FBS) or mMSC conditioned DMEM. Buffer and medium were replaced daily during the course of the experiments. Gels were weighed daily over the course of six days. Gels for each condition were prepared in triplicate. Gels containing PEG-ADH degraded in complete DMEM before the six days were over and could therefore not be measured for the full extent of the experiment.

mMSC Encapsulation

AO-RGD (0.1, 0.5 or 1 mM final concentration) and PEG-CHO were dissolved in phosphate buffer. The two solutions were mixed together at the calculated ratios and allowed to react at 37 °C for 3 hours prior to setting up cell experiments. mMSCs in complete DMEM (3,500 or 5,000 cells/ μ L final concentration) were added to the AO-RGD/PEG-CHO solution and vortexed gently. The final components of the gel solution (5 total wt.% PEG-CDH and/or PEG-AO) were added to the AO-RGD/PEG-CHO/cell solution. 5 μ L gels were pipetted onto a hydrophobic glass slide with 1 mm spacers and sandwiched using a second hydrophobic slide. The gels were incubated at 37 °C for 15 minutes to allow for gelation. The gels were then added into the wells of a 96-well plate containing 200 μ L complete DMEM.

Cell Viability and Spreading

mMSC viability was studied with a LIVE/DEAD® viability/cytotoxicity kit (Molecular Probes, Eugene, OR). Briefly, 1 μ L of ethidium homodimer-1 and 0.25 μ L of calcein AM from the kit were diluted with 500 μ L DMEM to make the staining solution. Each gel was stained with 150 μ L of staining solution for 30 min at 37 °C in the dark before imaging. To better analyze cell spreading, gels were fixed for 5 min at RT using 4% PFA, rinsed with PBS, treated with 0.1% triton-X for 10 min and stained for 90 min in the dark with DAPI for cell nuclei (1:500 dilution from 5 mg/mL stock, Invitrogen, Grand Island, NY) and Alexa Fluor 488-phalloidin (1:200 dilution, Invitrogen, Grand Island, NY) in 1% sterile filtered bovine serum albumin solution. The samples were then washed with 0.05% tween-20. For cell viability, an inverted Observer Z1 Zeiss fluorescent microscope was used to visualize samples. To better visualize the distribution throughout the hydrogel, multiple z-stacks 1.9–2.3 μ m thick were taken for each image, deconvolved to minimize background, and presented as orthogonal projections. For cell spreading, a Nikon C2 confocal microscope was utilized to visualize samples. For 20X images, z-stacks 160 μ m thick were imaged at 1.8 μ m intervals. For 40X images, z-stacks 110 μ m thick were imaged at 1 μ m intervals with a water immersion lens. All confocal images were presented as maximum intensity projections.

Cells

Mouse mesenchymal stem cells (mMSCs) and human dermal fibroblasts (HDFs) were cultured in Dulbecco's modified Eagle's medium (DMEM) with added 10% fetal bovine

serum (FBS) and 1% penicillin/ streptomycin at 37 °C with 5% CO₂. Standard procedures were followed for cell culture.

Cell Viability Assay

The cell compatibility of the PEG components of the hydrogels to mMSCs and HDFs was evaluated using a LIVE/DEAD viability/cytotoxicity assay (Invitrogen). A control containing no PEG was also prepared. Cells were cultured as described above. The cells were seeded in 96-well plates (BD Falcon) at a density of 1000 cells per well. After 24 hours, culture media was replaced with 100 μ L media containing PEG (PEG-AO, PEG-CHO, PEG-CDH, and PEG-ADH) concentrations of 5 and 10 mg/mL and the cells were incubated for 24 hours. Cells were then washed with pre-warmed Dulbecco's phosphate buffered saline (D-PBS) and stained with LIVE/DEAD reagents (2 μ M calcein AM and 4 μ M ethidium homodimer-1). Fluorescent images of each well were captured on an Axiovert 200 microscope. The number of live (green) and dead (red) cells were counted, and % cell viability was calculated by dividing the number of live cells by the total number of live and dead cells. All experiments were performed a total of six times. The data is presented by normalizing each set to the control containing no additive.

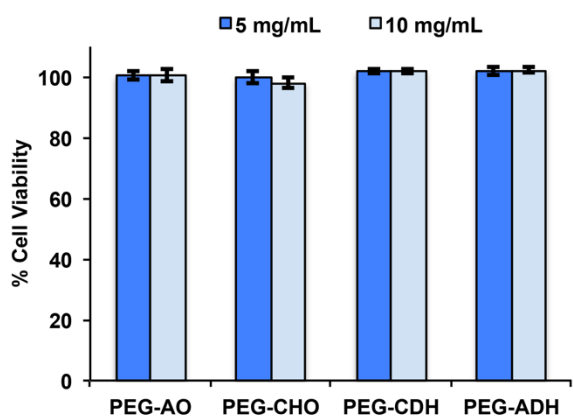


Figure 2.15. Cytotoxicity assays of PEGs with mMSCs with $p > 0.05$ for all conditions relative to the control. Experiments were repeated six times, and the results are represented as the average with standard deviation relative to the control with no PEG added.

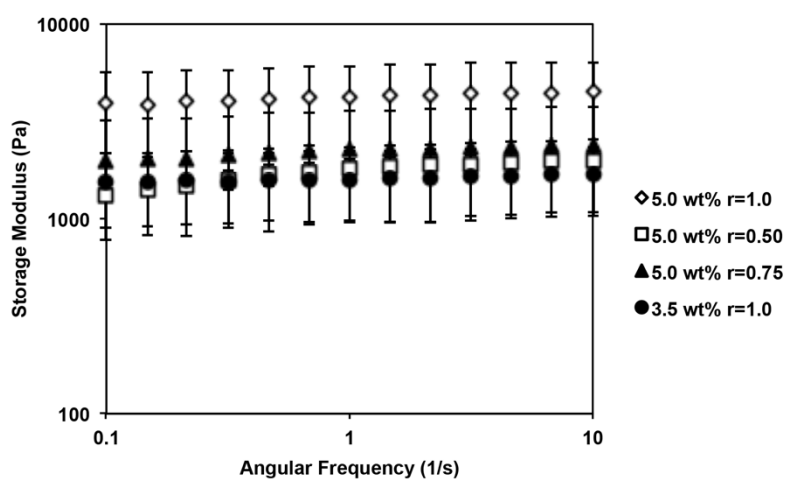
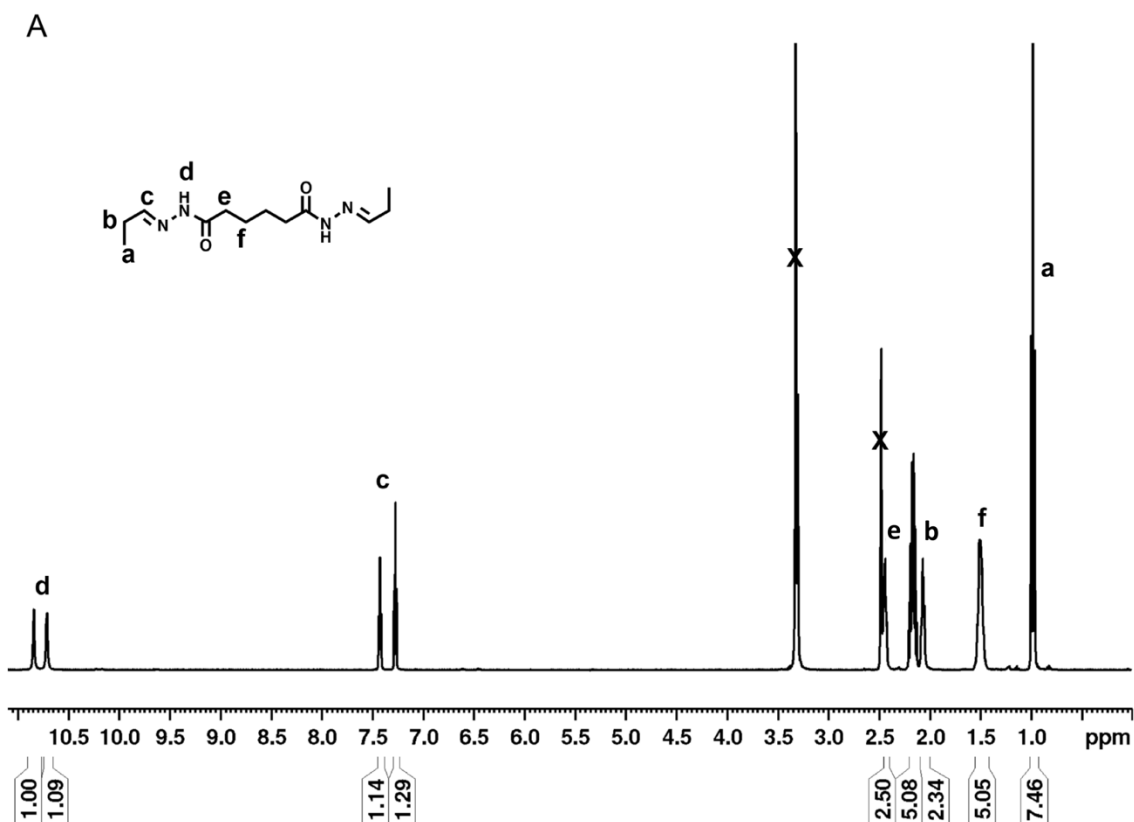


Figure 2.16. Rheological measurements of PEG-ADH based gels. 5.0 wt.% gels have a higher storage modulus than the more dilute 3.5 wt.% gels. Changing the ratio of aldehyde to hydrazide (r value) also decreases the storage modulus.

NMR Model Study

Adipohydrazide (20 mg, 0.115 mmol) was dissolved in H₂O (1 mL) in a vial with a stir bar. To this, propionaldehyde (18 μ L, 0.253 mmol) was added. The reagents were mixed at 23°C for 1 hour. As a result of the reaction, a white solid precipitated out of solution. Water was removed by lyophilization before re-dissolving the formed product in deuterated DMSO for NMR analysis. ¹H NMR (400 MHz, DMSO-d₆) δ 10.85-10.73 (s, 2H, NHCO), 7.43-7.28 (t, 2H, CHNH), 2.46-2.41 (m, 4H, OCCH₂CH₂), 2.19-2.12 (t, 2H, CH₂CH₃) 1.53-1.44 (t, 4H, CH₂CH₂CH₂CH₂), 0.99-0.94 (t, 6H, CH₃CH₂) ppm; ¹³C NMR (500 MHz, DMSO-d₆) δ 174.2, 168.5, 151.4, 148.1, 34.4, 32.0, 25.7, 25.3, 24.4, 11.0 ppm.

Note: both syn and anti peaks are observed.



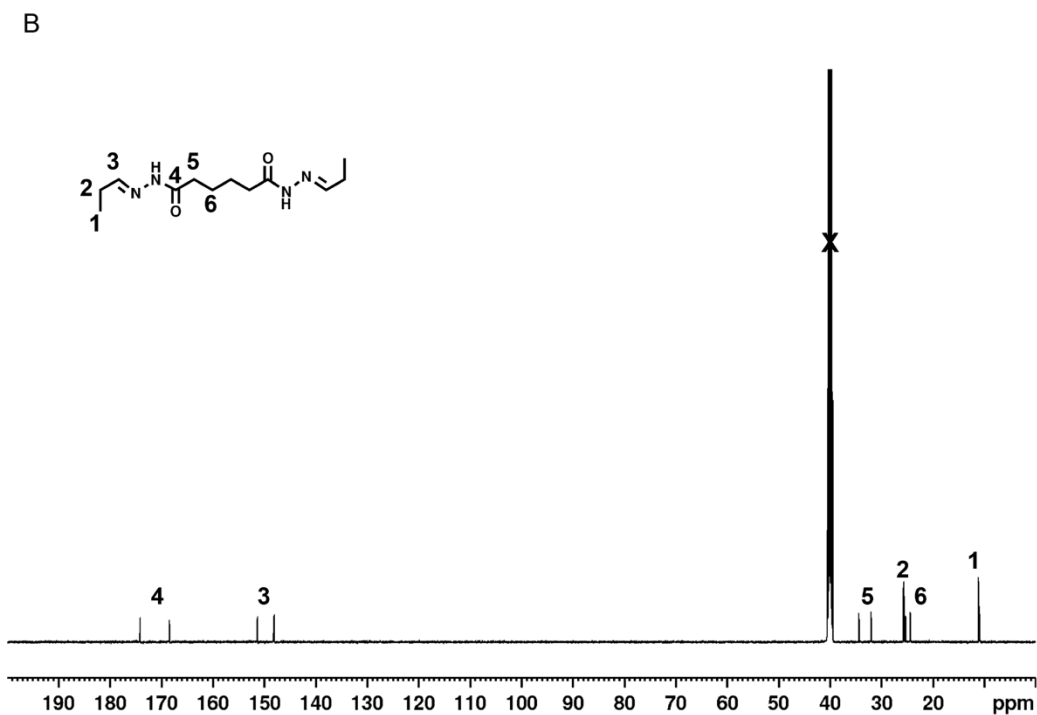


Figure 2.17. ^1H NMR (A) and ^{13}C NMR (B) of ADH-hydrazone in DMSO- d_6 .

Synthesis of Aminoxy-RGD Peptide (Aminoxy-GRGDSL-OH):

The aminoxy-GRGDSL integrin-binding peptide (AO-RGD) was synthesized using standard fmoc solid-phase peptide synthesis with a pre-loaded leucine 2-chlorotrityl resin (0.49 mmol/g substitution). (Boc-aminoxy) acetic acid was added to the N-terminus of the peptide via HBTU coupling. The peptide was cleaved from the resin using 95:2.5:2.5 TFA: TIPS: H_2O , which simultaneously deprotected the side chains, at 23 °C for two hours. The resin was rinsed with TFA and the solution reduced in volume before precipitation in cold diethyl ether. The sample was then purified using a preparative reverse-phase HPLC

equipped with a C18 column. A linear gradient from 95:5 to 5:95 of water: acetonitrile (containing 0.1% of trifluoroacetic acid) at 10 mL/min was used for optimal separation. The desired product was contained in the main peak, which eluted at 15 minutes. ESI-MS was used to verify the molecular mass (Figure 2.18). Mass of the peptide $[M+H]=677.2692$ Da, calculated $[M+H]=677.31$ Da.

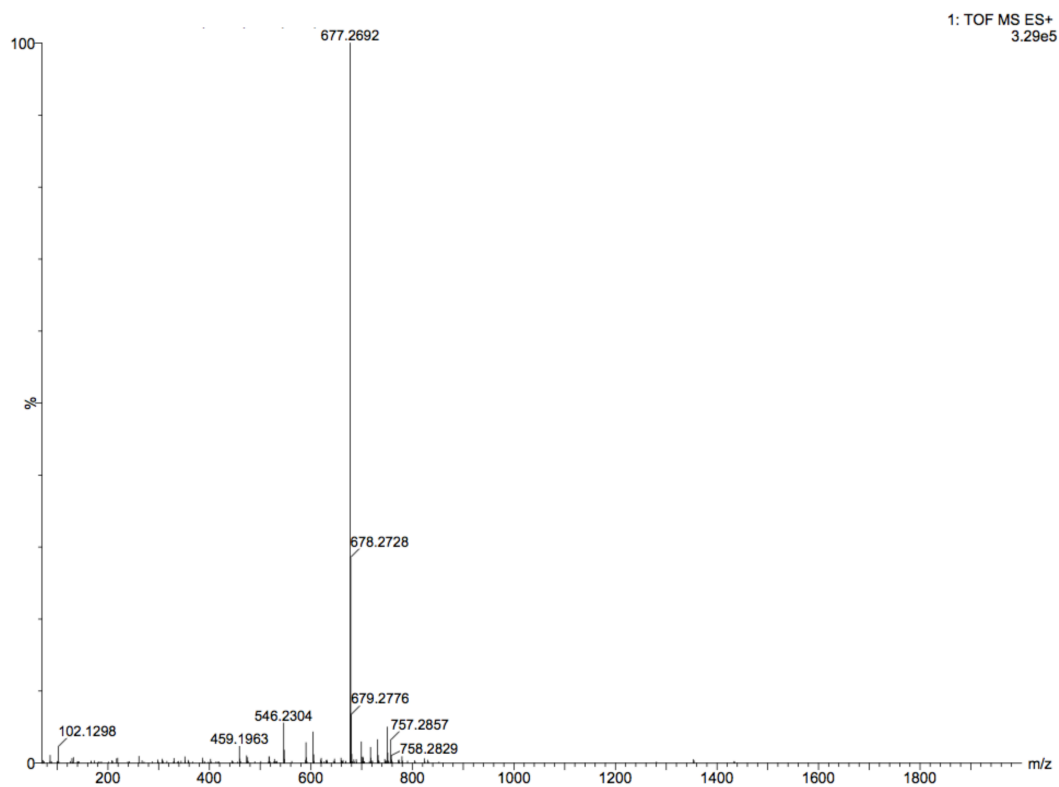


Figure 2.18. ESI-MS Spectrum of purified aminoxy-GRGDSL-OH.

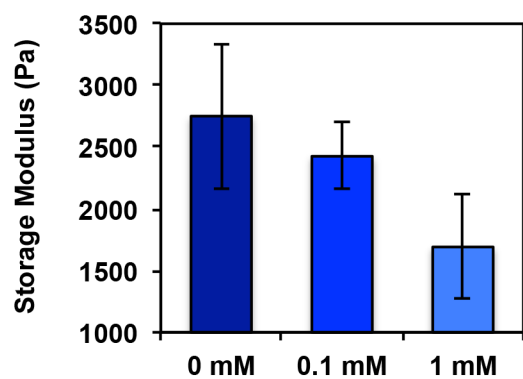


Figure 2.19. Rheological characterization of 3.5 wt.% PEG-CDH based hydrogels containing 1, 0.1, and 0 mM RGD. Statistical difference ($p < 0.05$) observed between 1-0.1 and 1-0 mM RGD containing gels.

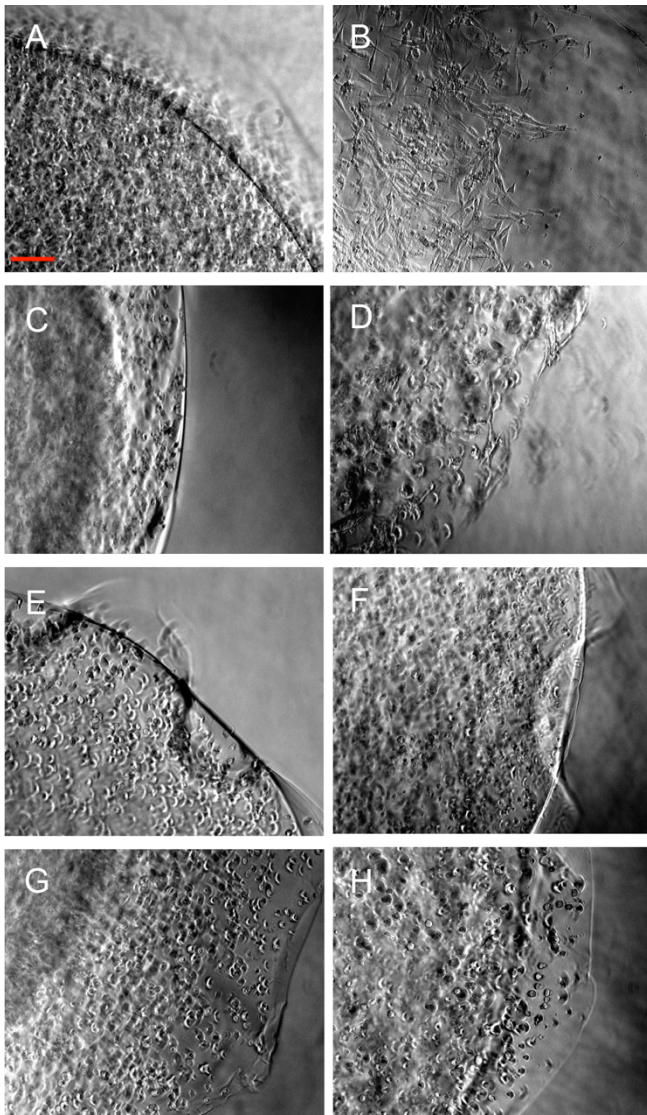


Figure 2.20. Light microscope images of 5.0 wt.% hydrazone (PEG-CDH) and mixed hydrazone/oxime gels containing mMSCs (5,000 cells/ μ L, 0.5 mM AO-RGD). Wells containing 100:0 hydrazone: oxime gels were imaged at day 1 (A) and day 6 (B) even though gels had degraded on day 5. Wells containing 75:25 hydrazone: oxime at day 1 (C) and day 6 (D), 50:50 hydrazone: oxime at day 1 (E) and day 6 (F), 0:100 hydrazone: oxime at day 1 (G) and day 6 (H) were also imaged. Scale bar = 100 μ m.

Monitoring of Hydrazone Displacement by Oxime by NMR

CDH Hydrazone:

Carbohydrazide (6.5 mg, 0.07 mmol) was dissolved in D₂O (1 mL) in a vial with a stir bar. To this, propionaldehyde (21 μ L, 0.14 mmol) was added. The reagents were mixed at 23°C for 30 minutes. As a result of the reaction, a white solid precipitated out of solution. Then, hydroxylamine HCl (10 mg, 0.14 mmol) was added to the vial and stirred for 30 minutes. Upon addition, the white solid dissolved almost immediately to give a clear colorless solution. Extent of hydrazone bond displacement was calculated by dividing sum of oxime proton integration by total imine proton integration.

ADH Hydrazone:

Adipohydrazide (12.5 mg, 0.07 mmol) was dissolved in D₂O (1 mL) in a vial with a stir bar. To this, propionaldehyde (21 μ L, 0.14 mmol) was added. The reagents were mixed at 23°C for 30 minutes. As a result of the reaction, a white solid precipitated out of solution. Then, hydroxylamine HCl (10 mg, 0.14 mmol) was added to the vial and stirred for 30 minutes. Upon addition, the white solid dissolved almost immediately to give a clear colorless solution. Extent of hydrazone bond displacement was calculated by dividing sum of oxime proton integration by total imine proton integration.

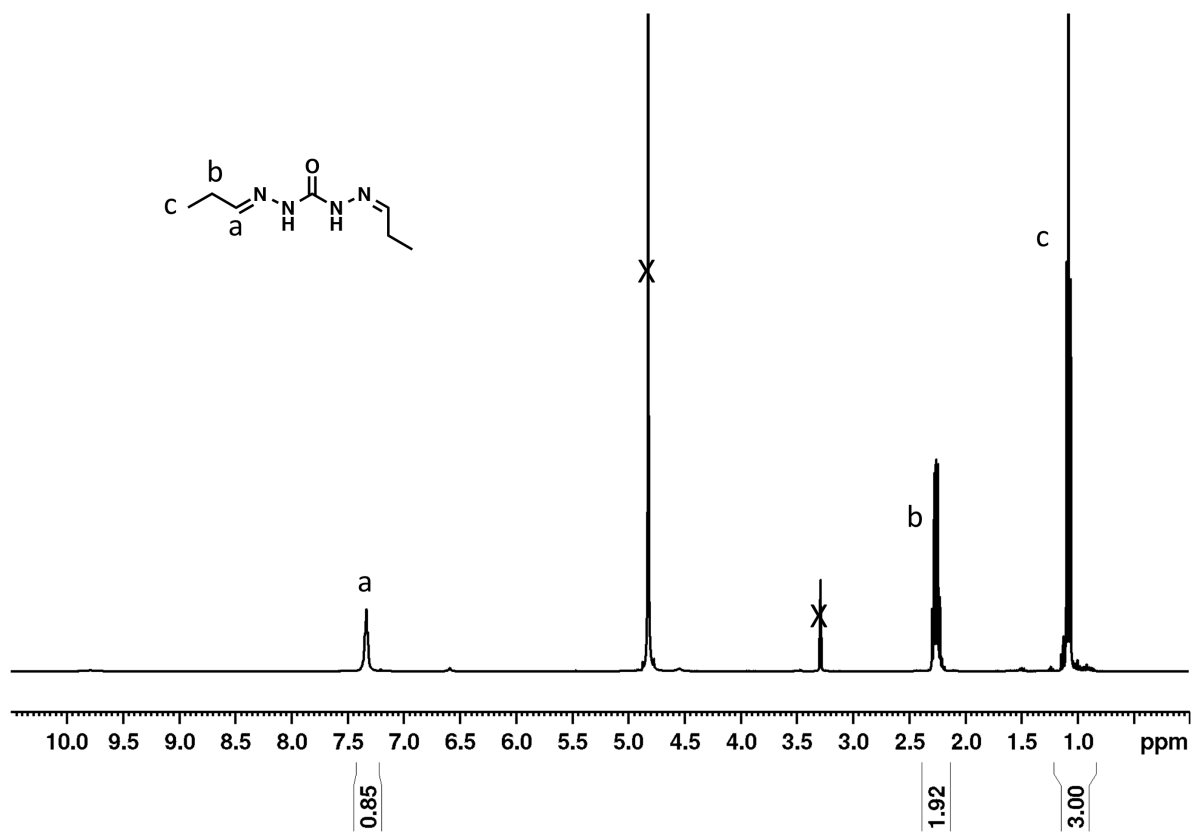


Figure 2.21. ^1H NMR of CDH hydrazone in MeOD.

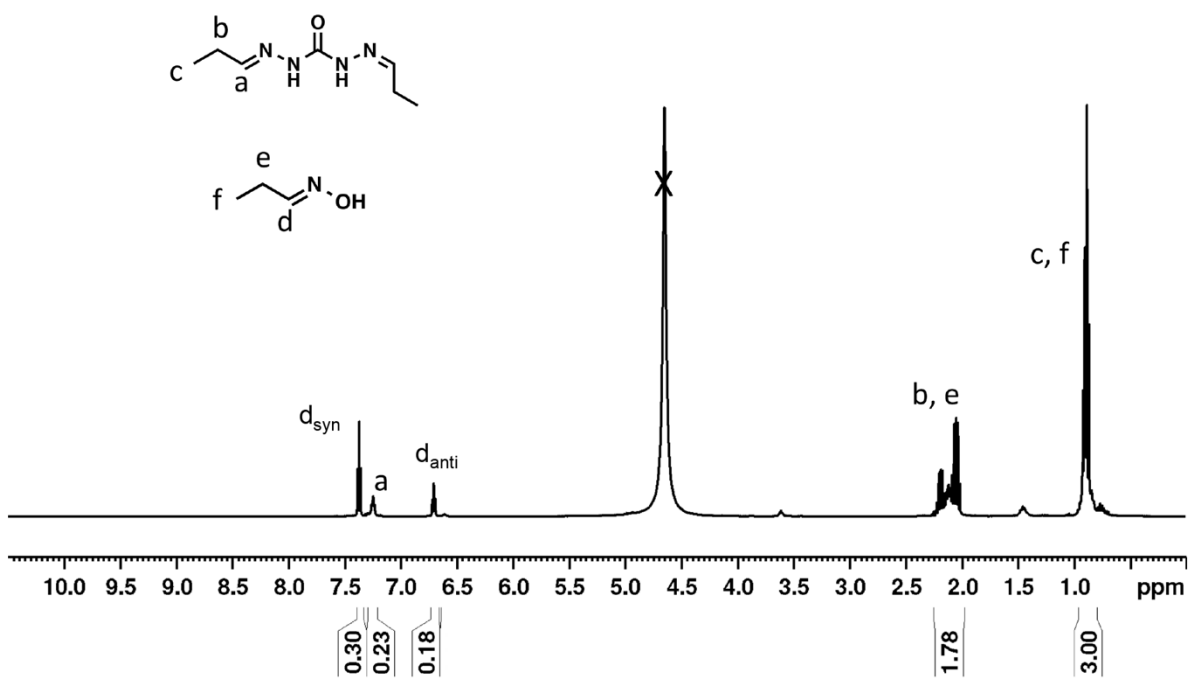


Figure 2.22. ^1H NMR of reaction of CDH hydrazone with hydroxylamine in D_2O .

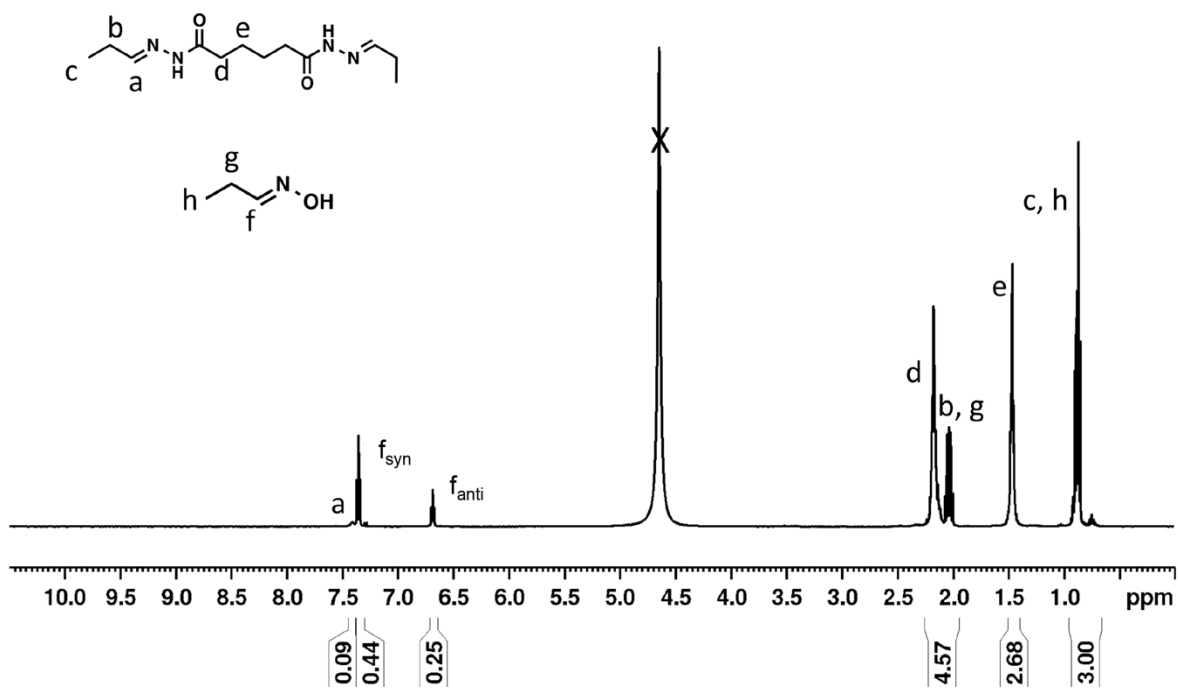


Figure 2.23. ^1H NMR of reaction of ADH hydrazone with hydroxylamine in D_2O .

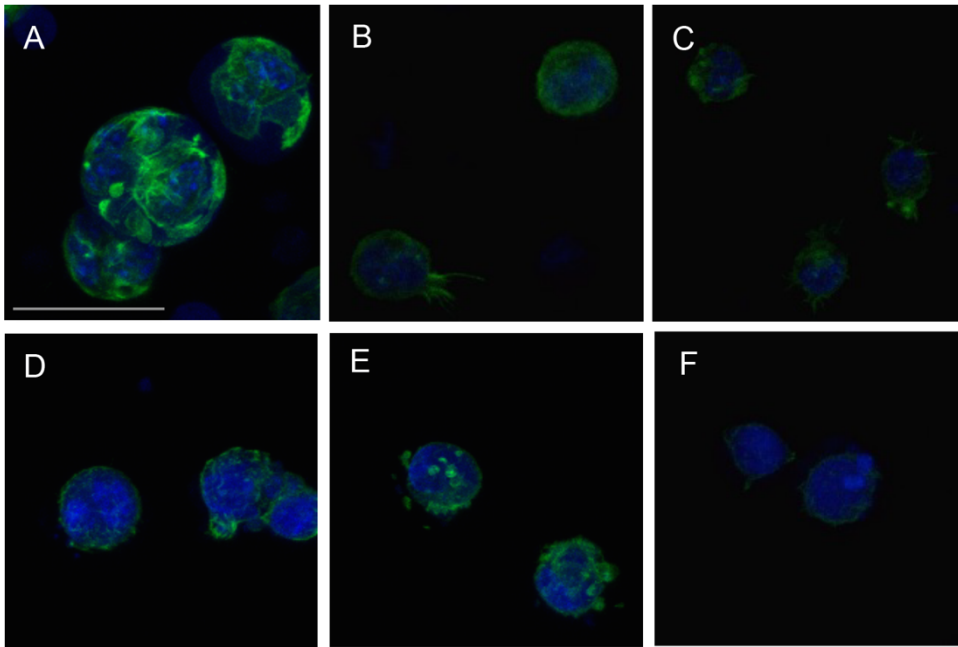


Figure 2.24. DAPI/Phalloidin staining for cell spreading at day 5. mMSCs were encapsulated in 5.0 wt.% 100:0 hydrazone: oxime (not shown due to gel degradation), 75:25 hydrazone: oxime (A), 50:50 hydrazone: oxime (B), and 0:100 hydrazone: oxime (C) gels containing 0.1 mM AO-RGD. Experiments were repeated using HDFs, encapsulated in 100:0 hydrazone: oxime (not shown due to gel degradation), 75:25 hydrazone: oxime (D), 50:50 hydrazone: oxime (E), and 0:100 hydrazone: oxime (F) gels also containing 0.1 mM AO-RGD. 40x magnification is shown for all images. Scale bar = 50 μm .

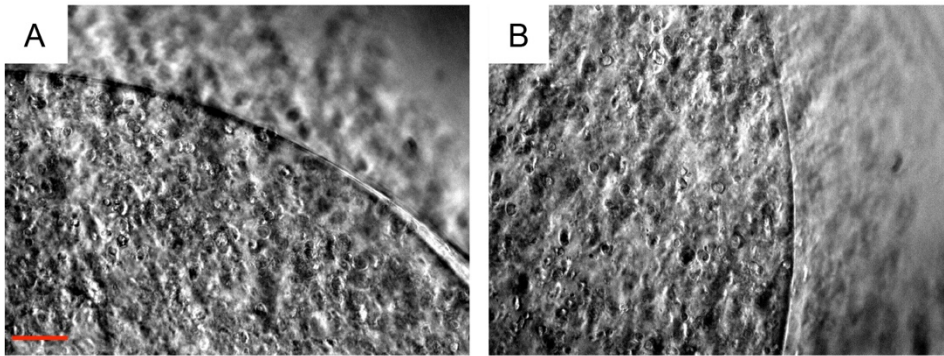


Figure 2.25. Light microscope images of 5 wt.% hydrazone (PEG-CDH) gels containing mMSCs (5,000 cells/ μ L) with (A) 0.1 mM AO-RGD and (B) 1 mM RGD on day 1 after encapsulation. Scale bar = 100 μ m.

2.5 References

† Chapter 2 has been published as: Boehnke, N.; Cam, C.; Bat, E.; Segura, T.; Maynard, H. D. *Biomacromolecules* **2015**, *16*, 2101-2108.

1. MacArthur, B. D.; Oreffo, R. O. C. *Nature* **2005**, *433*, 19-19.
2. Lenas, P.; Luyten, F. P. *Ind. Eng. Chem. Res.* **2011**, *50*, 482-522.
3. Lutolf, M. P.; Hubbell, J. A. *Nat. Biotechnol.* **2005**, *23*, 47-55.
4. DeLong, S. A.; Moon, J. J.; West, J. L. *Biomaterials* **2005**, *26*, 3227-3234.
5. Bryant, S. J.; Anseth, K. S. *J. Biomed. Mater. Res. A* **2003**, *64A*, 70-79.
6. DeForest, C. A.; Anseth, K. S. *Nat. Chem.* **2011**, *3*, 925-931.
7. DeForest, C. A.; Sims, E. A.; Anseth, K. S. *Chem. Mater.* **2010**, *22*, 4783-4790.
8. DeForest, C. A.; Polizzotti, B. D.; Anseth, K. S. *Nat. Mater.* **2009**, *8*, 659-664.
9. Tibbitt, M. W.; Anseth, K. S. *Biotechnol. Bioeng.* **2009**, *103*, 655-663.
10. Baker, E. L.; Bonnecaze, R. T.; Zamao, M. H. *Biophys. J.* **2009**, *97*, 1013-1021.
11. West, J. L.; Hubbell, J. A. *Macromolecules* **1999**, *32*, 241-244.
12. McKinnon, D. D.; Domaille, D. W.; Brown, T. E.; Kyburz, K. A.; Kiyotake, E.; Cha, J. N.; Anseth, K. S. *Soft Matter* **2014**, *10*, 9230-9236.
13. Kolb, H. C.; Finn, M. G.; Sharpless, K. B. *Angew. Chem. Int. Ed.* **2001**, *40*, 2004-2021.
14. Nimmo, C. M.; Shoichet, M. S. *Bioconjugate Chem.* **2011**, *22*, 2199-2209.
15. Agard, N. J.; Prescher, J. A.; Bertozzi, C. R. *J. Am. Chem. Soc.* **2004**, *126*, 15046-15047.

16. Grover, G. N.; Lam, J.; Nguyen, T. H.; Segura, T.; Maynard, H. D. *Biomacromolecules* **2012**, *13*, 3013-3017.
17. Lin, F.; Yu, J.; Tang, W.; Zheng, J.; Defante, A.; Guo, K.; Wesdemiotis, C.; Becker, M. L. *Biomacromolecules* **2013**, *14*, 3749-3758.
18. Anderson, S. B.; Lin, C. C.; Kuntzler, D. V.; Anseth, K. S. *Biomaterials* **2011**, *32*, 3564-3574.
19. Lei, Y. G.; Gojgini, S.; Lam, J.; Segura, T. *Biomaterials* **2011**, *32*, 39-47.
20. Yang, B.; Zhang, Y. L.; Zhang, X. Y.; Tao, L.; Li, S. X.; Wei, Y. *Polym. Chem.* **2012**, *3*, 3235-3238.
21. Zhang, Y. L.; Tao, L.; Li, S. X.; Wei, Y. *Biomacromolecules* **2011**, *12*, 2894-2901.
22. Lee, K. Y.; Alsberg, E.; Mooney, D. J. *J. Biomed. Mater. Res.* **2001**, *56*, 228-233.
23. Varghese, O. P.; Sun, W. L.; Hilborn, J.; Ossipov, D. A. *J. Am. Chem. Soc.* **2009**, *131*, 8781-8783.
24. Hudson, S. P.; Langer, R.; Fink, G. R.; Kohane, D. S. *Biomaterials* **2010**, *31*, 1444-1452.
25. Ding, C. X.; Zhao, L. L.; Liu, F. Y.; Cheng, J.; Gu, J. X.; Shan-Dan; Liu, C. Y.; Qu, X. Z.; Yang, Z. Z. *Biomacromolecules* **2010**, *11*, 1043-1051.
26. McKinnon, D. D.; Domaille, D. W.; Cha, J. N.; Anseth, K. S. *Chem. Mater.* **2014**, *26*, 2382-2387.
27. McKinnon, D. D.; Domaille, D. W.; Cha, J. N.; Anseth, K. S. *Adv. Mater.* **2014**, *26*, 865-872.
28. Patenaude, M.; Hoare, T. *Biomacromolecules* **2012**, *13*, 369-378.

29. Patenaude, M.; Hoare, T. *ACS Macro Lett.* **2012**, *1*, 409-413.
30. Alves, M. H.; Young, C. J.; Bozzetto, K.; Poole-Warren, L. A.; Martens, P. J. *Biomed. Mater.* **2012**, *7*.
31. Deng, G.; Tang, C.; Li, F.; Jiang, H.; Chen, Y. *Macromolecules* **2010**, *43*, 1191-1194.
32. Dahlmann, J.; Krause, A.; Moller, L.; Kensah, G.; Mowes, M.; Diekmann, A.; Martin, U.; Kirschning, A.; Gruh, I.; Drager, G. *Biomaterials* **2013**, *34*, 940-951.
33. Kool, E. T.; Park, D. H.; Crisalli, P. *J. Am. Chem. Soc.* **2013**, *135*, 17663-17666.
34. Crisalli, P.; Kool, E. T. *J. Org. Chem.* **2013**, *78*, 1184-1189.
35. Drury, J. L.; Mooney, D. J. *Biomaterials* **2003**, *24*, 4337-4351.
36. Sun, H. W.; Feigal, R. J.; Messer, H. H. *Pediatr. Dent.* **1990**, *12*, 303-307.
37. Zhao, Y. J.; Zhai, Y. Q.; Ma, G. H.; Su, Z. G. *J. Appl. Polym. Sci.* **2009**, *111*, 1638-1643.
38. Dirksen, A.; Hackeng, T. M.; Dawson, P. E. *Angew. Chem. Int. Ed.* **2006**, *45*, 7581-7584.
39. Deng, G. H.; Tang, C. M.; Li, F. Y.; Jiang, H. F.; Chen, Y. M. *Macromolecules* **2010**, *43*, 1191-1194.
40. Oommen, O. P.; Wang, S. J.; Kisiel, M.; Sloff, M.; Hilborn, J.; Varghese, O. P. *Adv. Funct. Mater.* **2013**, *23*, 1273-1280.
41. Krylov, I. B.; Terent'ev, A. O.; Timofeev, V. P.; Shelimov, B. N.; Novikov, R. A.; Merkulova, V. M.; Nikishin, G. I. *Adv. Synth. Catal.* **2014**, *356*, 2266-2280.
42. Ruoslahti, E.; Pierschbacher, M. D. *Cell* **1986**, *44*, 517-518.

43. Ruoslahti, E. *Annu. Rev. Cell Dev. Biol.* **1996**, *12*, 697-715.
44. Merrifield, R. B. *J. Am. Chem. Soc.* **1963**, *85*, 2149-2154.
45. Moon, J. J.; Saik, J. E.; Poche, R. A.; Leslie-Barbick, J. E.; Lee, S. H.; Smith, A. A.; Dickinson, M. E.; West, J. L. *Biomaterials* **2010**, *31*, 3840-3847.
46. Phelps, E. A.; Enemchukwu, N. O.; Fiore, V. F.; Sy, J. C.; Murthy, N.; Sulchek, T. A.; Barker, T. H.; Garcia, A. J. *Adv. Mater.* **2012**, *24*, 64-70, 62.
47. Bott, K.; Upton, Z.; Schrobback, K.; Ehrbar, M.; Hubbell, J. A.; Lutolf, M. P.; Rizzi, S. C. *Biomaterials* **2010**, *31*, 8454-8464.
48. Adeloew, C.; Segura, T.; Hubbell, J. A.; Frey, P. *Biomaterials* **2008**, *29*, 314-326.
49. Bat, E.; van Kooten, T. G.; Feijen, J.; Grijpma, D. W. *Biomaterials* **2009**, *30*, 3652-3661.
50. Wei, Z.; Yang, J. H.; Liu, Z. Q.; Xu, F.; Zhou, J. X.; Zrínyi, M.; Osada, Y.; Chen, Y. M. *Adv. Funct. Mater.* **2015**, *25*, 1352-1359.
51. Levental, I.; Georges, P. C.; Janmey, P. A. *Soft Matter* **2007**, *3*, 299-306.

Chapter 3

Synthesis of Redox-Responsive Trehalose

Glycopolymer Nanogels

3.1 Introduction

Systemic delivery of therapeutic agents can lead to off target effects.¹ Therefore, there is a need to incorporate stimuli responsive characteristics into materials that allow for the selective release and delivery of therapeutic agents.² Because of their tunable size, physical properties, and high degree of functionality, nanogels are commonly used for such applications.^{1, 3-4} Nanogels can be prepared through a number of different approaches, including emulsion,⁵ polymerization,⁶⁻⁷ and cross-linking of polymeric materials.⁸⁻⁹ Cargo can be encapsulated either covalently or non-covalently, though covalent incorporation, or conjugation, can improve pharmacokinetic properties and therapeutic benefits.¹⁰

To act as an effective therapeutic delivery vehicle, nanogels should be biocompatible, contain tunable physical properties, and release their cargo in response to specific stimuli. Many examples of degradable nanogels have been reported, particularly ones that degrade in reducing environments which allow for intracellular delivery.⁵ The Thayumanavan group has reported the synthesis of nanogels through self-cross-linking of random pyridyl disulfide ethyl methacrylate (PDSMA) poly(ethylene glycol) methacrylate (PEGMA) copolymers in the presence of substoichiometric amounts of a reducing agent.¹⁰ They utilized the lower critical solution temperature (LCST) behavior of their polymers to create temperature responsive nanogels to non-covalently encapsulate hydrophobic compounds. No release was observed unless a reducing agent was added to break the nanogel cross-links. They additionally demonstrated that their particles were biocompatible and readily taken up by cells.¹¹⁻¹² Thayumanavan and coworkers further expanded on their work to demonstrate that their mild nanogel formation is compatible

with covalent encapsulation of therapeutic proteins, such as caspase 3, with retention of activity.¹³ Recently, the group utilized a new strategy in which an amine reactive disulfide was incorporated into their copolymer instead of PDS groups. This allowed for efficient conjugation and nanogel formation in one step without the need to add reducing agent.¹⁴ In collaboration with the Thayumanavan group, we have previously reported the biocompatible synthesis of nanogel-protein conjugates which were used to covalently attach thiolated bovine serum albumin (BSA) to PDSMA-*co*-PEGMA nanogels through disulfide bonds.¹⁵ Using disulfide cross-links, nanogels could be degraded in the presence of dithiothreitol (DTT), releasing intact BSA.

A similar cross-linking strategy has been utilized by the Davis and Bulmus groups. PDSMA homopolymers prepared via RAFT were used to form water-insoluble scaffolds. After functionalizing the polymers with the tripeptide glutathione (GSH), a shift in solubility was observed.¹⁶ Block copolymers containing PDSMA were also prepared by polymerizing with *N*-(2-hydroxypropyl)methacrylamide (HMPA) and PEG to form drug¹⁷ and protein-functionalized nanoparticles,¹⁸ respectively.

Glycopolymers or nanocarriers that contain carbohydrates either in the backbone or side chains have also been utilized to form nanoparticles and nanogels to further stabilize sensitive cargo, as well as to tune solubility and improve targeting.¹⁹⁻²¹ Additionally, glycopolymers have been employed to create stimuli responsive particles. The Stenzel group has reported the synthesis of disulfide cross-linked glycopolymer nanocapsules for the encapsulation of the anticancer drug gemcitabine, leading to a two-fold increase in drug efficacy.²² Moreover, they developed a block copolymer system containing sugar side

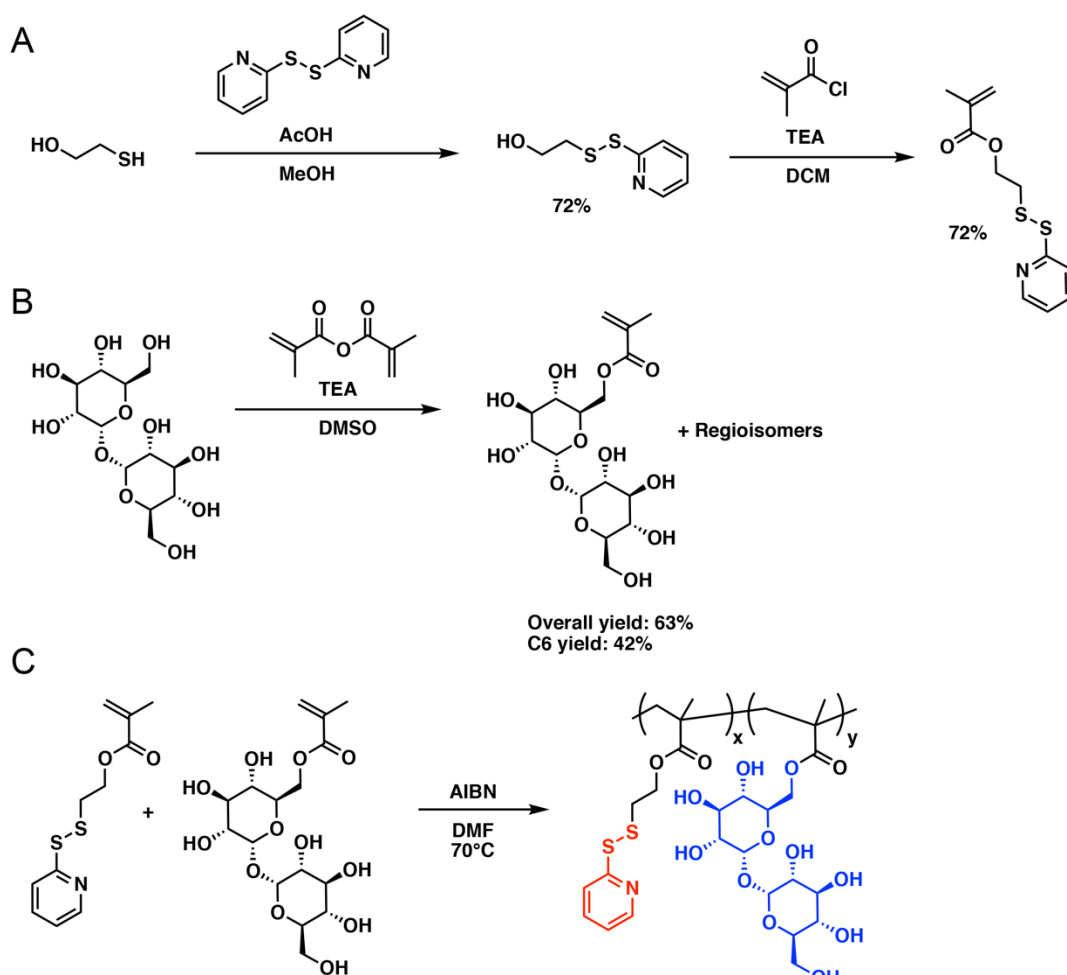
chains, wherein the nanoparticle morphology could be tuned based on sugar content.²³⁻²⁴ The Reineke group has reported the synthesis of nanoparticles that stabilize pDNA in the presence of serum. Their particles were prepared from polymers containing trehalose, a natural non-reducing disaccharide formed by α,α -1,1-linked glucose units,²⁵ in the backbone.²⁶ Trehalose-functionalized polymers have also been utilized to create serum stable micelles²⁷ and cationic nanocomplexes.²⁸ Due to the biocompatibility of glycopolymers, they have also been prepared for *in vivo* therapeutics delivery.²⁹ Additionally, we have previously shown that polymers containing side chains functionalized with trehalose were able to stabilize proteins to a variety of environmental stressors, including heat and electron beam irradiation, as conjugates and excipients.³⁰⁻³⁵ Trehalose glycopolymers can also be used to form bulk hydrogels to protect proteins against heat,³⁶ which inspired us to design degradable nanogels containing trehalose for protein stabilization and delivery applications. Degradability was installed by incorporation of redox-responsive disulfide cross-links. Herein, we present the design and synthesis of trehalose glycopolymer nanogels for potential use to stabilize and deliver proteins. The synthesis and characterization of monomers, copolymers, and resulting redox-responsive trehalose nanogels will be described.

3. 2. Results and Discussion

3. 2. 1. Monomer and Polymer Synthesis

In order to create redox-responsive nanogels, copolymers containing pyridyl disulfide and trehalose side chains were prepared for cross-linking via disulfide exchange.

PDSMA was synthesized following a previously reported procedure (Scheme 3.1A).³⁷ We initially used a styrenyl ether functionalized trehalose monomer because of its established protein stabilizing properties.^{30-31, 35-36} However, after copolymerizing with PDSMA, we obtained polymers with inconsistent monomer incorporation. Therefore, we chose to utilize a methacrylate-functionalized trehalose monomer (TrMA) that we had synthesized previously, although our previously reported synthetic route required multiple protecting groups and was low yielding.³¹ To simplify the synthesis, we reacted trehalose with methacrylic anhydride in the presence of triethylamine and found that this gave the desired monomer as a mix of regioisomers with the C6 isomer as the predominant product (Scheme 3.1B). We screened several ratios of trehalose to methacrylic anhydride and found that a five-fold excess of trehalose gave the highest yield of TrMA after HPLC purification (Table 3.2). A 10-60% methanol gradient was used to purify the monomers by HPLC, and we found that we could recover unreacted trehalose for resubjection (Figure 3.9). The overall yield of all regioisomers was 63% and the yield of C6 was 42%, an improvement over the previously reported overall yield of 14%. To ensure that the correct regioisomer was isolated, 1D and 2D NMR analysis was carried out (Figure 3.10-Figure 3.12). We also compared the NMR spectrum of purified C6 TrMA to TrMA synthesized using our previous synthetic route and found that they matched, suggesting our assignment was correct (Figure 3.13).



Scheme 3.1. Syntheses of PDSMA (A) and TrMA (B) monomers. The copolymer containing PDS and trehalose side chains, PDSMA-*co*-TrMA, was synthesized using free radical polymerization conditions (C).

Free radical polymerization (FRP) conditions were utilized to synthesize PDSMA-*co*-TrMA polymers at two different ratios, 1:1 and 1:3 PDSMA to TrMA (Scheme 3.1c). We chose to use methacrylates for both monomers in an attempt to match their reactivities. We found that the feed ratio matched the monomer incorporation fairly well, as determined by NMR, obtaining 1:0.8 (PDSMA₁-*co*-TrMA_{0.8}) and 1:1.7 PDSMA to TrMA (PDSMA₁-

co-TrMA_{1.7}) incorporation, respectively (Figure 3.1, Figures 3.14- 3.15). These monomer feed ratios were chosen to create nanogels with trehalose content for protein stabilization applications, yet with enough PDSMA content to allow for efficient cross-linking and uniform nanogel formation.

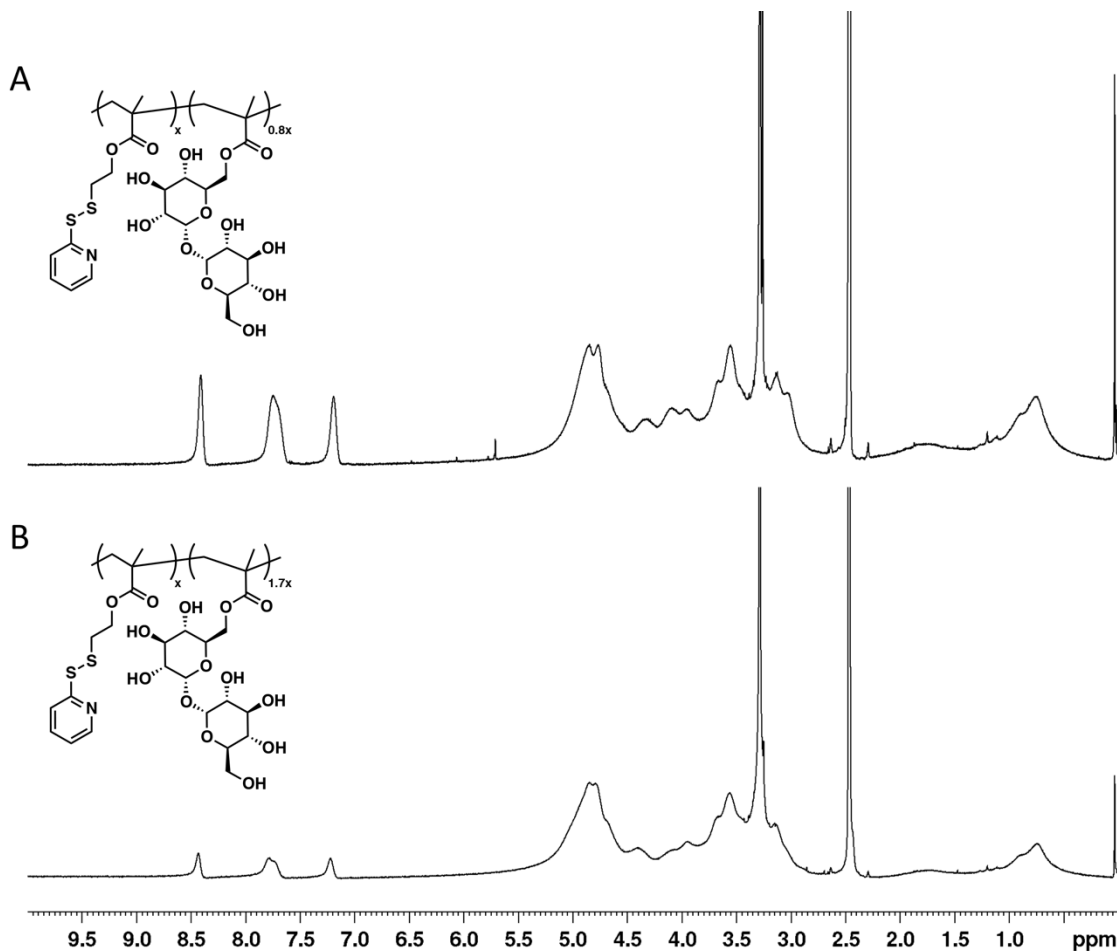


Figure 3.1. ¹H NMR spectra of PDSMA₁-*co*-TrMA_{0.8} (A) and PDSMA₁-*co*-TrMA_{1.7} (B) acquired in DMSO-d₆.

The resulting polymers were characterized using gel permeation chromatography (GPC) with dimethylformamide (DMF) + 0.1 M LiBr as the eluent with near-monodisperse

poly(methylmethacrylate) (PMMA) standards and using size exclusion chromatography (SEC) with 0.03 M NaNO₃ + 20 mM phosphate buffer pH 7 + 20% acetonitrile with near-monodisperse PEG standards (Table 3.1). Interestingly, two different trends in M_n were observed when comparing the results. When using PEG standards, a significant size increase was observed when comparing PDSMA_{1-co}-TrMA_{1.7} to PDSMA_{1-co}-TrMA_{0.8}, which could be explained by the increased hydrophilicity of the polymer. The opposite trend was observed when comparing our polymers to more hydrophobic PMMA standards wherein an increase in trehalose content resulted in a decrease in M_n values. While PMMA and PDSMA-*co*-TrMA contain the same methacrylate backbone, hydrophilic trehalose groups on PDSMA-*co*-TrMA alter the solubility and properties compared to PMMA, especially when in an organic solvent. Because no standards exist that match the properties of these polymers, a more accurate polymer size could not be determined. The broad dispersities of the resulting polymers were typical of trehalose glycopolymers synthesized by FRP.³¹ We attempted to use reversible addition-fragmentation chain-transfer (RAFT) polymerization with a variety of chain transfer agents (CTAs) to obtain polymers with lower dispersity (Đ), though these attempts were unsuccessful.

Table 3.1. GPC characterization of PDSMA-*co*-TrMA polymers.

Polymer	Feed (PDSMA: TrMA)	Polymer (PDSMA: TrMA)	Targeted Size (Da)	M _n (Da)	Đ	Yield (%)
PDSMA _{1-co} -TrMA _{0.8}	1:1	1:0.8	10,000	4,900* 2,700**	2.90* 1.18**	60

PDSMA ₁ - <i>co</i> - TrMA _{1.7}	1:3	1:1.7	10,000	9,700* 1,600**	2.38* 1.02**	70
--	-----	-------	--------	-------------------	-----------------	----

* Values obtained using a PEG standard. ** Values obtained using a PMMA standard.

3. 2. 2. Nanogel Synthesis and Characterization

Initially, nanogel formation was attempted using the conditions described by the Thayumanavan group wherein substoichiometric amounts of reducing agent were used to facilitate cross-linking.¹⁰ However, TEM images of polymer plus TCEP indicated no nanogels had formed, and no change in morphology was observed when compared to polymer only (Figure 3.16). We hypothesized that the lack of cross-linking was caused by the steric bulk of the trehalose side chains. To circumvent this issue, we introduced 1,000 Da PEG-dithiol as a cross-linker (Figure 3.2a). Resulting PDSMA₁-*co*-TrMA_{0.8} nanogels were characterized using dynamic light scattering (DLS) and transmission electron microscopy (TEM), and we observed fairly uniform particles approximately 9 nm in diameter (Figure 3.2b-c). Four different PEG-dithiol cross-linker amounts were investigated: 12.5, 25, 37.5, and 50 mol%, corresponding to 25, 50, 75, and 100% cross-linking if quantitative conversion were achieved. We were surprised to find that changing the amount of PEG-dithiol cross-linker did not appear to have an effect on overall nanogel size. We hypothesized that this was due to trehalose's large hydrodynamic radius³⁸ that may prevent nanogels from being contracted smaller than the observed sizes. We did, however, observe that we could change nanogel size by changing overall polymer concentration. The abovementioned nanogels were formed at a PDSMA₁-*co*-TrMA_{0.8} concentration of 2 mg/mL. At a PDSMA₁-*co*-TrMA_{0.8} concentration of 10 mg/mL,

nanogels closer to 50 nm in diameter were obtained. These nanogels were more disperse, as evidenced by TEM imaging, which can be explained by the higher polymer concentration causing nanogels to cross-link with each other in solution, leading to larger aggregates (Figure 3.17).

Switching from self-cross-linking to the use of a cross-linker could have several advantages. Cross-linkers of different sizes and structures could be added to tune nanogel properties further. Moreover, because we eliminated the need to add reducing agent in order to form nanogels, we anticipated that this strategy would be useful for the encapsulation of sensitive peptides and proteins that might lose activity in a reducing environment.

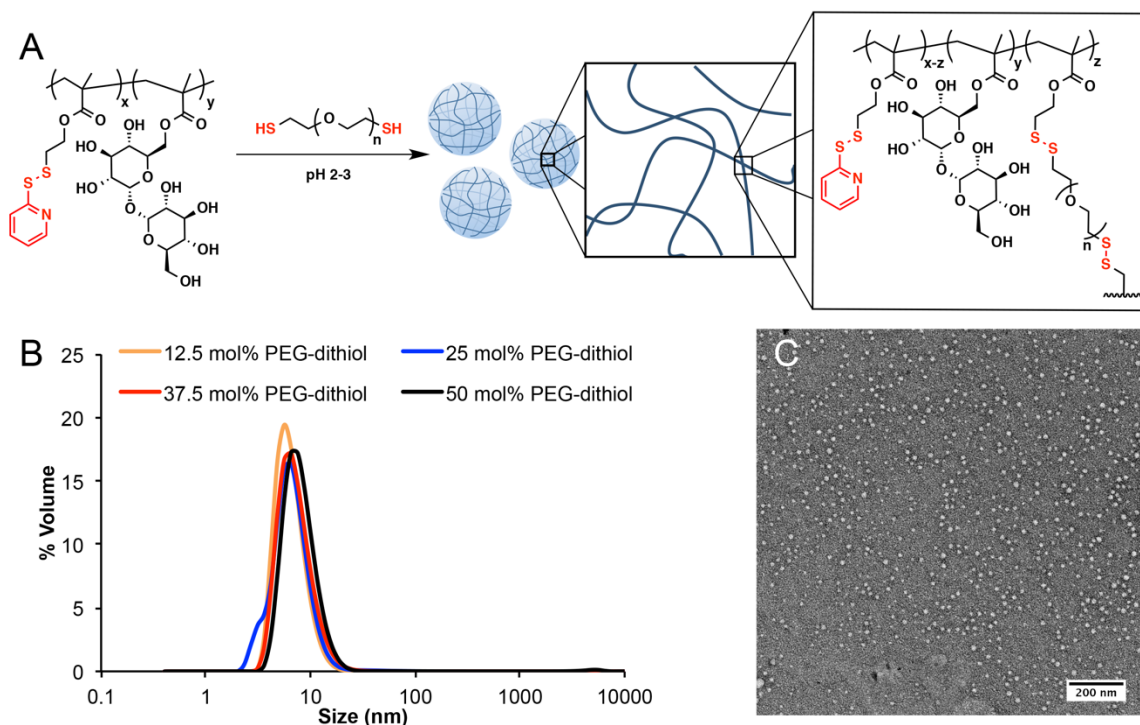


Figure 3.2. PDSMA₁-co-TrMA_{0.8} nanogels were formed using PEG-dithiol as a cross-linker (A) and characterized using DLS (B) and TEM (C).

3. 2. 3. Protein Encapsulation

We chose to non-covalently encapsulate two model proteins, lysozyme (lyz) and BSA, by adding the proteins during the nanogel formation step. We chose these two proteins because they have different sizes and properties. Lyz is a 14.3 kDa protein³⁹ with an isoelectric point of 11.35⁴⁰ whereas BSA is much larger at 66.5 kDa⁴¹ with an isoelectric point of 4.7.⁴² It is known that these proteins form aggregates in the presence of reducing agents,⁴³ and we hypothesized that our reducing agent free process might retain a higher degree of protein activity. Both proteins have free cysteines that could be used for conjugation, although we have previously shown that the addition of a thiolating linker is needed for efficient conjugation of PDSMA-*co*-PEGMA nanogels to BSA,¹⁵ likely due to the increased steric bulk of the nanoparticles compared to linear polymers. After mixing the polymer and protein solutions for three hours using either 5 or 10 weight equivalents of PDSMA₁-*co*-TrMA_{1.7} in the presence of PEG-dithiol cross-linker, no protein encapsulation was observed by SDS-PAGE (Figure 3.3). While these conditions were far from optimized, we chose a relatively short mixing time because therapeutic proteins are often unstable in solution⁴⁴ and longer encapsulation times may result in loss of protein activity. It may be worthwhile to explore the effect of cross-linking density and polymer size on encapsulation efficiency. The cross-linking density and resulting mesh size of our system were limited by the bulky trehalose side chains, which may have increased the mesh size and allowed proteins to easily slip out of the nanogels, although larger polymers may be able to encapsulate cargo more efficiently. However, we were more interested in

pursuing a covalent encapsulation strategy to improve overall protein retention since it is known that non-covalent encapsulation of proteins inside nanogels is usually lower yielding than covalent encapsulation.¹⁵ Therefore, we chose to focus on developing a reversible covalent conjugation strategy that would allow us to use a therapeutic protein as the cross-linker. This will be described in Chapter 4.

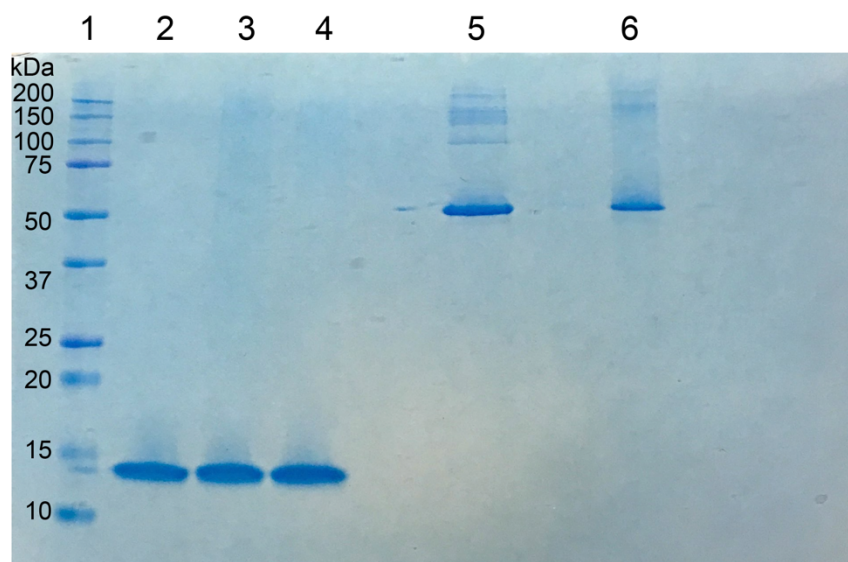


Figure 3.3. SDS PAGE of Lyz and BSA encapsulation attempt using PDSMA-*co*-TrMA nanogels cross-linked with PEG-dithiol. Lane 1: protein ladder; lane 2: lyz; lane 3: PDSMA-*co*-TrMA (3 wt. eq. PDSMA₁-*co*-TrMA_{0.8}) nanogels + Lyz; lane 4: PDSMA-*co*-TrMA (4 wt. eq. PDSMA₁-*co*-TrMA_{1.7}) nanogels + Lyz; lane 5: BSA; lane 6: PDSMA-*co*-TrMA (4 wt. eq. PDSMA₁-*co*-TrMA_{1.7}) nanogels + BSA. Non-reducing conditions.

In order to ensure our polymers and nanogels were biocompatible for potential *in vitro* and *in vivo* applications, cytotoxicity was assessed using LIVE/DEAD assay. It was found that PDSMA₁-*co*-TrMA_{1.7} was non-cytotoxic to human dermal fibroblasts (HDFs)

up to 2.5 mg/mL (Figure 3.4A). It is important to note that at this concentration, the cells exhibited a rounded morphology, indicating they may not be healthy, and at 5 mg/mL polymer, no live cells were observed (Figure 3.18). However, at 1 mg/mL, normal cell morphology was observed. Nanogels were tested up to 1 mg/mL and high cell viability was observed (Figure 3.4B), indicating that these particles would be compatible with further biological applications.

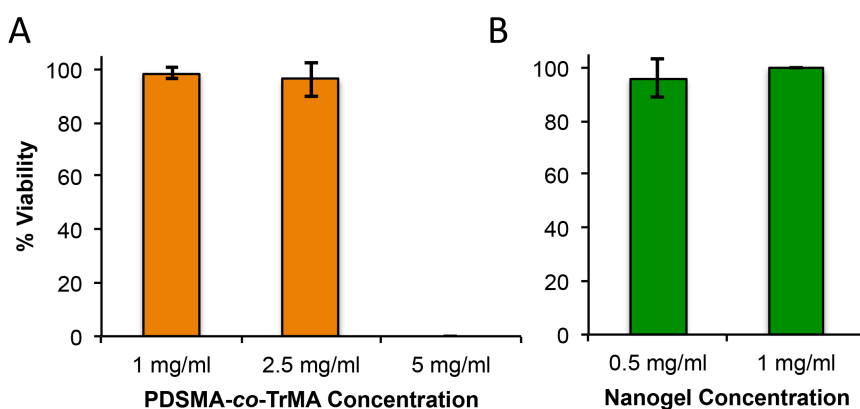


Figure 3.4. Cytotoxicity studies of PDSMA₁-*co*-TrMA_{1.7} (A) and nanogels (B) with HDFs.

3.3. Conclusions

We optimized the synthesis of a methacrylate-functionalized trehalose monomer (TrMA) and copolymerized it with PDSMA to create PDSMA-*co*-TrMA using FRP conditions. While self-cross-linking of the polymers was not observed under reducing conditions, we were able to form uniform nanogels through the addition of a PEG cross-linker, which circumvented the need to add reducing agent to form nanogels. Non-covalent encapsulation of two model proteins, lysozyme and bovine serum albumin, was investigated. Neither protein was retained inside the nanogels suggesting that covalent

encapsulation may be required. Further, cytotoxicity experiments indicated that our polymers and nanogels are non-cytotoxic up to 1 mg/mL and may be compatible for future *in vitro* and *in vivo* applications.

3. 4. Experimental

3. 4. 1. Materials and Analytical Techniques

Chemicals were purchased from Sigma Aldrich or Fisher Scientific without further purification unless mentioned otherwise. Azobis(isobutyronitrile) (AIBN) was recrystallized from acetone before use. Trehalose (Healthy Essential Management Corporation, Houston TX) was azeotropically dried from ethanol and kept under vacuum until use. ¹H NMR and ¹³C NMR spectroscopy were performed on an Avance DRX 400 MHz or 500 MHz instrument. GPC was carried out on a Shimadzu HPLC system equipped with a refractive index (RI) detection RID-10A, a Polymer Laboratories PLgel guard column, and two Polymer Laboratories PLgel 5 μm mixed D columns. DMF + 0.1 M LiBr at 50 °C was used as the eluent at a flow rate of 0.8 mL/min. Calibration was performed using near-monodisperse PMMA standards from Polymer Laboratories. SEC was conducted on a Shimadzu HPLC system with a RI detection RID-10A, a Tosoh TSKGel guard column, and a Tosoh TSKGel G4000PW column. 0.3 M NaNO₃ + 20 mM phosphate buffer pH 7 + 20% acetonitrile was used as the eluent at a flow rate of 0.7 mL/min. Calibration was carried out using near mono-disperse PEG standards from Polymer Laboratories. DLS measurements were carried out using a Malvern Zetasizer Nano.

3. 4. 2. Methods

Synthesis of Pyridyl Disulfide Alcohol (PDSOH)³⁷

Aldrithiol-2 (1.25 g, 5.65 mmol) was dissolved in methanol (15 mL). Then, acetic acid (2.5 mL) was added to the solution drop wise. A pale, clear yellow solution resulted. β -mercaptoethanol (300 μ L, 4.3 mmol) was dissolved in methanol (10 mL) and added to the stirring reaction drop wise. The reaction was stirred for 18 hours at room temperature (19 °C). Solvent volume was reduced via rotary evaporator. Then, methylene chloride was added before extracting twice with sat. NaHCO₃ and once with water. The methylene chloride layer was washed with sat. NaCl before drying over MgSO₄. The crude product was purified using column chromatography (2:3 hexanes: ethyl acetate). The product had an R_f value of 0.5 by TLC with these solvents and was obtained in 72% yield. NMR (400 MHz, CDCl₃) δ 8.46-8.41 (m, 1H, CHN), 7.57-7.50 (m, 1H, CHCHCN), 7.40-7.36 (dt, 1H, CHCHCN), 7.12-7.07 (m, 1H, CHCHN), 5.83-5.50 (broad s, 1H, OH), 3.80-3.72 (2H, t, CH₂OH), 2.94-2.86 (2H, t, CH₂S) ppm; ¹³C NMR (400 MHz, CDCl₃) δ 159.2, 149.8, 136.9, 121.9, 121.5, 58.4, 42.7 ppm.

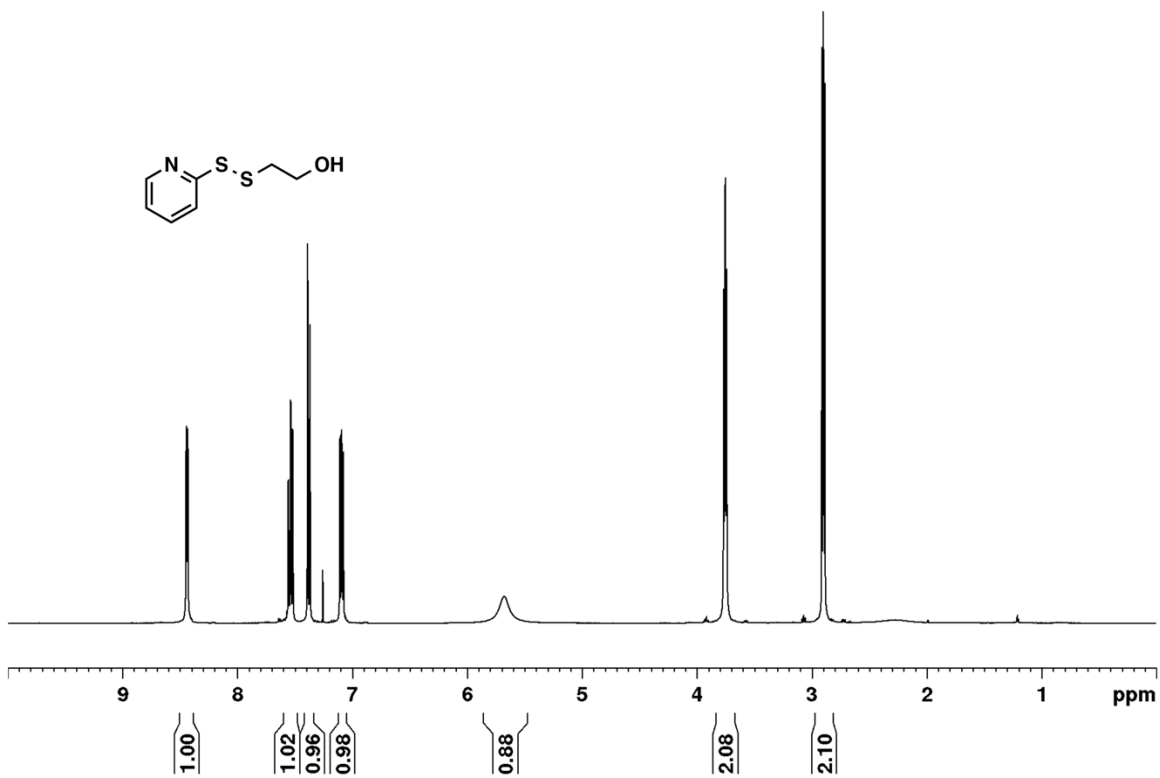


Figure 3.5. ^1H NMR spectrum of PDSOH in CDCl_3 .

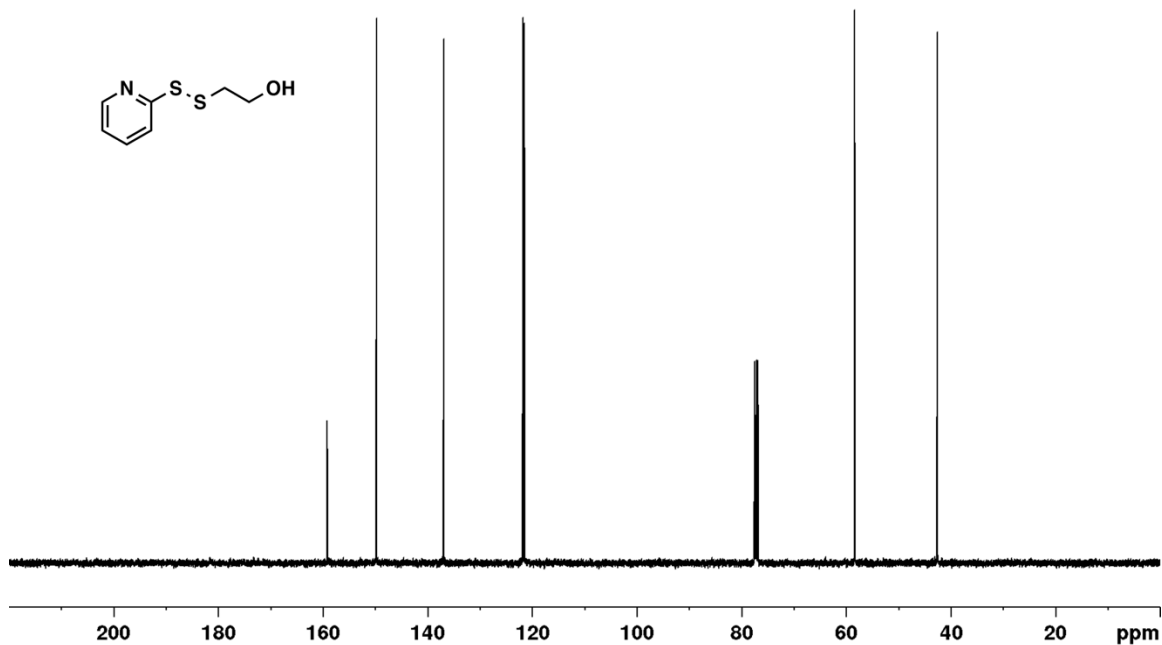


Figure 3.6. ¹³C NMR spectrum of PDSOH in CDCl₃.

Synthesis of Pyridyl Disulfide Ethyl Methacrylate (PDSMA)³⁷

PDSOH (500 mg, 2.67 mmol) was dissolved in anhydrous methylene chloride (9 mL) and transferred to an oven dried flask under argon. Triethylamine (1119 μL, 8.02 mmol) was then added to the flask. The reaction was cooled to 0 °C using an ice bath before adding methacryloyl chloride (784 μL, 8.02 mmol) drop wise over 5 minutes. The reaction was stirred for 18 hours, letting it warm to room temperature (21 °C). A color change from cloudy beige to dark brown was observed. The solution was transferred to a separatory funnel. The organic layer was washed with 1M HCl, 1M NaOH, and sat. NH₄Cl. The organic layer was then dried over MgSO₄ before reduce volume via rotary evaporator. The

crude product was purified via column chromatography (9:1 hexanes: ethyl acetate). The product had an R_f of 0.2 by TLC with these solvents and was obtained in 72% yield. NMR (400 MHz, CDCl_3) δ 8.47-8.43 (m, 1H, CHN), 7.70-7.65 (m, 1H, CHCHCHN), 7.64-7.58 (m, 1H, CHCN), 7.11-7.05 (m, 1H, CHCHN), 6.13-6.09 (m, 1H, CHHC), 5.58-5.55 (m, 1H, CHHC), 4.42-4.35 (t, 2H, CH_2O , $J = 6.3$ Hz), 3.10-3.05 (t, 2H, $\text{CH}_2\text{CH}_2\text{O}$, $J = 6.3$ Hz), 1.94-1.90 (3H, s, CH_3) ppm; ^{13}C NMR (400 MHz, CDCl_3) δ 167.0, 159.8, 149.8, 137.1, 136.0, 126.0, 120.9, 119.8, 62.4, 37.5, 18.31 ppm.

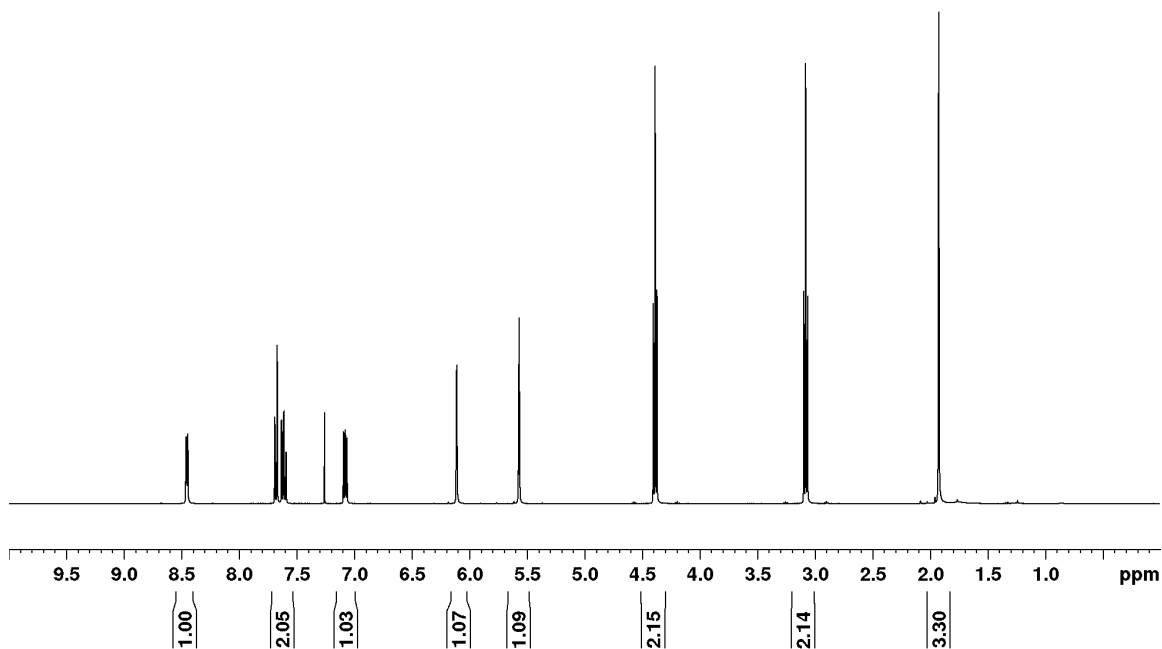


Figure 3.7. ^1H NMR spectrum of PDSMA in CDCl_3 .

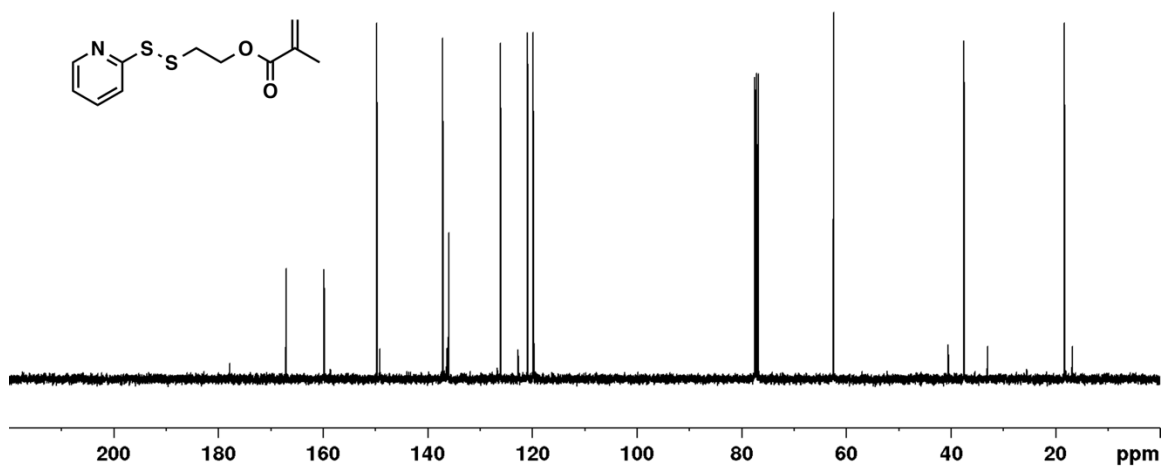


Figure 3.8. ¹³C NMR spectrum of PDSMA in CDCl₃.

Synthesis of Methacrylate Trehalose Monomer (TrMA)

Trehalose was added to 10 mL of anhydrous dimethylsulfoxide (DMSO) under argon and stirred 10-15 minutes to dissolve. Triethylamine was added to the stirring solution before adding methacrylic anhydride dropwise. The solution was stirred for 17 h at 21 °C during which time it turned a faint clear yellow color. To purify, the reaction solution was added to ice cold 8:2 hexanes/DCM (200 mL) and stirred for 5-10 minutes. The organic layer was decanted, leaving a sticky solid on the bottom of the flask, which was re-dissolved in deionized water (20 mL). The remaining organic solvent was removed via rotary evaporator prior to HPLC purification (C18 column, 20 ml/min flow, 10-60% MeOH, 20 min run). The product (C6 regioisomer), which had a retention time of 14 minutes, was

collected and lyophilized to yield a white, fluffy solid. NMR (500 MHz, D₂O) δ 6.06-6.01 (s, 1H, **CHHCCH**₃), 5.65-5.61 (s, 1H, **CHHCCH**₃), 5.08-5.06 (d, 1H, **OCHO** $J = 4$ Hz), 5.05-5.02 (d, 1H, $J = 4$ Hz, **OCHO**), 4.41-4.36 (m, 1H, trehalose protons), 4.28-4.22 (m, 1H, trehalose protons), 3.99-3.94 (m, 1H, trehalose protons), 3.78-3.60 (m, 5H, trehalose protons), 3.59-3.48 (m, 2H, trehalose protons), 3.46-3.39 (m, 1H, trehalose protons), 3.36 (t, 1H, $J = 9.3$ Hz, trehalose protons), 1.84-1.80 (s, 3H, **CH**₃) ppm; ¹³C NMR (500 MHz, DMSO-d₆) δ 166.9, 136.5, 126.3, 93.7, 93.6, 73.3, 73.1, 72.1, 72.0, 70.7, 70.5, 70.1, 64.3, 61.2, 18.4 ppm.

Table 3.2. Reagent amounts for TrMA syntheses.

Condition	Eq. Trehalose	Eq. TEA	Eq. Methacrylic Anh.	% Overall yield (% C6)
1:1	1	15	1	<5 (<1)
2:1	2	15	1	25 (16)
5:1	5	15	1	63 (42)

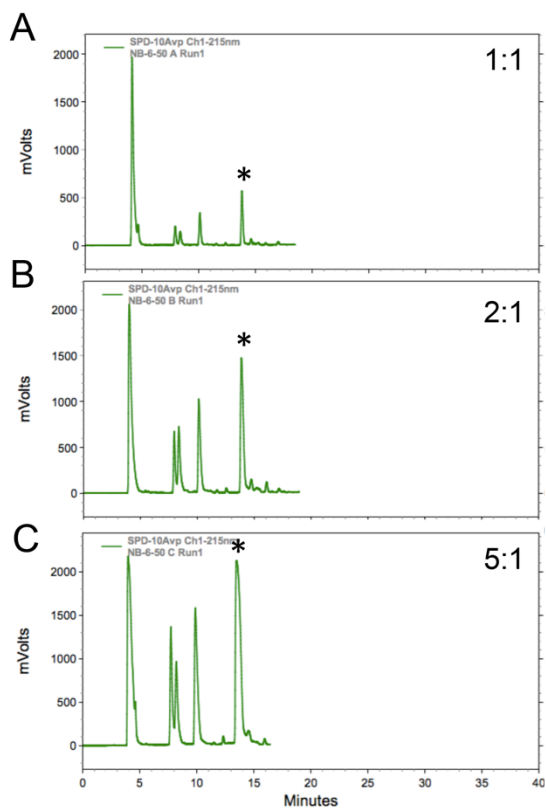


Figure 3.9. HPLC traces of TrMA at 1:1 (A), 2:1 (B), and 5:1 (C) trehalose to methacrylic anhydride. Unreacted trehalose elutes first, at 4 min, followed by the other TrMA regioisomers between 7 and 10 min. C6 TrMA regioisomer elutes at 14 min, as indicated by an asterisk.

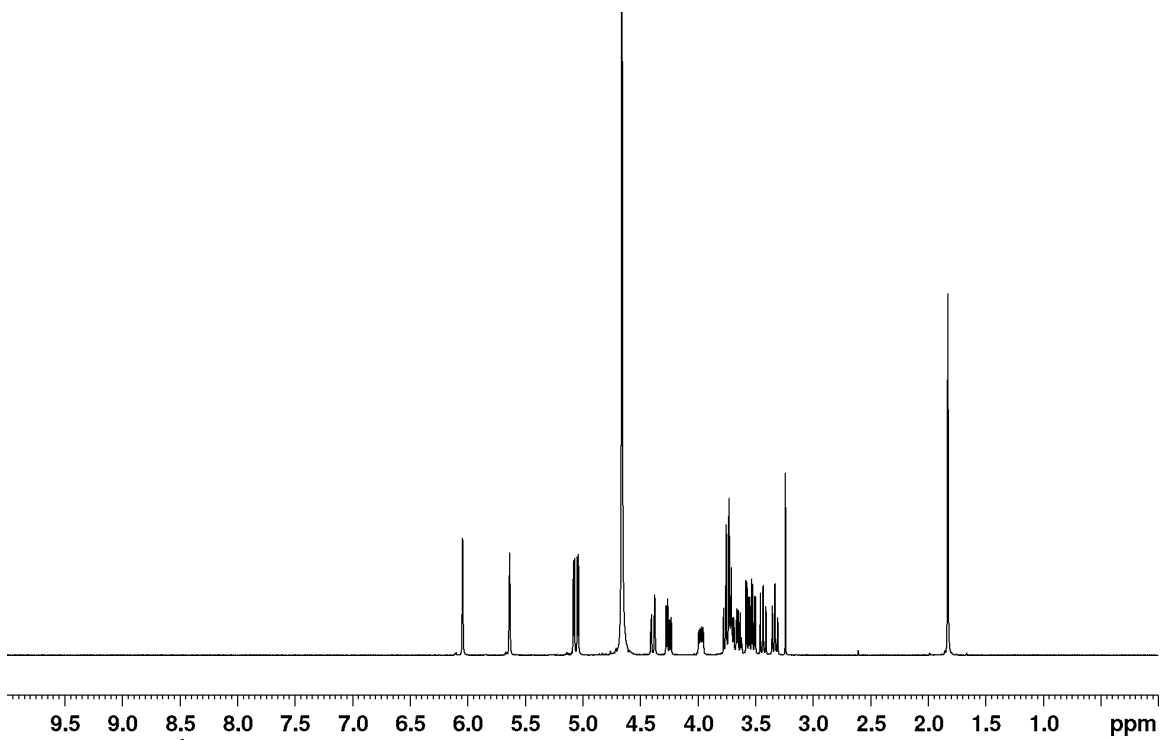


Figure 3.10. ^1H NMR spectrum of TrMA (C6) in D_2O .

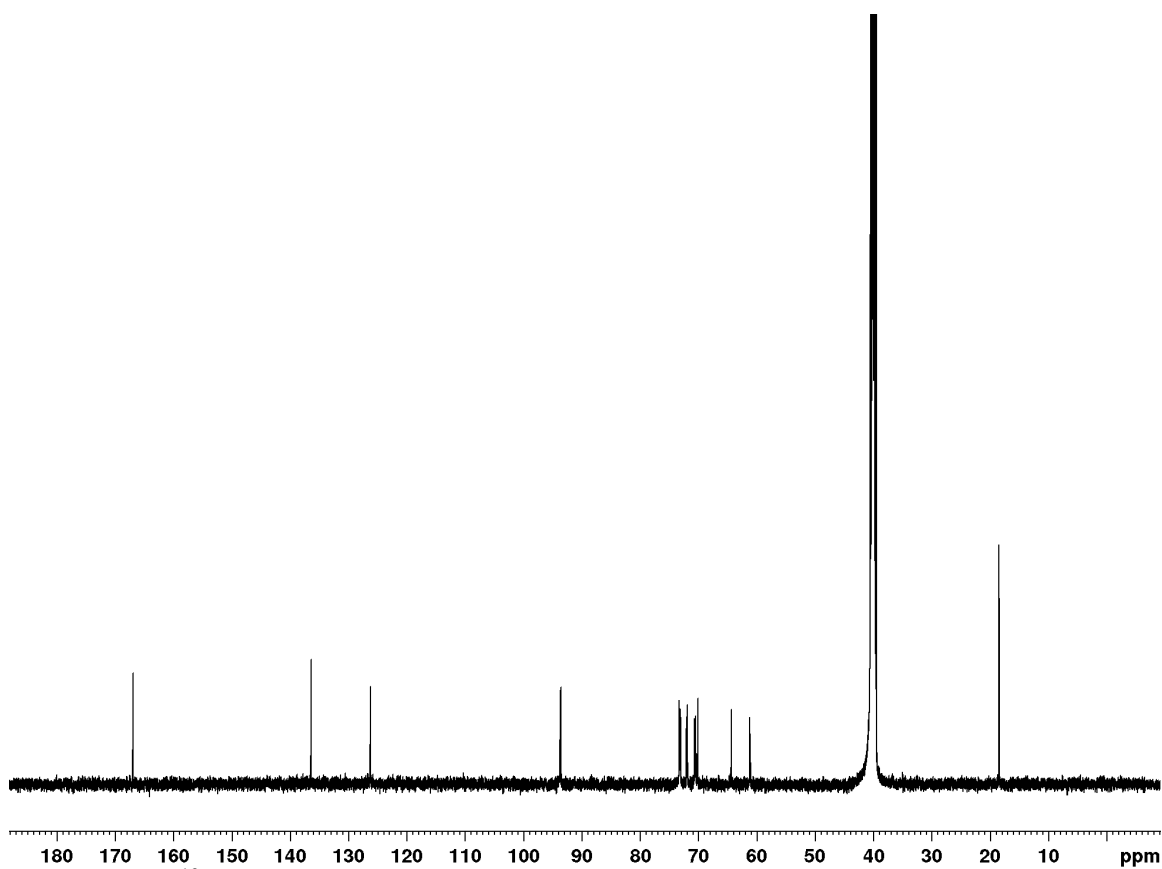


Figure 3.11. ^{13}C NMR Spectrum of TrMA (C6) in DMSO-d_6 .

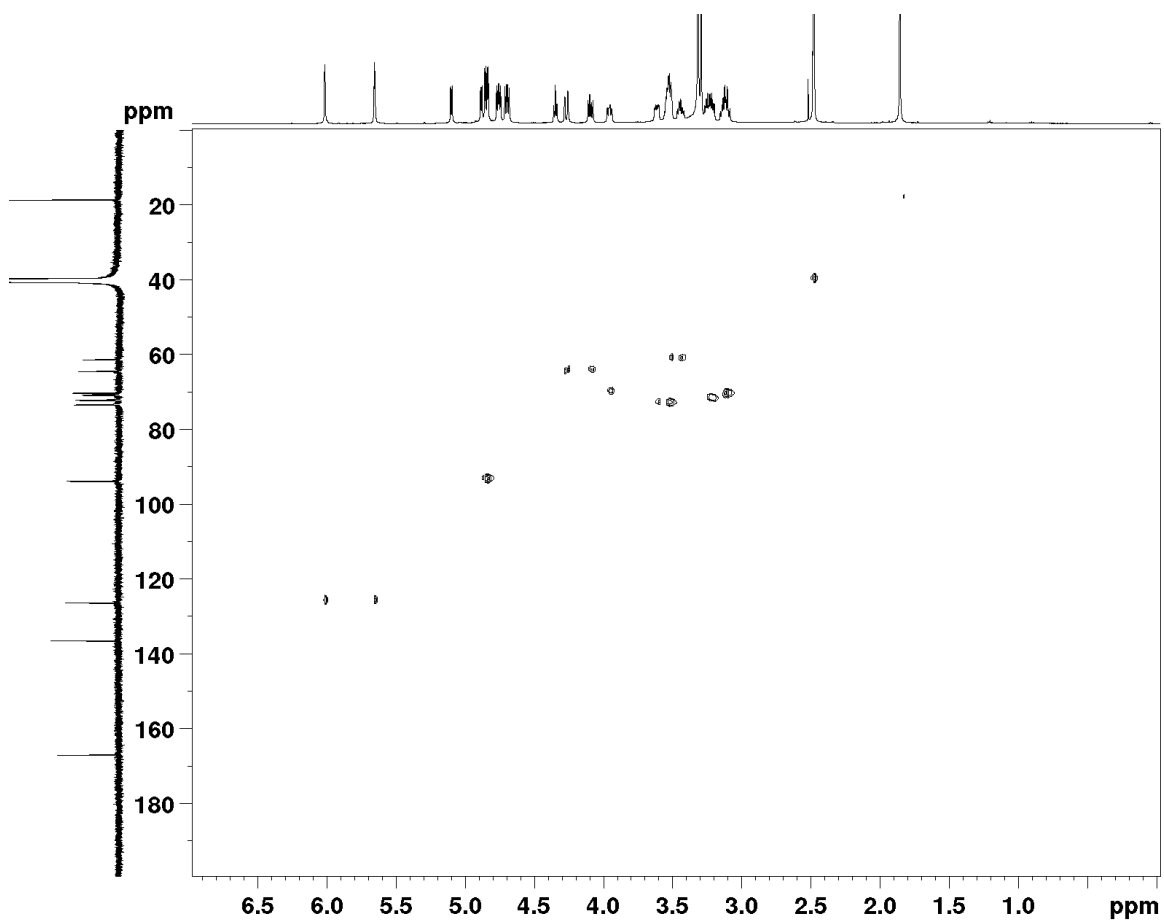


Figure 3.12. HSQC NMR spectrum of TrMA in DMSO-d₆.

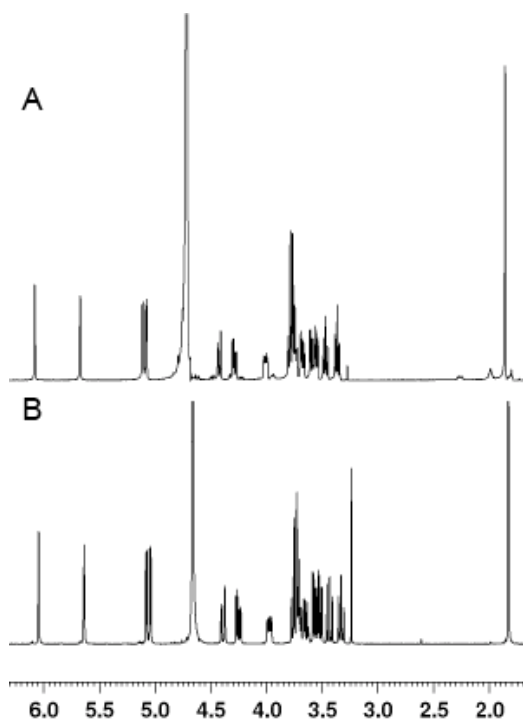


Figure 3.13. ^1H NMR spectra of C6 regioisomer of TrMA prepared from previously reported method (A) and method described in this manuscript (B) in D_2O .

Polymerization of TrMA and PDSMA

For 1:1 PDSMA:TrMA (C6 regioisomer) feed ratio, TrMA (65 mg, 0.16 mmol), PDSMA (40.4 mg, 0.16 mmol), and AIBN (0.65, 0.004 mmol) were dissolved in DMF (0.60 mL) to give a [TrMA]: [PDSMA]: [initiator] ratio of 40: 40: 1. For 1 PDSMA: 3 TrMA (C6 regioisomer) feed ratio, TrMA (60 mg, 0.15 mmol), PDSMA (12.4 mg, 0.05 mmol), and AIBN (0.4 mg, 0.002 mmol) were dissolved in DMF (0.46 mL) to give a [TrMA]: [PDSMA]: [initiator] ratio of 20: 60: 1. The solutions were degassed by freeze-pump-thawing five times before initiating polymerization at 70 °C in an oil bath. The polymerizations were stopped after 5 and 6 hours, respectively, by exposing the solutions to air. The resulting polymers were purified by precipitating once into ethyl acetate and

dialyzing against water using 3.5 kDa MWCO tubing for two days. The polymers were obtained in 60% and 70% yield after lyophilization, respectively. Monomer incorporation was calculated to be 0.8 to 1 and 1.7 to 1 by comparing the integration of the PDS protons (8.55-8.35 ppm, 1H) to the CH₃ protons (1.40-0.45 ppm) of the backbone by ¹H NMR. Analysis of polymers by GPC is tabulated in Table 3.1.

PDSMA-*co*-TrMA NMR (400 MHz, DMSO-d₆) δ 8.55-8.35 (CHN), 7.90-7.63 (aromatic), 7.28-7.14 (aromatic), 5.30-4.50 (trehalose OHs), 4.50-2.70 (CH₂CH₂O, CH₂CH₂O, CH₂CHO, CHOH), 2.30-1.40 (CH₂ polymer backbone), 1.40-0.45 (CH₃, polymer backbone) ppm.

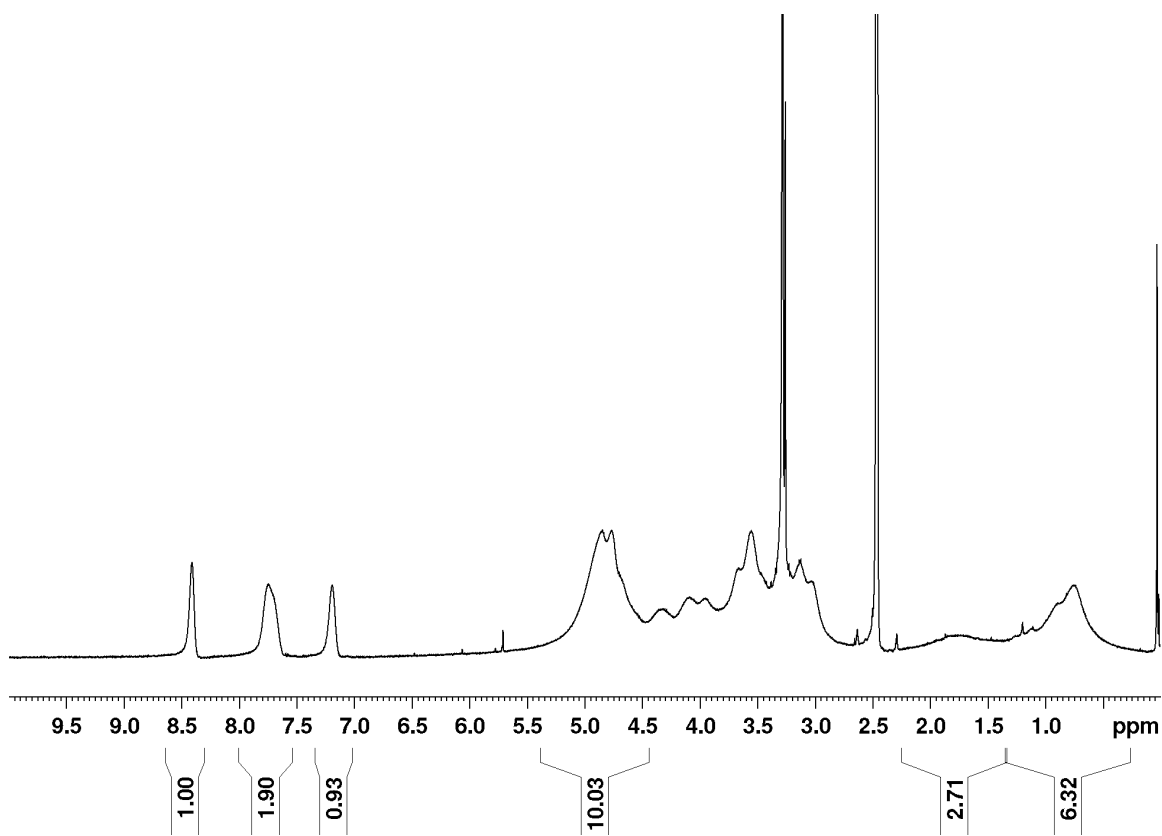


Figure 3.14. ¹H NMR spectrum of PDSMA₁-co-TrMA_{0.8} (1:1 feed ratio) acquired in DMSO-d₆.

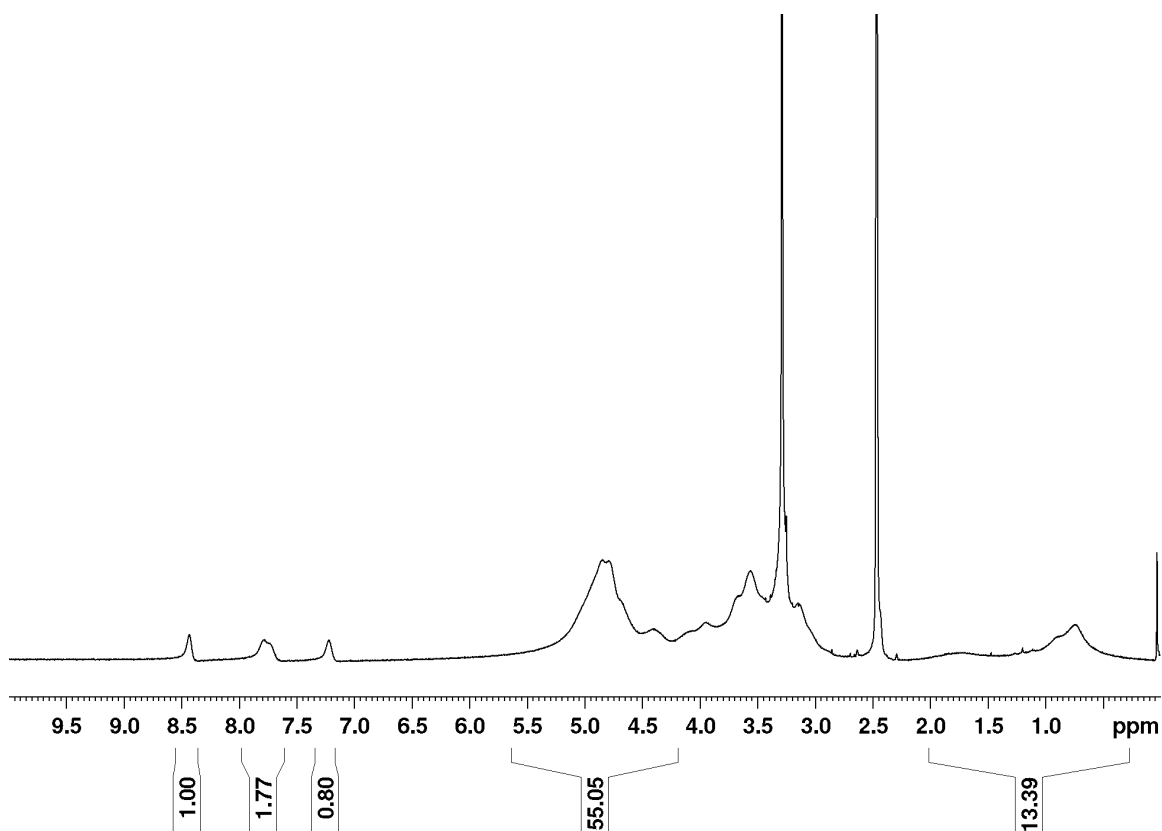


Figure 3.15. ^1H NMR spectrum of PDSMA₁-*co*-TrMA_{1.7} (1:3 feed ratio) acquired in DMSO- d_6 .

Representative Nanogel Formation with PEG-dithiol

PDSMA₁-*co*-TrMA_{0.8} (1 mg) was dissolved in 300 μL pH 7.4 PBS. A solution of 1 kDa PEG-dithiol (0.37 mg) was prepared separately in 10 mM HCl (200 μL). The two solutions were transferred to a glass vial equipped with a stir bar and mixed at 1000 rpm for 3 hours. The resulting nanogel solution was purified using 10 kDa MWCO centriprep filters.

TEM Imaging:

TEM images were acquired on a FEI T12 instrument using formvar/carbon coated grids (200 mesh, Cu, Ted Pella). Grids were glow discharged for 15 seconds. 2.5 μL of sample were placed on the grid and allowed to adhere for 5 minutes. After, the grids were washed 3x with 1 drop of water, followed by staining with uranyl acetate.

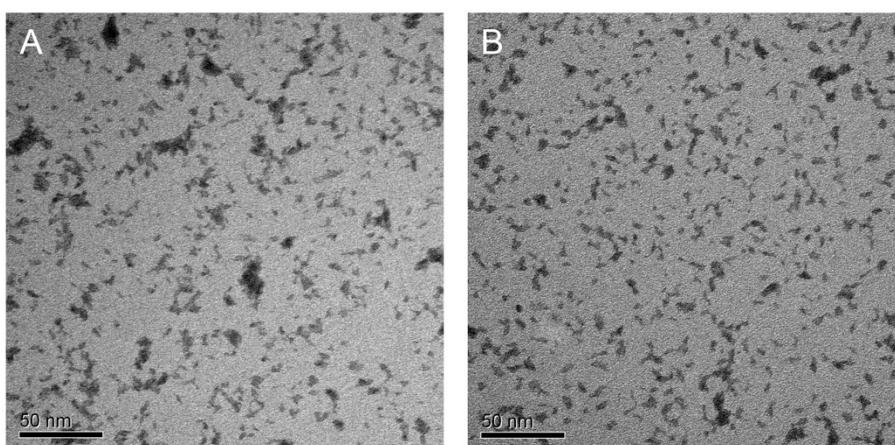


Figure 3.16. TEM Images of PDSMA₁-*co*-TrMA_{0.8} only (A) and of PDSMA₁-*co*-TrMA_{0.8} (+) TCEP.

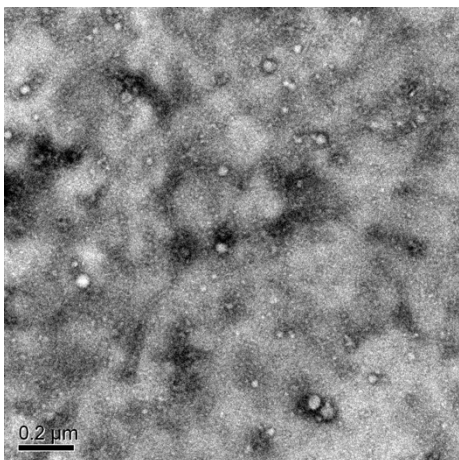


Figure 3.17. TEM image of PDSMA-*co*-TrMA nanogels formed at 10 mg/ml PDSMA₁-*co*-TrMA_{0.8} using PEG-dithiol as the cross-linker.

Protein Encapsulation

For lyz encapsulation:

PDSMA₁-*co*-TrMA_{0.8} (0.13 mg) or PDSMA₁-*co*-TrMA_{1.7} (0.19 mg) was dissolved in pH 7.4 PBS (50 μL). Lysozyme (0.05 mg) was separately dissolved in pH 7.4 PBS (10 μL). A 1 kDa PEG-dithiol solution was also prepared by dissolving the polymer (0.02 mg) in PBS (50 μL). PDSMA-*co*-TrMA and 100 μL 10 mM HCl were transferred to a glass vial equipped with a stir bar. The solution was stirred at 1000 rpm and then lyz and PEG solutions were transferred to the vial. The solution was stirred for 3 hours before SDS PAGE (180V, 45 min) analysis of the crude nanogel solutions.

For BSA encapsulation:

PDSMA₁-*co*-TrMA_{1.7} (0.19 mg) was dissolved in pH 7.4 PBS (50 μL). BSA (0.05 mg) was separately dissolved in PBS (10 μL). A 1 kDa PEG-dithiol solution was also prepared by dissolving the polymer (0.02 mg) in PBS (50 μL). PDSMA-*co*-TrMA and 100 μL 10 mM

HCl were transferred to a glass vial equipped with a stir bar. The solution was stirred at 1000 rpm and then BSA and PEG solutions were transferred to the vial. The solution was stirred for 3 hours before SDS PAGE (180V, 45 min) analysis of the crude nanogel solutions.

Cytotoxicity Studies

The cell compatibility of the polymer and nanogel components to HDFs was evaluated using a LIVE/DEAD viability/cytotoxicity assay (Invitrogen). A control containing no polymer or nanogel was also prepared. Cells were cultured using fibroblast basal medium supplemented with a low serum growth kit (ATCC) at 37 °C with 5% CO₂. The cells were seeded in 96-well plates (BD Falcon) at a density of 1000 cells per well. After 24 hours, culture media was replaced with 100 µL media containing PDSMA-*co*-TrMA or PEG cross-linked nanogels and the cells were incubated for 24 hours. Cells were then washed with pre-warmed Dulbecco's phosphate buffered saline (D-PBS) and stained with LIVE/DEAD reagents (2 µM calcein AM and 4 µM ethidium homodimer-1). Fluorescent images of each well were captured on an Axiovert 200 microscope. The number of live (green) and dead (red) cells were counted, and % cell viability was calculated by dividing the number of live cells by the total number of live and dead cells. All experiments were performed a total of three times. The data is presented by normalizing each set to the control containing no additive.

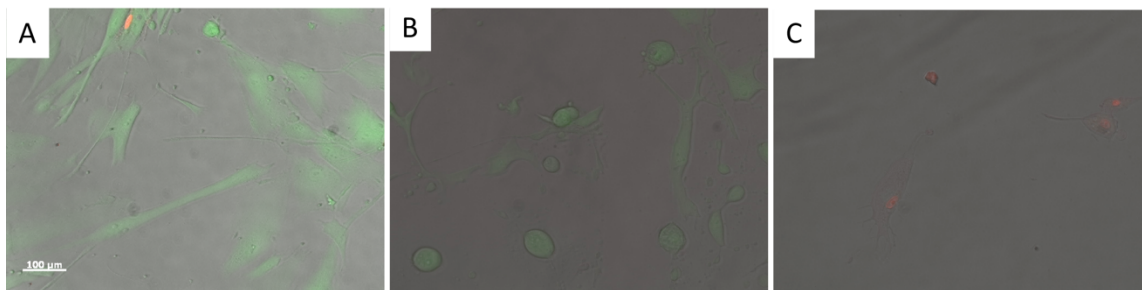


Figure 3.18. Characteristic fluorescence microscopy images of HDFs incubated with 1.0 (A), 2.5 (B) and 5.0 (C) mg/mL PDSMA_{1-co}-TrMA_{1.7} using LIVE/DEAD staining.

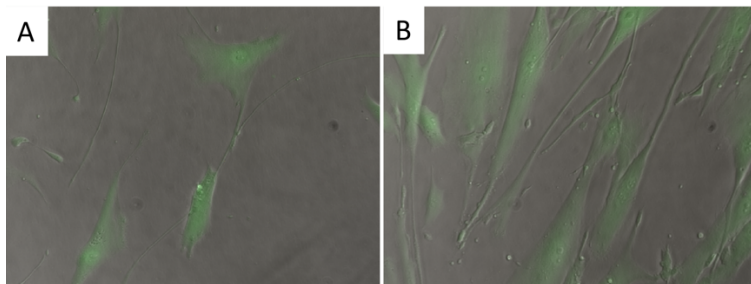


Figure 3.19. Characteristic fluorescence microscopy images of HDFs incubated with 0.5 (A) and 1.0 (B) mg/mL PDSMA_{1-co}-TrMA_{1.7} nanogels cross-linked with PEG-dithiol using LIVE/DEAD staining.

3. 5. References

1. Li, Y. L.; Maciel, D.; Rodrigues, J.; Shi, X. Y.; Tomas, H. *Chem. Rev.* **2015**, *115*, 8564-8608.
2. Mavila, S.; Eivgi, O.; Berkovich, I.; Lemcoff, N. G. *Chem. Rev.* **2016**, *116*, 878-961.
3. Chacko, R. T.; Ventura, J.; Zhuang, J. M.; Thayumanavan, S. *Adv. Drug Del. Rev.* **2012**, *64*, 836-851.
4. Molina, M.; Asadian-Birjand, M.; Balach, J.; Bergueiro, J.; Miceli, E.; Calderon, M. *Chem. Soc. Rev.* **2015**, *44*, 6161-6186.
5. Zhang, X. J.; Malhotra, S.; Molina, M.; Haag, R. *Chem. Soc. Rev.* **2015**, *44*, 1948-1973.
6. Rieger, J.; Gazon, C.; Charleux, B.; Alaimo, D.; Jerome, C. *J. Polym. Sci. A Polym. Chem.* **2009**, *47*, 2373-2390.
7. Shen, W. Q.; Chang, Y. L.; Liu, G. Y.; Wang, H. F.; Cao, A. N.; An, Z. S. *Macromolecules* **2011**, *44*, 2524-2530.
8. Thurmond, K. B.; Kowalewski, T.; Wooley, K. L. *J. Am. Chem. Soc.* **1996**, *118*, 7239-7240.
9. Rijcken, C. J.; Snel, C. J.; Schiffelers, R. M.; van Nostrum, C. F.; Hennink, W. E. *Biomaterials* **2007**, *28*, 5581-5593.
10. Ryu, J. H.; Chacko, R. T.; Jiwanich, S.; Bickerton, S.; Babu, R. P.; Thayumanavan, S. *J. Am. Chem. Soc.* **2010**, *132*, 17227-17235.
11. Ryu, J. H.; Jiwanich, S.; Chacko, R.; Bickerton, S.; Thayumanavan, S. *J. Am. Chem. Soc.* **2010**, *132*, 8246-8247.
12. Li, L. Y.; Raghupathi, K.; Yuan, C. H.; Thayumanavan, S. *Chem. Sci.* **2013**, *4*, 3654-3660.

13. Ventura, J.; Eron, S. J.; Gonzalez-Toro, D. C.; Raghupathi, K.; Wang, F.; Hardy, J. A.; Thayumanavan, S. *Biomacromolecules* **2015**, *16*, 3161-3171.
14. Dutta, K.; Hu, D.; Zhao, B.; Ribbe, A. E.; Zhuang, J. M.; Thayumanavan, S. *J. Am. Chem. Soc.* **2017**, *139*, 5676-5679.
15. Matsumoto, N. M.; Gonzalez-Toro, D. C.; Chacko, R. T.; Maynard, H. D.; Thayumanavan, S. *Polym. Chem.* **2013**, *4*, 2464-2469.
16. Wong, L. J.; Boyer, C.; Jia, Z. F.; Zareie, H. M.; Davis, T. P.; Bulmus, V. *Biomacromolecules* **2008**, *9*, 1934-1944.
17. Jia, Z. F.; Wong, L. J.; Davis, T. P.; Bulmus, V. *Biomacromolecules* **2008**, *9*, 3106-3113.
18. Jia, Z. F.; Liu, J. Q.; Boyer, C.; Davis, T. P.; Bulmus, V. *Biomacromolecules* **2009**, *10*, 3253-3258.
19. Li, X.; Chen, G. *J. Polym. Chem.* **2015**, *6*, 1417-1430.
20. Miura, Y.; Hoshino, Y.; Seto, H. *Chem. Rev.* **2016**, *116*, 1673-1692.
21. Sunasee, R.; Adokoh, C. K.; Darkwa, J.; Narain, R. *Expert. Opin. Drug. Del.* **2014**, *11*, 867-884.
22. Utama, R. H.; Jiang, Y. Y.; Zetterlund, P. B.; Stenzel, M. H. *Biomacromolecules* **2015**, *16*, 2144-2156.
23. Dag, A.; Lu, H. X.; Stenzel, M. *Polym. Chem.* **2015**, *6*, 7812-7820.
24. Chen, Y.; Espeel, P.; Reinicke, S.; Du Prez, F. E.; Stenzel, M. H. *Macromol. Rapid Commun.* **2014**, *35*, 1128-1134.
25. Teramoto, N.; Sachinvala, N. D.; Shibata, M. *Molecules* **2008**, *13*, 1773-1816.
26. Srinivasachari, S.; Liu, Y. M.; Zhang, G. D.; Prevette, L.; Reineke, T. M. *J. Am. Chem. Soc.* **2006**, *128*, 8176-8184.
27. Tale, S. R.; Yin, L. G.; Reineke, T. M. *Polym. Chem.* **2014**, *5*, 5160-5167.

28. Sizovs, A.; Xue, L.; Tolstyka, Z. P.; Ingle, N. P.; Wu, Y. Y.; Cortez, M.; Reineke, T. M. *J. Am. Chem. Soc.* **2013**, *135*, 15417-15424.
29. Yin, L. G.; Dalsin, M. C.; Sizovs, A.; Reineke, T. M.; Hillmyer, M. A. *Macromolecules* **2012**, *45*, 4322-4332.
30. Mancini, R. J.; Lee, J.; Maynard, H. D. *J. Am. Chem. Soc.* **2012**, *134*, 8474-8479.
31. Lee, J.; Lin, E. W.; Lau, U. Y.; Hedrick, J. L.; Bat, E.; Maynard, H. D. *Biomacromolecules* **2013**, *14*, 2561-2569.
32. Bat, E.; Lee, J.; Lau, U. Y.; Maynard, H. D. *Nat. Commun.* **2015**, *6*.
33. Lau, U. Y.; Saxer, S. S.; Lee, J.; Bat, E.; Maynard, H. D. *ACS Nano* **2016**, *10*, 723-729.
34. Pelegri-O'Day, E. M.; Maynard, H. D. *Acc. Chem. Res.* **2016**, *49*, 1777-1785.
35. Liu, Y.; Lee, J.; Mansfield, K. M.; Ko, J. H.; Sallam, S.; Wesdemiotis, C.; Maynard, H. D. *Bioconjugate Chem.* **2017**.
36. Lee, J.; Ko, J. H.; Lin, E. W.; Wallace, P.; Ruch, F.; Maynard, H. D. *Polym. Chem.* **2015**, *6*, 3443-3448.
37. Ghosh, S.; Basu, S.; Thayumanavan, S. *Macromolecules* **2006**, *39*, 5595-5597.
38. Sakurai, M., Biological Functions of Trehalose as a Substitute for Water. In *Water and Biomolecules*, Kuwajima, K.; Goto, Y.; Hirata, F.; Kataoka, M.; Terazima, M., Eds. Springer: 2009; pp 219-240.
39. Canfield, R. E. *J. Biol. Chem.* **1963**, *238*, 2698-&.
40. Wetter, L. R.; Deutsch, H. F. *J. Biol. Chem.* **1951**, *192*, 237-242.
41. Hirayama, K.; Akashi, S.; Furuya, M.; Fukuhara, K. *Biochem. Biophys. Res. Commun.* **1990**, *173*, 639-646.
42. Ge, S. R.; Kojio, K.; Takahara, A.; Kajiyama, T. *J. Biomat. Sci.; Polym. E.* **1998**, *9*, 131-150.

43. Yang, M.; Dutta, C.; Tiwari, A. *J. Phys. Chem. B* **2015**, *119*, 3969-3981.
44. Carpenter, J. F.; Manning, M. C.; Randolph, T. W. *Curr. Protoc. Protein Sci.* **2009**, *Supp.* 27, 4.6.1-4.6.6.

Chapter 4

Trehalose Glycopolymer Nanogels for the Stabilization and Release of a Peptide Hormone

4.1 Introduction

Glucagon is a peptide hormone that interacts with glucagon receptors in the liver to trigger the conversion of glycogen into glucose, raising blood glucose levels.¹ It is commonly used to raise blood sugar in hypoglycemic patients² and to treat bradycardia resulting from beta-blocker overdose; however, high cost, limited availability, and instability currently thwart its clinical potential.³ The clinical limitations of glucagon arise from two different reasons. First, the isoelectric point of glucagon is near seven, making it insoluble at neutral pH.⁴ Therefore, glucagon is typically dissolved in dilute HCl when administered to patients, which can cause discomfort. Second, any unused solution must be discarded immediately due to glucagon's instability.⁵ In solution, glucagon begins aggregating within hours, mainly through side chain deamidation,⁶⁻⁷ forming amyloid fibers that are cytotoxic and severely limit its clinical usefulness.⁸⁻⁹ In addition to instability in solution, peptides can also be susceptible to degradation in the solid state.¹⁰ Therefore, there is a great need to create stable glucagon formulations.

Several approaches have been developed to stabilize glucagon in solution. One strategy developed by DiMarchi and coworkers involved chemically modifying glucagon to change its isoelectric point, resulting in a more soluble analog at physiological pH.^{4, 11} Additionally, the same group developed glucagon prodrugs with increased stability that convert to active glucagon at slightly basic pH.¹² A second strategy to prevent glucagon aggregation involves the covalent attachment of poly(ethylene glycol) (PEG), known as PEGylation, to glucagon, which has been shown to improve glucagon stability to lyophilization cycles as well as resistance to adsorption onto surfaces.¹³⁻¹⁴ Further,

Anderson and coworkers showed that supramolecular PEGylation could stabilize glucagon against aggregation in solution.¹⁵ It is important to note that none of these reports mentions whether or not the conjugates retain bioactivity. Since glucagon interacts with its receptor on the cell surface,¹⁶ irreversibly attached conjugates may not be active because the steric shield of the polymer could prevent interactions between the small peptide ligand and receptor. Therefore, any conjugation strategy should include a responsive and reversible linkage between peptide and polymer to allow for glucagon release once at the site of interest. A final strategy to stabilize glucagon is through the addition of excipients, such as sugars, to the formulation. It has been shown that glucagon can be stabilized by lactose, trehalose, cyclodextrins, and hydroxyethyl starch.^{5, 17} It was noted that trehalose was particularly effective at stabilizing glucagon's secondary structure via hydrogen bonding.¹⁷

Trehalose is a commonly used excipient for many pharmaceutical formulations due to its stabilizing properties.¹⁸⁻¹⁹ Consisting of two alpha-linked glucose units, it is a non-reducing sugar commonly accumulated in large amounts by organisms with tolerance to desiccation, known as anhydrobiotes.²⁰ The addition of trehalose to living cells, such as *Saccharomyces cerevisiae*²¹ and primary human fibroblasts,²² has also been shown to confer desiccation tolerance. As an excipient, trehalose acts as a chemical chaperone and can reduce aggregation and adsorption of proteins because of its ability to stabilize biological structures.²³⁻²⁵ The protection by trehalose against additional environmental stressors, including freezing²⁶⁻²⁷, heating,²⁸ and oxidation²⁹ has also been reported. To date, three main hypotheses on the mechanism of trehalose stabilization have been proposed: vitrification, water replacement, and water entrapment.³⁰ These hypotheses suggest that

protein movement is restricted by glassy sugars,³¹ that the hydrogen bonding capabilities of trehalose could potentially displace water and stabilize protein structure,³¹ and that trehalose is able to trap water near the protein surface, stabilizing protein structure,³²⁻³³ respectively, all protecting proteins from damage. Current research suggests that potentially trehalose stabilization occurs due to a combination of the above three hypotheses.³¹

Our group and others have shown that trehalose is able to more effectively stabilize proteins and other biomacromolecules to environmental stressors as a polymer. We have prepared trehalose glycopolymers with various hydrophobic backbones containing trehalose side chains and have shown that when used as either excipients or conjugates, the glycopolymers can stabilize proteins to heat stress, lyophilization, and electron beam irradiation.³⁴⁻³⁸ Moreover, conjugation to insulin has shown to improve the circulation time *in vivo*.³⁹ Trehalose glycopolymers have also been utilized as hydrogels, allowing for protein stabilization as well as controlled release,⁴⁰⁻⁴¹ and to form serum stable nanocomplexes to stabilize nucleic acids.⁴²⁻⁴⁴

Herein, we report the use of trehalose glycopolymer nanogels to encapsulate, stabilize, and release glucagon. We chose to use copolymers containing trehalose and pyridyl disulfide (PDS) side chains to form redox-responsive nanogels via disulfide exchange in order to encapsulate glucagon. This design is based a similar nanogel system that we reported on in collaboration with the Thayumanavan group.⁴⁵ Because glucagon is administered via injection, we envision cargo release from our nanogels could occur either in the blood stream or upon arrival at the liver, both of which contain millimolar levels of

glutathione (GSH).⁴⁶⁻⁴⁷ In order to maximize encapsulation efficiency, glucagon was modified with two thiol groups, allowing us to use the therapeutic payload as the cross-linker, eliminating the need to add any additional reagents. The synthesis and characterization of modified glucagon and resulting nanogels, as well as stabilization and release will be described below.

4.2 Results and Discussion

4.2.1. Glucagon Modification

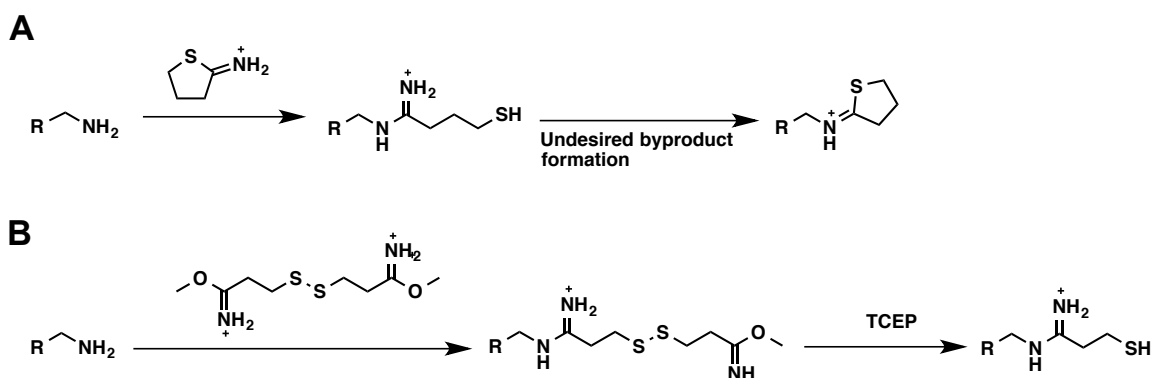
Trehalose copolymers were synthesized using methacrylate functionalized trehalose (TrMA) and pyridyl disulfide ethyl methacrylate (PDSMA) using free radical polymerization conditions as described in Chapter 3. Polymers containing 1:1 and 1:2 ratios of PDS and trehalose side chains were prepared, called PDSMA_{1-co}-TrMA_{0.8} and PDSMA_{1-co}-TrMA_{1.7}, respectively. We first explored non-covalent encapsulation of cargo using our PDSMA-co-TrMA nanogels and found that the resulting encapsulation efficiency was quite low (see Chapter 3), prompting us to covalently conjugate glucagon to our polymeric nanogels. For this application, the ideal encapsulation strategy would allow for glucagon to remain attached to the nanogels through covalent yet reversible attachment until release is triggered by an external stimulus, such as GSH. Since native glucagon does not contain any cysteines, thiol groups needed to be installed through modification of amino acid side chains. It has previously been shown that preservation of the positive charge at lysine 12 is essential for binding and glucagon activity, yet there is some tolerance for structural modification, as changing this residue to arginine retained up

to 50% activity *in vivo*.⁴⁸ Additionally, modification of the N terminal histidine either by acetylation or methylation has minimal effect on glucagon efficacy.⁴⁸ Therefore, we were interested in using a modification strategy that would retain the positive charges of amines while simultaneously installing thiol groups at these sites that might tolerate minor modification. Because glucagon has two amine groups in its structure, at the N terminus and lysine 12, we aimed to modify both in order to use the peptide as a cross-linker.

Initially, glucagon was modified with 2-iminothiolane (2-IT), resulting in the formation of an amidine group linked to a thiol (Scheme 4.1A). While thiolation attempts were successful, we observed the formation of a cyclic non-thiol byproduct via LCMS that has also been reported in the literature (Figure 4.10).⁴⁹ Because this byproduct forms after thiolation, we attempted to trap the thiol prior to cyclization using both PDS and PDSMA-*co*-TrMA, which was monitored using Ellman's assay (Figure 4.11). After mixing glucagon and 2-IT, an initial increase in absorbance was observed that suggested thiolation was occurring, while a decrease in signal after addition of PDS or polymer indicated the thiols were being consumed. While this approach was successful, exact reaction conditions, such as concentration and extent of modification, were difficult to control.

Switching to dimethyl-3,3'-dithio-bis(propionimidate) (DTBP) as the thiolating reagent allowed for efficient modification of glucagon under mild conditions without noticeable side reactions (Scheme 4.1B).⁵⁰⁻⁵¹ While DTBP is less commonly used than 2-IT, it has been found to be biocompatible⁵² and has previously been used to create pluronic-horse radish peroxidase conjugates for enhanced cellular delivery.⁵³ Moreover, DTBP is a dimeric disulfide that can be used as a built in protecting group when the reagent is used in

excess. Glucagon thiolation with DTBP was monitored using Ellman's assay and LCMS. Because TCEP is added after modification to reduce disulfides, the wash solutions after reduction were also analyzed by Ellman's assay (Figure 4.12). The lack of absorbance increase for the wash solution indicated the modification of glucagon with DTBP and subsequent reduction were successful. Via LCMS, we were able to monitor the disappearance of glucagon ($m/z = 1161$, $z = 3$) and the appearance of two new peaks, $m/z = 1191$ and 1219 ($z = 3$), corresponding to singly and doubly modified glucagon, respectively, after modification with DTBP and reduction with TCEP (Figure 4.13). We anticipated that the mixture of products would allow us to link glucagon to our polymers both as a cross-linker and conjugate by mixing PDSMA-*co*-TrMA with thiolated glucagon at acidic pH (Figure 4.1).



Scheme 4.1. Thiolation with 2-IT (A) and DTBP (B).

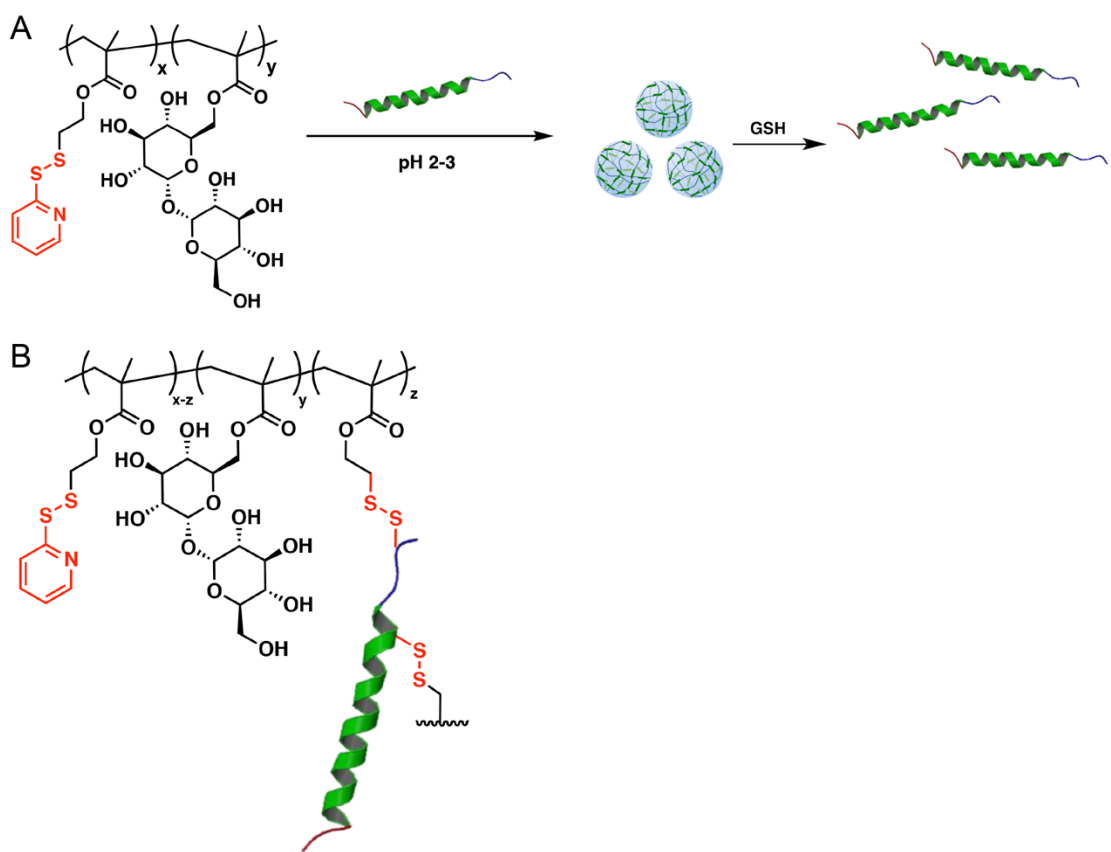


Figure 4.1. General glucagon nanogel formation and release (A) and representative structure of glucagon cross-linked PDSMA-*co*-TrMA (B).

4. 2. 2. Nanogel Synthesis and Characterization

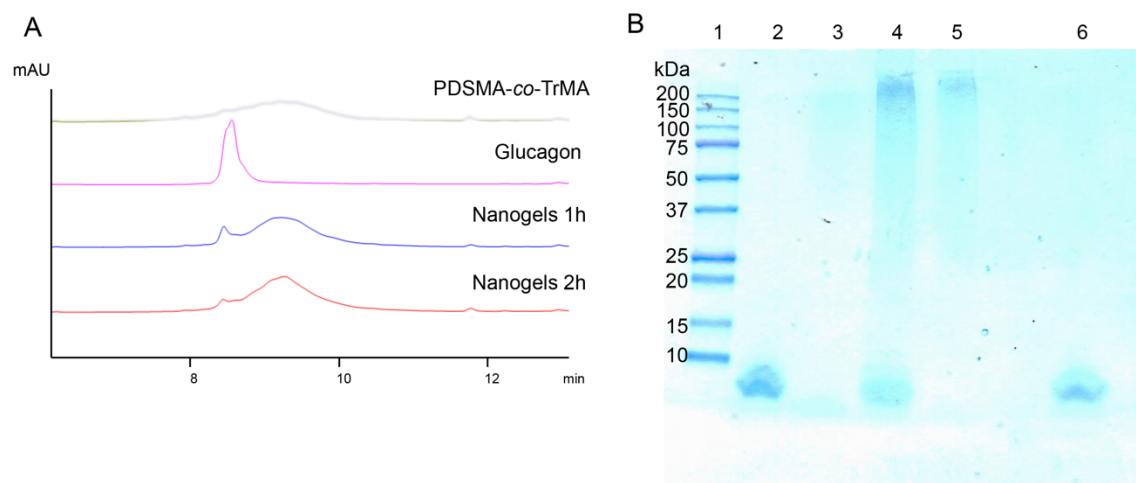


Figure 4.2. Glucagon conjugation to PDSMA₁-co-TrMA_{0.8} was monitored via HPLC at 280 nm (A) and SDS-PAGE (B). Lane 1: protein ladder; lane 2: thiolated glucagon; lane 3: PDSMA₁-co-TrMA_{0.8}; lane 4: crude nanogel; lane 5: purified nanogel; lane 6: nanogel from lane 5 reduced with TCEP (10 mg/mL).

Conjugation of glucagon to PDSMA₁-co-TrMA_{0.8} was initially monitored using HPLC (Figure 4.2A). Polymer and thiolated glucagon were analyzed separately before mixing the two components and taking measurements at one and two hour time points. After one hour, a significant decrease in the glucagon peak intensity was observed as well as a narrowing of the polymer peak, suggesting peptide and polymer were reacting. Narrowing of the polymer peak indicated that cross-linking may have occurred, contracting the overall polymer structure. After two hours, the glucagon peak was almost completely consumed. Moreover, an increase in polymer peak height was also observed, suggesting the successful conjugation of glucagon to PDSMA-co-TrMA. To confirm glucagon

conjugation to our polymer, we utilized SDS-PAGE to analyze the individual components and resulting glucagon-nanogel conjugate (Figure 4.2B). Lane 2 contained only thiolated glucagon which appeared below the 10 kDa band after staining with Coomassie; this shift makes sense since the molecular mass is 3.7 kDa (doubly thiolated). Lane 3 contained PDSMA-*co*-TrMA and could be seen as a very faint high molecular weight smear. Glucagon and polymer were mixed together for two hours before running SDS-PAGE analysis, as shown in lane 4. The appearance of an intense high molecular weight band was observed as well as a decrease in glucagon band intensity, suggesting the peptide successfully reacted with the polymer. After purification, as shown in lane 5, only the high molecular weight band corresponding to nanogel remained. The purified glucagon-nanogel conjugate was then subjected to reducing conditions (10 mg/mL TCEP), as shown in lane 6. Upon reduction of the disulfide cross-links, glucagon was released, as indicated by the reappearance of an approximately 3.7 kDa band and the disappearance of the nanogel band.

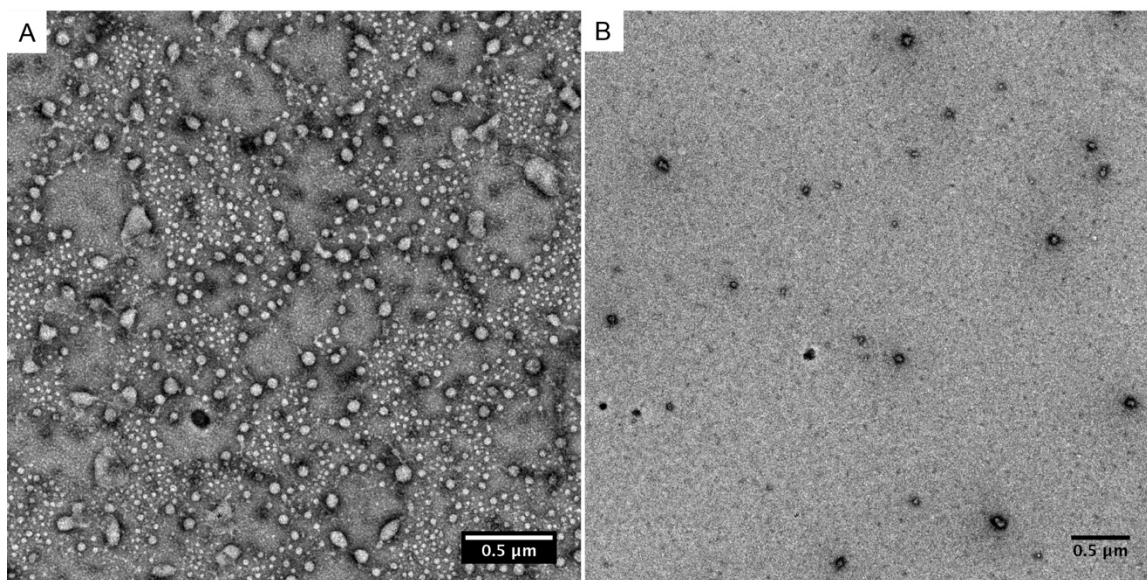


Figure 4.3. TEM images of glucagon nanogels formed at 2 mg/mL PDSMA_{1-co}-TrMA_{0.8} (A) and 0.65 mg/mL PDSMA_{1-co}-TrMA_{0.8} (B).

After confirming that thiolated glucagon could be used to assemble and cross-link PDSMA_{1-co}-TrMA_{0.8} nanogels, the effect of polymer concentration on nanogel morphology was assessed. We found that using 2 mg/mL PDSMA-*co*-TrMA to form nanogels resulted in fairly disperse nanogels ranging from 10-100 nm in diameter by transmission electron microscopy (TEM) (Figure 4.3A). When PDSMA-*co*-TrMA concentration was decreased to 1.0-0.5 mg/mL, a decrease in particle size and dispersity was observed (Figure 4.3B). Particles observed via TEM corresponded well to dynamic light scattering (DLS) results, which indicated that nanogels were approximately 9 nm in diameter (Figure 4.4-Figure 4.5). We hypothesized that at higher concentrations, thiolated glucagon could be able to interact with multiple polymers, potentially even linking several smaller nanogels together, accounting for the observed aggregates and dispersity.

Concentrations lower than 0.5 mg/mL were low yielding and therefore not investigated further.

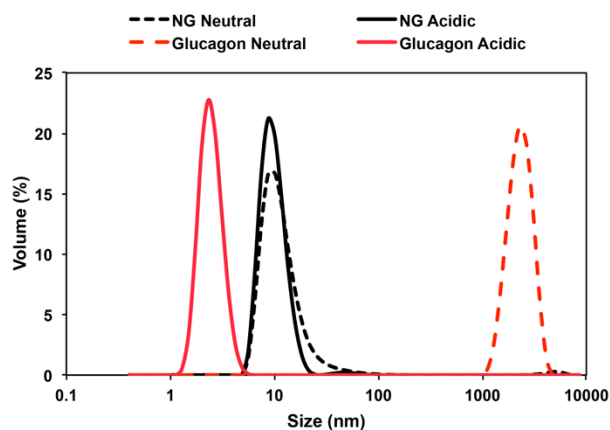


Figure 4.4. DLS data of glucagon and PDSMA₁-*co*-TrMA_{0.8} nanogels at acidic and neutral pH.

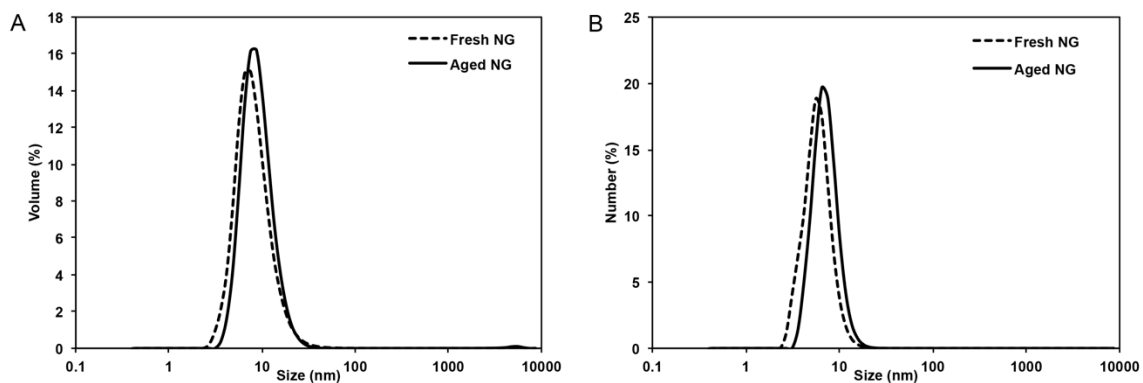


Figure 4.5. Volume (A) and number (B) DLS measurements of glucagon nanogels formed with PDSMA₁-*co*-TrMA_{1.7} at 0 and 5 days in solution.

Additionally, the effect of cross-linking density and trehalose content on glucagon encapsulation was investigated using two PDSMA-*co*-TrMA polymers, PDSMA_{1-*co*}-TrMA_{0.8} and PDSMA_{1-*co*}-TrMA_{1.7}, containing different ratios of PDSMA and TrMA. Two different ratios of polymer to glucagon were also explored when forming nanogels: 5:1 and 10:1 with respect to thiol groups. A 5:1 thiol ratio of PDSMA_{1-*co*}-TrMA_{0.8} to glucagon would contain approximately equal amounts by weight of polymer and peptide, indicating high load capacity of the gels. On average, nanogels were obtained in 60-70% yield after purification. Nanogel conjugation was quantified by comparing the amount of remaining glucagon in the crude nanogel solutions to a thiolated glucagon control (Table 4.1). Interestingly, it was found that using 5:1 thiol ratio of polymer to glucagon resulted in higher yielding conjugations than nanogels prepared at a 10:1 thiol ratio. Moreover, after examining nanogels by TEM, 5:1 nanogels were more uniform and well defined than 10:1 nanogels (Figure 4.14). This could be because large excess of polymer could effectively cap thiol groups on glucagon with a single chain, resulting in uncross-linked glucagon conjugates instead of nanogels. It was also observed that nanogels formed using PDSMA_{1-*co*}-TrMA_{0.8} retained more glucagon than PDSMA_{1-*co*}-TrMA_{1.7}, most likely due to the higher density of PDS groups capable of conjugating to glucagon. At 10:1 PDSMA_{1-*co*}-TrMA_{1.7} to glucagon, only a few irregular nanogels were observed by TEM, and the conjugation yield could not be calculated because no defined nanogel band was obtained by SDS PAGE (Table 4.1). Therefore, we chose to use nanogels prepared at the 5:1 ratio for the majority of subsequent experiments.

4. 2. 3. Nanogel Solubility

We were interested in studying the solubilizing effect of our glucagon nanogel conjugates because glucagon is not soluble at neutral pH, making administration to patients challenging.⁴ Using DLS, the particle sizes of unencapsulated glucagon and glucagon nanogels were measured at neutral and acidic pH (Figure 4.4). As expected, analysis of glucagon solubilized in 10 mM HCl showed small particles approximately 2-3 nm in diameter. When glucagon was neutralized however, a dramatic shift to 2000-3000 nm particles was observed, which was additionally confirmed visually as glucagon precipitated out of solution. Glucagon nanogels, on the other hand, did not change in size in either acidic or neutral pH. Under both conditions, approximately 9 nm particles were observed, indicating that encapsulated glucagon does not aggregate or precipitate out of solution with pH change, which was also confirmed visually as the solution remained homogeneous and clear.

4. 2. 4. Nanogel Stability

One of the main challenges preventing broader clinical application of glucagon is its instability. Upon dissolution, fibrillation, which is associated with cytotoxicity and loss of activity, is observed within hours.⁵⁴ Therefore, when assessing glucagon stability, extent of fibrillation is frequently used as an indirect measure of retention of activity.¹³ The stabilizing effect of PDSMA-*co*-TrMA nanogels on glucagon was investigated using TEM imaging (Figure 4.6). Nanogel solutions were prepared using PDSMA₁-*co*-TrMA_{0.8}, imaged, reduced, and then imaged at 0 (just after reduction) and 24 hours. Immediately after reduction with TCEP, no nanogels, fibrils, or aggregates were observed (Figure 4.6B).

This indicates that while encapsulated, glucagon does not aggregate, suggesting the nanogels are able to stabilize the peptide cargo. After letting the reduced solution sit at 22 °C for 24 hours, fibrils and aggregates were clearly observed (Figure 4.6C). This indicates that glucagon was successfully released under reducing conditions and begins to aggregate when no longer bound inside the nanogels. The experiment was repeated over a longer time period switching to the higher trehalose content polymer to maximize stabilization, reducing and imaging nanogel solutions after two days in solution and re-imaging after three additional days (Figure 4.15). These results were similar to the first experiment, which perhaps may be even more significant, since no glucagon aggregates were observed when imaged directly after release from aged nanogels after the nanogels were kept two days in solution. After re-imaging the released nanogel solution at day 5, fibril formation was observed. Since we typically observed glucagon fibrillation within less than 24 hours, this indicated to us that the nanogels were able to stabilize glucagon up to at least two days.

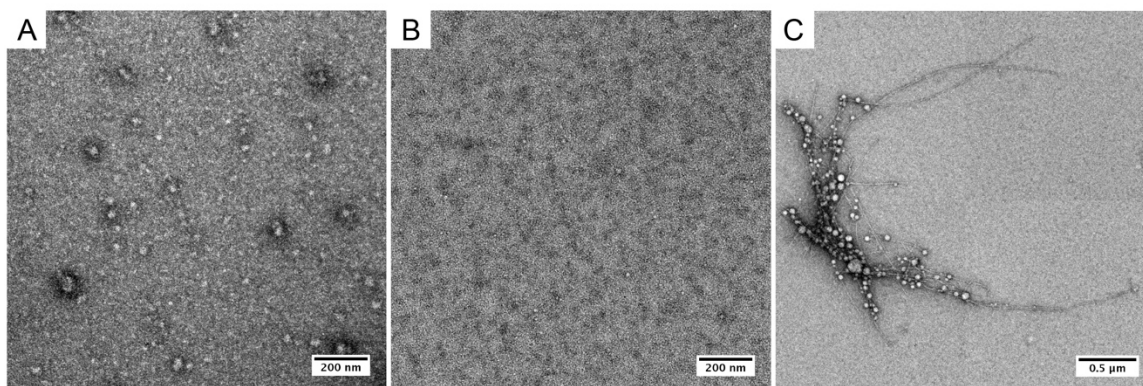


Figure 4.6. TEM images of PDSMA₁-*co*-TrMA_{0.8} glucagon nanogels in solution (A), immediately after reduction (B), and 24h after reduction (C).

To further assess stability, PDSMA_{1-co}-TrMA_{1.7} NGs were examined by DLS after five days in solution, and no significant shift in size was observed compared to fresh NGs, again indicating that they remained stable for the duration of the experiment (Figure 4.5). However, TEM imaging of aged PDSMA_{1-co}-TrMA_{1.7} nanogels indicated that several small aggregates had started to form that were not indicated by the DLS data (Figure 4.7). While these aggregates looked different compared to the fibrils imaged in previous experiments, it is known that glucagon goes through several different stages of fibrillation, and this type of structure has been reported previously.⁵⁴ It is important to note that the extent of fibrillation is drastically slowed compared to unencapsulated glucagon which is completely fibrillated within 24 hours. The NGs used for this experiment contained approximately 1:1 (PDSMA_{1-co}-TrMA_{0.8}) or 2:1 (PDSMA_{1-co}-TrMA_{1.7}) polymer to glucagon by weight, so higher polymer concentration or molecular weight might be able to slow aggregation more effectively by acting as an even larger steric shield.

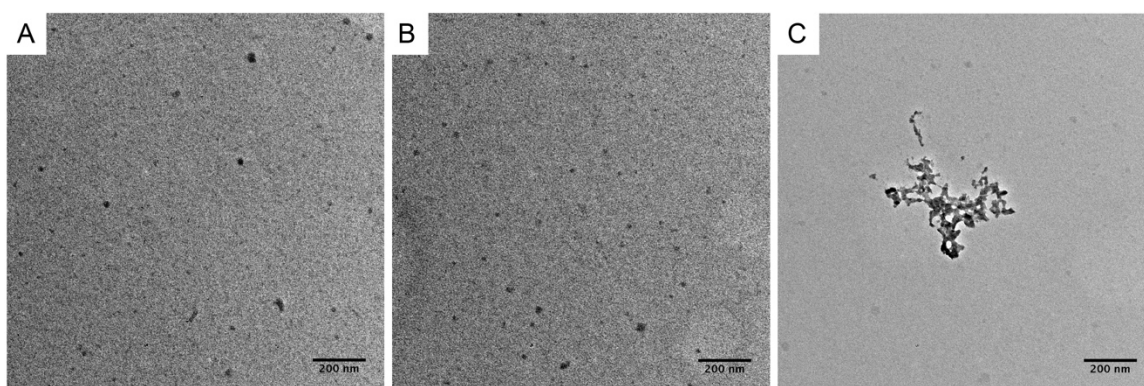


Figure 4.7. TEM images of PDSMA_{1-co}-TrMA_{1.7} glucagon nanogels on day 0 (A) and day 5 (B). In addition to nanogels, small glucagon aggregates were observed in solution after 5 days (C).

Long-term PDSMA_{1-co}-TrMA_{1.7} NG stability was also assessed using native PAGE to ensure glucagon was not released over time through hydrolysis (Figure 4.8). We also compared native and thiolated glucagon (lanes 1-2) and observed no shift in the bands, indicating the two compounds run comparably on the gel. No differences were observed when comparing fresh nanogels and nanogels aged in pH 7.4 PBS for five days (lanes 4-5), and the lack of a glucagon band indicated nonspecific release was not occurring. After addition of reducing agent, a single band corresponding to glucagon was obtained (lane 7), comparable to the result observed via SDS-PAGE, indicating successful nanogel degradation and glucagon release.

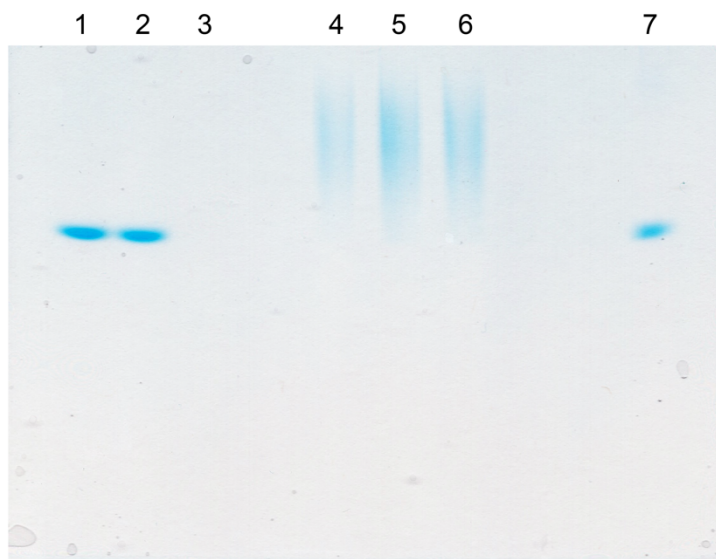


Figure 4.8. Native PAGE of glucagon and nanogels. Lane 1: glucagon; lane 2: thiolated glucagon; lane 3: PDSMA_{1-co}-TrMA_{1.7}; lane 4: glucagon- PDSMA_{1-co}-TrMA_{1.7} nanogel; lane 5: glucagon- PDSMA_{1-co}-TrMA_{1.7} nanogel aged 5 days; lane 6: glucagon- PDSMA_{1-co}-

co-TrMA_{1.7} nanogel after lyophilization; lane 7: glucagon- PDSMA₁-*co*-TrMA_{1.7} nanogel from lane 5 reduced with TCEP (10 mg/mL).

We also subjected our nanogel solutions to a lyophilization cycle, and by native PAGE no glucagon release after reconstitution in buffer was observed (Figure 4.8, lane 6). However, TEM imaging revealed the formation of micron-sized aggregates, indicating the nanogels were not stable (Figure 4.16). While trehalose polymers have been used previously to create particles stable to lyophilization,⁴² the high loading of our nanogels may limit the polymer's stabilizing effects to lyophilization. Also, as discussed previously, optimization with larger polymers or different polymer to glucagon ratios may yield more promising results for lyophilization. Additionally, glucagon is currently commercially available as a lyophilized powder that must be reconstituted before administration and is considered more stable to lyophilization than when in solution.⁵⁵ Therefore, most research efforts are focusing on developing liquid stable glucagon formulations.

4. 2. 5. Bioactivity Studies

In vitro glucagon activity studies were carried out to assess the extent of bioactivity of thiolated glucagon compared to native glucagon (Figure 4.9). A commercially available assay kit containing hematopoietic rat cells expressing human glucagon receptor on the cell surface was utilized for these experiments. Using a four-parameter logistic fit, we obtained an EC₅₀ value of 113 ± 1 nM ($R^2 = 0.99$) for native glucagon and a value of 126 ± 10 nM ($R^2 = 0.98$) for thiolated glucagon (Figure 4.9A-B). While this value for glucagon is approximately ten-fold higher than what has been reported previously using a different

assay,⁵⁶ license restrictions on the assay kit prevented us from passaging the cells and required us to assay the thawed cells, which retained rounded morphologies for the duration of the experiment, indicating they may not be healthy. However, it is important to note that the values for both unmodified and modified peptides are not statistically different ($p > 0.05$), suggesting that the thiolated compound retains bioactivity.

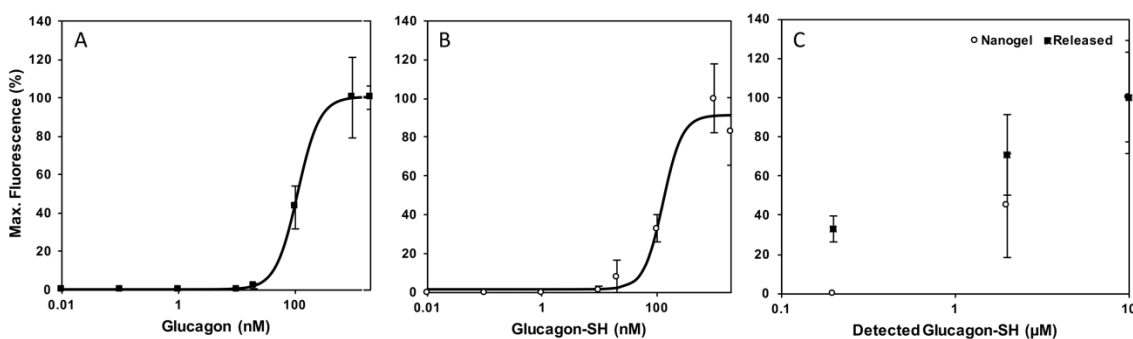


Figure 4.9. Dose response curves of glucagon (A) and thiolated glucagon (B) using Chem-1 cells expressing human glucagon receptor. A signal in response to PDSMA₁-co-TrMA_{1.7} glucagon nanogels was also measured (C). Calculated EC₅₀ values of 113 ± 1 nM ($R^2 = 0.99$) and 126 ± 10 nM ($R^2 = 0.98$) for native glucagon and thiolated glucagon, respectively, were obtained.

Additionally, glucagon nanogels also produced a positive response, suggesting the peptide is able to interact with its receptor even when covalently bound to polymer (Figure 4.9C). While it is possible that the nanogels were taken up by cells and cleaved by GSH present inside the cell,⁵⁷ the released glucagon would need to be expelled from the cells in order to act on its extracellular receptor.⁵⁸ Because the signal response was observed within

seconds of compound addition, and endo- and exocytosis of nanoparticles has been reported to occur within minutes or hours,⁵⁹ we believe the signal we observed was elicited by the intact glucagon nanogels. Further, as mentioned previously, thiolation of glucagon resulted in a mixture of singly and doubly modified peptide and we anticipate that singly thiolated glucagon could be covalently conjugated to the outside of the nanogel, allowing for interaction with the receptor. After reduction of glucagon nanogels with 10 mM DTT, a stronger signal was observed, corresponding to release of glucagon from the interior of the nanogel, further strengthening our hypothesis. These results demonstrated that we successfully synthesized a bioactive glucagon analog with reactive functional handles for easy conjugation and stabilization. Further studies will be undertaken by the Maynard lab to examine the effect of polymer size and number of conjugation sites on glucagon stability and efficacy, as well as *in vivo* bioactivity characterization.

4.3. Conclusions

We described the use of a modified glucagon to assemble and cross-link PDSMA-*co*-TrMA polymers into nanogels without the need for any additional reagents or cross-linkers. Uniform nanogels approximately 9 nm in diameter were obtained with conjugation efficiency greater than 80%. Moreover, glucagon nanogel conjugates exhibited superior stability in solution to aggregation compared to unencapsulated glucagon with the additional benefit of being soluble at both acidic and neutral pH. Glucagon release was observed under mild reducing conditions, suggesting that this encapsulation strategy may

be a useful delivery vehicle. In addition to presenting a stabilizing nanogel system, we also synthesized a novel modified glucagon compound with a reactive functional handle. The bioactivity of this modified glucagon compound was found to be comparable to native glucagon, suggesting it may be a promising candidate for further *in vivo* study. Additionally, the glucagon within the nanogel was also found to retain bioactivity when conjugated and upon release.

4. 4. Experimental

4. 4. 1. Materials and Analytical Techniques

All reagents were purchased from Sigma Aldrich or Fisher Scientific and used without further purification unless specified. Glucagon was purchased from ChemPep. Glucagon characterization was carried out on an Agilent 1100/1200 HPLC system equipped with a G1312A binary pump, a G1314A autosampler, and a G1314A VWD. Mass spectra were recorded using an Agilent 6130 LC/MS system equipped with an ESI source. Stationary phase and gradient profiles are noted below. DLS measurements were carried out using a Malvern Zetasizer Nano.

4. 4. 2. Methods

Thiolation of Glucagon with Traut's Reagent

Glucagon (1 mg) was solubilized in 1:1 ACN/50 mM HCl (200 μ L). 2-IT was dissolved in pH 9 PBS immediately before use (0.08 mg/50 μ L). Glucagon solution (100 μ L) and 2-IT

solution (50 μ L) plus an additional 300 μ L pH 9 PBS were mixed in a 0.5 mL lo-bind tube for 90 min before analyzing sample via LCMS.

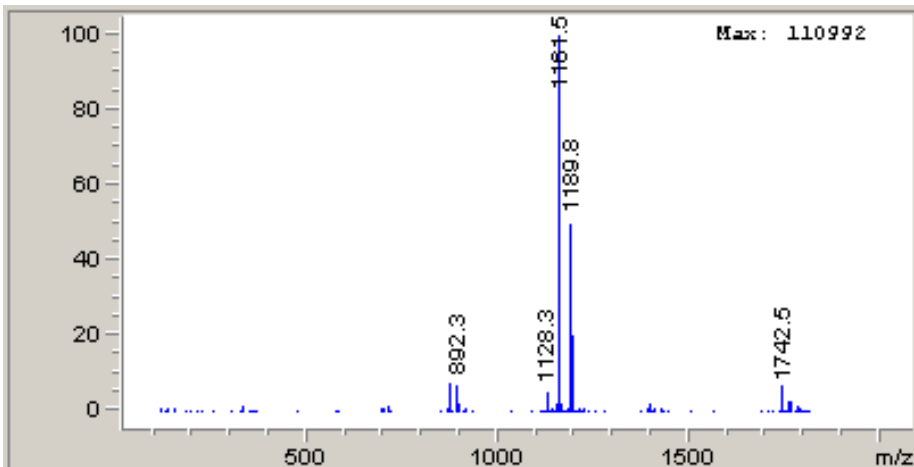


Figure 4.10. ESI-MS of glucagon thiolated with Traut's reagent. $m/z = 1161.5$ corresponds to glucagon and $m/z = 1189.8$ corresponds to the byproduct of singly thiolated glucagon ($z = 3$).

Trapping Thiolated Glucagon with PDS and PDSMA-*co*-TrMA

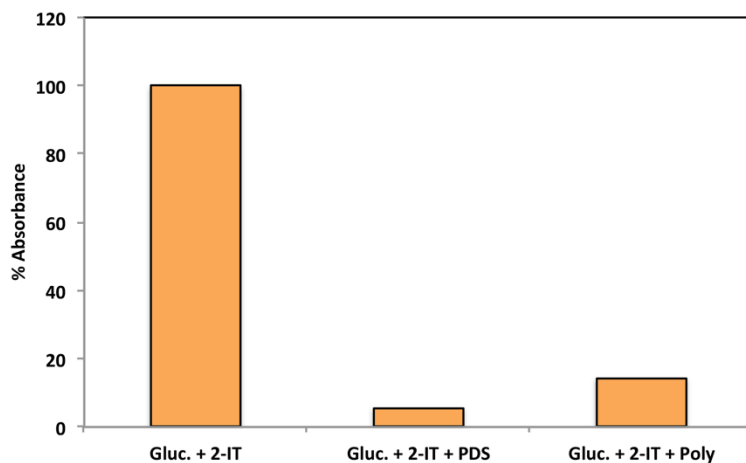


Figure 4.11. Ellman's assay results of glucagon thiolated with 2-IT trapped with PDS or PDSMA-*co*-TrMA.

Thiolation of Glucagon with DTBP

Glucagon (3 mg) was dissolved in 1 mL 0.1 M NaOH. Separately, DTBP (5 mg) was dissolved in 0.5 ml pH 9 100 mM borate buffer and added to the glucagon solution. The solution was mixed for five minutes before adding additional DTBP (2 mg) in 0.2 mL borate buffer. The same addition was repeated two minutes later. After mixing for 40 minutes, DTBP (1 mg) in 0.1 mL borate buffer was added to the solution. Cloudiness developed in the solution over time, but the addition of 0.1 M NaOH caused the solution to return to clear. DTBP-modified glucagon was purified using 3kDa MWCO centriprep filters, centrifuged at 12,000 rpm for 20 minute cycles. To reduce the disulfides, 10 mM TCEP was added to the solution and mixed for 10-15 minutes before continuing centriprep cycles until TCEP was completely removed.

Ellman's Assay

5,5'-dithiobis-(2-nitrobenzoic acid (DTNB) (0.5 mg) was dissolved in pH 7.9 PBS + 1 mM EDTA (1 mL). To each well of a polystyrene 96 well plate, 250 μ L pH 7.9 PBS + 1 mM EDTA, 10 μ L DTNB solution were added followed by 25 μ L sample solution. After letting the color develop, absorbance measurements were performed at 405 nm on ELX800 Universal Microplate Reader. Results were reported as the average and standard deviation of three independent repeats.

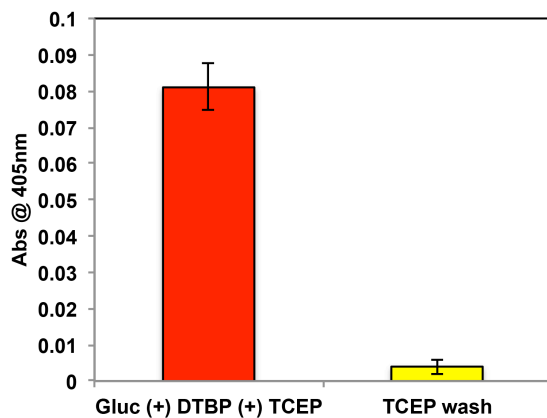


Figure 4.12. Ellman's assay results of thiolated glucagon and wash solution.

HPLC Method

An Eclipse XDB-C18 (4.6 x 150 mm, 5 μ m) column was utilized to analyze glucagon thiolation using a gradient of 10-100% H₂O + 0.1% TFA/ACN + 0.1% TFA over 13 minutes. Glucagon and modified glucagon eluted at approximately 8.3 minutes.

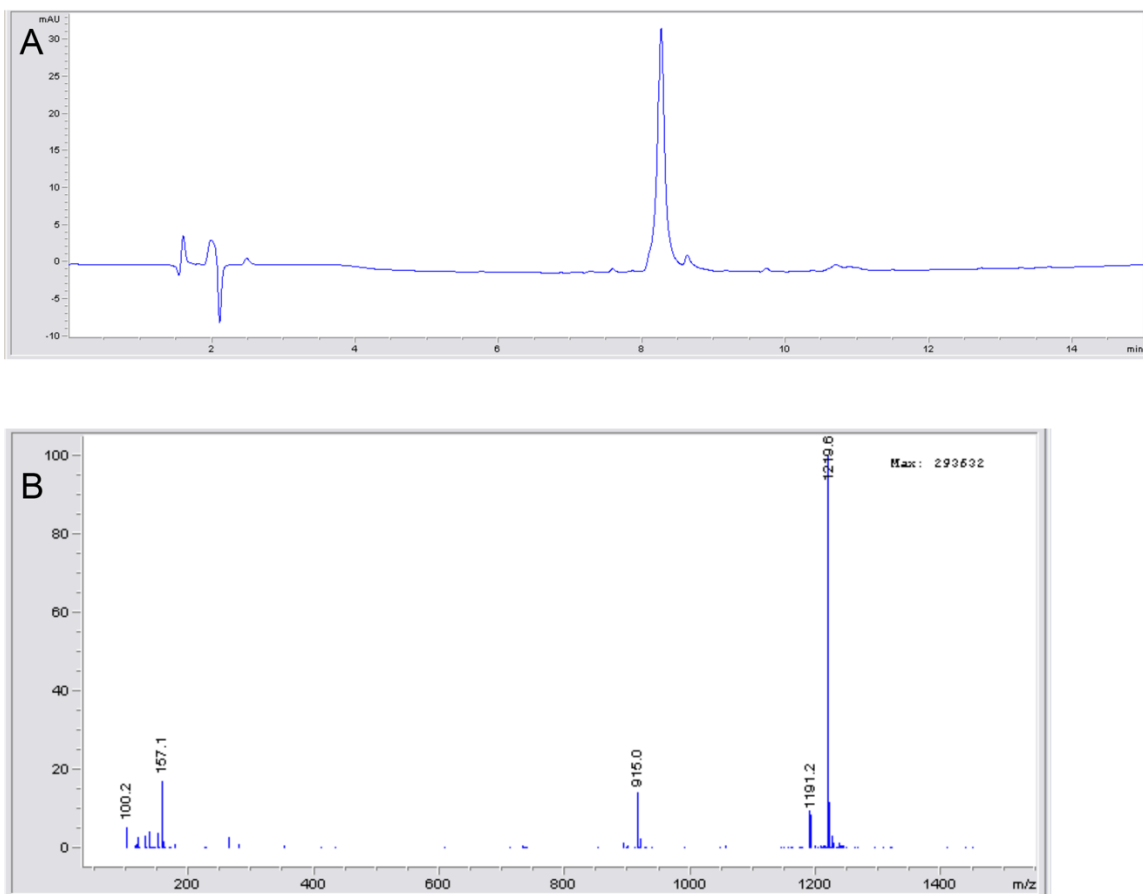


Figure 4.13. LC trace after TCEP reduction of glucagon thiolated with DTBP (peak at 8.3 min) (A) and ESI-MS data of thiolated glucagon after TCEP reduction (B). $m/z = 1191.2$ corresponds to singly thiolated glucagon and $m/z = 1219.6$ corresponds to doubly thiolated glucagon ($z = 3$).

Representative Nanogel Formation with Thiolated Glucagon

Thiolated glucagon (0.1 mg, approximately 1:1 singly to doubly thiolated peptide), lyophilized from 10 mM HCl, was dissolved in deionized water (100 μ L). Separately, PDSMA_{1-co}-TrMA_{0.8} (0.13 mg) or PDSMA_{1-co}-TrMA_{1.7} (0.21 mg) was dissolved in 100 μ L pH 7.4 PBS. The polymer solution along with additional 100 μ L 10 mM HCl were

transferred to a glass vial equipped with a stir bar. The solution was stirred at 1000 rpm, at which point the glucagon solution was added in dropwise. After stirring for 2 hours, crude nanogels were purified using 30 kDa MWCO centriprep filters by centrifuging at 12,000 rpm for 20 min for three cycles. In between, the solution was replenished with 10 mM HCl then PBS.

Gel Electrophoresis

SDS-PAGE:

Samples were loaded using 2X Laemmli sample buffer and run on Mini-Protean TGX, Any kD gels (Bio-Rad) at 180V for 25-30 minutes using Tris/Glycine/SDS buffer (Bio-Rad).

Gels were stained with Coomassie.

Native-PAGE:

Samples were loaded using native sample buffer (Bio-Rad) and run on Mini-Protean TGX, 4-20% gels (Bio-Rad) at 180V for 90 minutes using Tris/Glycine buffer (Bio-Rad). Gels

were stained with Coomassie.

Estimating Conjugation Yield

Conjugation yields were calculated using ImageJ software to compare glucagon band intensity before and after conjugation.

Table 4.1. Conjugation yields of nanogels made from PDSMA₁-*co*-TrMA_{0.8} and PDSMA₁-*co*-TrMA_{1.7} at two different ratios.

Polymer	Polymer to Glucagon (w.r.t. thiols)	Conjugation Yield (%)
PDSMA ₁ - <i>co</i> -TrMA _{0.8}	5	84
PDSMA ₁ - <i>co</i> -TrMA _{0.8}	10	76
PDSMA ₁ - <i>co</i> -TrMA _{1.7}	5	77
PDSMA ₁ - <i>co</i> -TrMA _{1.7}	10	N/A

TEM Imaging

TEM images were acquired on a FEI T12 instrument using formvar/carbon coated grids (200 mesh, Cu, Ted Pella). Grids were glow discharged for 15 seconds. 2.5 μ L of sample were placed on the grid and allowed to adhere for 5 minutes. After, the grids were washed 3x with 1 drop of water, followed by staining with uranyl acetate.

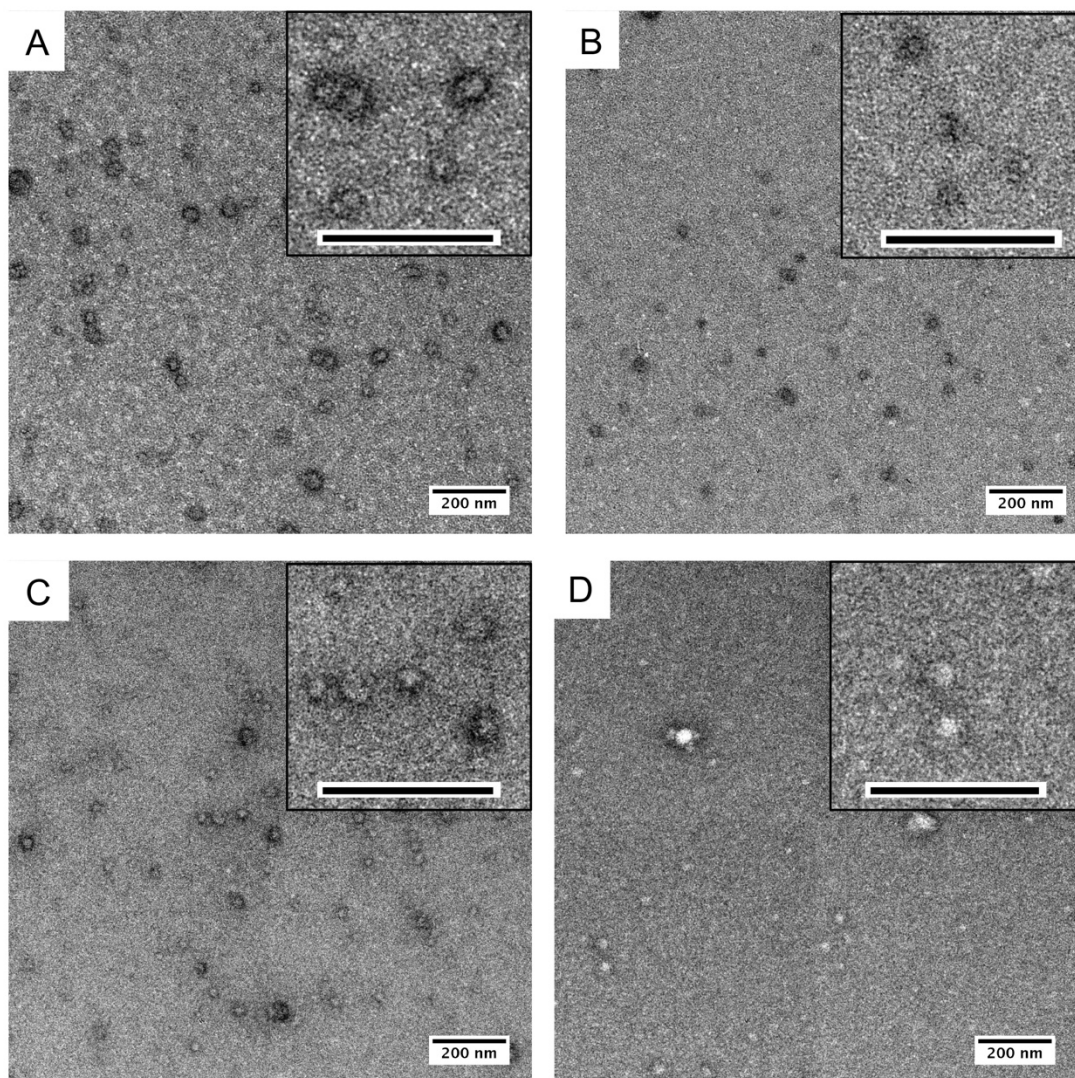


Figure 4.14. TEM images of nanogels formed using 5:1 (A) and 10:1 (B) PDSMA_{1-co}-TrMA_{0.8} and 5:1 (C) and 10:1 PDSMA_{1-co}-TrMA_{1.7} to thiolated glucagon. Scale bars = 200 nm.

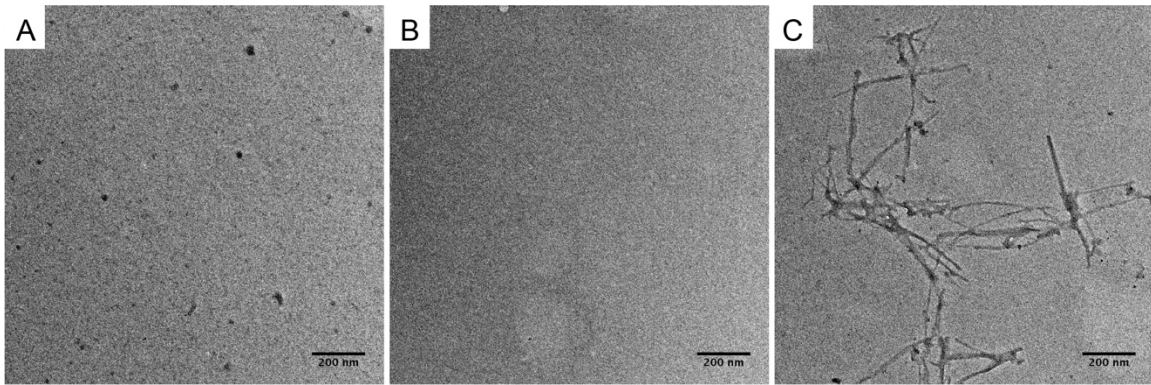


Figure 4.15. TEM images of fresh PDSMA₁-*co*-TrMA_{1.7} glucagon nanogels in solution (A), aged (2 days) nanogels imaged immediately after TCEP reduction (B), and three days after reduction (C).

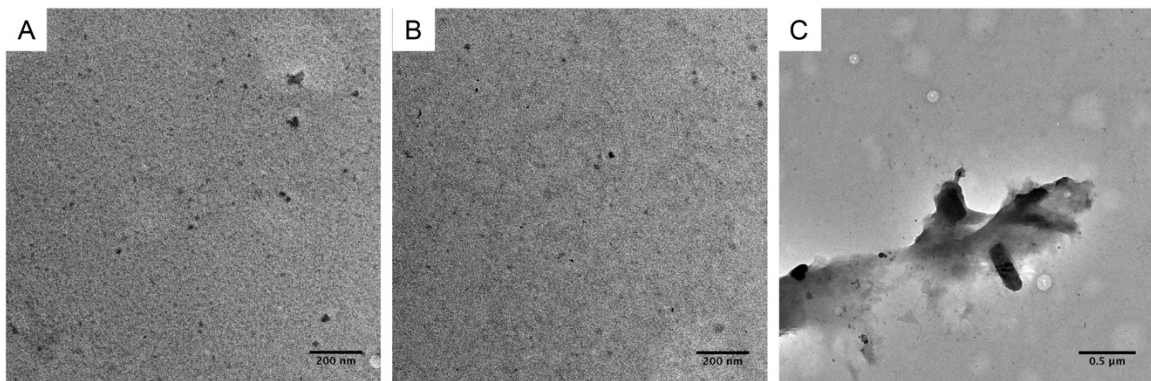


Figure 4.16. TEM images of PDSMA₁-*co*-TrMA_{1.7} glucagon nanogels in solution (A). However, after lyophilization and reconstitution a mixture of nanogels (B) and micron sized aggregates was observed after lyophilization (C).

Glucagon Activity Assay:

A commercial assay kit containing Chem-1 cells expressing the human glucagon receptor was purchased from Eurofins (HTS112RTA) and used in conjunction with Fluo-8 dye kit

from AAT Bioquest (36314). Cells were plated according to manufacturer's protocol for 96 well plate assay (2 vials of cells/96 well plate). After 24 hours, media was removed from the wells and replaced with 100 μ L dye solution, which was prepared according to manufacturer's instructions. Plates were incubated in the dark at 37 $^{\circ}$ C for 30 min and at 22 $^{\circ}$ C (room temperature) for an additional 30 minutes. Glucagon compounds were prepared in 0.05 M AcOH, then diluted 1:10 into Hank's Buffered Saline Solution (HBSS) without calcium, magnesium, or phenol red, supplemented with 1% dimethylsulfoxide and 10% v/v phosphate buffered saline. The thiolated glucagon sample used for these studies contained approximately 1:1 singly to doubly thiolated peptide as characterized by LC-MS. Imaging was carried out on a FlexStation II plate reader from Molecular Devices using the following conditions:

Ex/Em: 490/525 nm

Pipet height: 50 μ L

Pipet rate: 3 (78 μ L/sec)

Volume added: 10 μ L at $t = 20$ s

No mixing

Assay duration: 80 s

A blank correction was applied to the data by subtracting the first data point from all subsequent data points. All data were expressed as the % maximum for each condition tested. A four-parameter logistic fit was applied to the results to obtain EC50 values. The mean and errors of two to three independent repeats were used for calculations.

4. 5. References

1. Unger, R. H. *Diabetologia* **1985**, *28*, 574-578.
2. Cryer, P. E.; Davis, S. N.; Shamoon, H. *Diabetes Care* **2003**, *26*, 1902-1912.
3. Peterson, C. D.; Leeder, J. S.; Sterner, S. *Drug Intell. Clin. Pharm.* **1984**, *18*, 394-398.
4. Chabenne, J. R.; DiMarchi, M. A.; Gelfanov, V. M.; DiMarchi, R. D. *Biopolymers* **2011**, *96*, 468-468.
5. Matilainen, L.; Maunu, S. L.; Pajander, J.; Auriola, S.; Jaaskelainen, I.; Larsen, K. L.; Jarvinen, T.; Jarho, P. *Eur. J. Pharm. Sci.* **2009**, *36*, 412-420.
6. Joshi, A. B.; Kirsch, L. E. *J. Pharm. Sci.* **2002**, *91*, 2332-2345.
7. Caputo, N.; Castle, J. R.; Bergstrom, C. P.; Carroll, J. M.; Bakhtiani, P. A.; Jackson, M. A.; Roberts, C. T.; David, L. L.; Ward, W. K. *Peptides* **2013**, *45*, 40-47.
8. Pedersen, J. S. *J. Diabetes Sci. Technol.* **2010**, *4*, 1357-1367.
9. Onoue, S.; Ohshima, K.; Debari, K.; Koh, K.; Shioda, S.; Iwasa, S.; Kashimoto, K.; Yajima, T. *Pharm. Res.* **2004**, *21*, 1274-1283.
10. Costantino, H. R.; Langer, R.; Klibanov, A. M. *J. Pharm. Sci.* **1994**, *83*, 1662-1669.
11. Chabenne, J.; Chabenne, M. D.; Zhao, Y.; Levy, J.; Smiley, D.; Gelfanov, V.; DiMarchi, R. *Mol. Metab.* **2014**, *3*, 293-300.
12. Mroz, P. A.; Perez-Tilve, D.; Liu, F.; Mayer, J. P.; DiMarchi, R. D. *ACS Chem. Biol.* **2016**, *11*, 3412-3420.
13. Stigsnaes, P.; Frokjaer, S.; Bjerregaard, S.; van de Weert, M.; Kingshott, P.; Moeller, E. H. *Int. J. Pharm.* **2007**, *330*, 89-98.

14. Pinholt, C.; Bukrinsky, J. T.; Hostrup, S.; Frokjaer, S.; Norde, W.; Jorgensen, L. *Eur. J. Pharm. Biopharm.* **2011**, *77*, 139-147.
15. Webber, M. J.; Appel, E. A.; Vinciguerra, B.; Cortinas, A. B.; Thapa, L. S.; Jhunjhunwala, S.; Isaacs, L.; Langer, R.; Anderson, D. G. *Proc. Natl. Acad. Sci. U. S. A.* **2016**, *113*, 14189-14194.
16. Authier, F.; Desbuquois, B. *Cell. Mol. Life Sci.* **2008**, *65*, 1880-1899.
17. Fang, W. J.; Qi, W.; Kinzell, J.; Prestrelski, S.; Carpenter, J. F. *Pharm. Res.* **2012**, *29*, 3278-3291.
18. Ohtake, S.; Wang, Y. J. *J. Pharm. Sci.* **2011**, *100*, 2020-2053.
19. Kaushik, J. K.; Bhat, R. *J. Biol. Chem.* **2003**, *278*, 26458-26465.
20. Tapia, H.; Koshland, D. E. *Curr. Biol.* **2014**, *24*, 2758-2766.
21. Tapia, H.; Young, L.; Fox, D.; Bertozzi, C. R.; Koshland, D. *Proc. Natl. Acad. Sci. U. S. A.* **2015**, *112*, 6122-6127.
22. Guo, N.; Puhlev, I.; Brown, D. R.; Mansbridge, J.; Levine, F. *Nat. Biotechnol.* **2000**, *18*, 168-171.
23. Kale, S. S.; Akamanchi, K. G. *Mol. Pharm.* **2016**, *13*, 4082-4093.
24. Jain, N. K.; Roy, I. *Protein Sci.* **2009**, *18*, 24-36.
25. Wendorf, J. R.; Radke, C. J.; Blanch, H. W. *Biotechnol. Bioeng.* **2004**, *87*, 565-573.
26. Ring, R. A.; Danks, H. V. *Cryo Lett.* **1998**, *19*, 275-282.
27. Montiel, P. O. *Cryo Lett.* **2000**, *21*, 83-90.
28. Sola-Penna, M.; Meyer-Fernandes, J. R. *Arch. Biochem. Biophys.* **1998**, *360*, 10-14.

29. Herdeiro, R. S.; Pereira, M. D.; Panek, A. D.; Eleutherio, E. C. A. *Biochim. Biophys. Acta* **2006**, *1760*, 340-346.
30. Sakurai, M., Biological Functions of Trehalose as a Substitute for Water. In *Water and Biomolecules*, Kuwajima, K.; Goto, Y.; Hirata, F.; Kataoka, M.; Terazima, M., Eds. Springer: 2009; pp 219-240.
31. Crowe, J. H.; Carpenter, J. F.; Crowe, L. M. *Annu. Rev. Physiol.* **1998**, *60*, 73-103.
32. Belton, P. S.; Gil, A. M. *Biopolymers* **1994**, *34*, 957-961.
33. Cottone, G.; Ciccotti, G.; Cordone, L. *J. Chem. Phys.* **2002**, *117*, 9862-9866.
34. Mancini, R. J.; Lee, J.; Maynard, H. D. *J. Am. Chem. Soc.* **2012**, *134*, 8474-8479.
35. Lee, J.; Lin, E. W.; Lau, U. Y.; Hedrick, J. L.; Bat, E.; Maynard, H. D. *Biomacromolecules* **2013**, *14*, 2561-2569.
36. Lau, U. Y.; Saxer, S. S.; Lee, J.; Bat, E.; Maynard, H. D. *ACS Nano* **2016**, *10*, 723-729.
37. Bat, E.; Lee, J.; Lau, U. Y.; Maynard, H. D. *Nat. Commun.* **2015**, *6*.
38. Pelegri-O'Day, E. M.; Paluck, S. J.; Maynard, H. D. *J. Am. Chem. Soc.* **2017**, *139*, 1145-1154.
39. Liu, Y.; Lee, J.; Mansfield, K. M.; Ko, J. H.; Sallam, S.; Wesdemiotis, C.; Maynard, H. D. *Bioconjugate Chem.* **2017**.
40. O'Shea, T. M.; Webber, M. J.; Aimetti, A. A.; Langer, R. *Adv. Healthcare Mater.* **2015**, *4*, 1802-1812.
41. Lee, J.; Ko, J. H.; Lin, E. W.; Wallace, P.; Ruch, F.; Maynard, H. D. *Polym. Chem.* **2015**, *6*, 3443-3448.

42. Sizovs, A.; Xue, L.; Tolstyka, Z. P.; Ingle, N. P.; Wu, Y. Y.; Cortez, M.; Reineke, T. M. *J. Am. Chem. Soc.* **2013**, *135*, 15417-15424.
43. Srinivasachari, S.; Liu, Y. M.; Zhang, G. D.; Prevette, L.; Reineke, T. M. *J. Am. Chem. Soc.* **2006**, *128*, 8176-8184.
44. Tale, S. R.; Yin, L. G.; Reineke, T. M. *Polym. Chem.* **2014**, *5*, 5160-5167.
45. Matsumoto, N. M.; Gonzalez-Toro, D. C.; Chacko, R. T.; Maynard, H. D.; Thayumanavan, S. *Polym. Chem.* **2013**, *4*, 2464-2469.
46. Richie, J. P.; Skowronski, L.; Abraham, P.; Leutzinger, Y. *Clin. Chem.* **1996**, *42*, 64-70.
47. Kaplowitz, N. *Yale J. Biol. Med.* **1981**, *54*, 497-502.
48. Sueirasdiaz, J.; Lance, V. A.; Murphy, W. A.; Coy, D. H. *J. Med. Chem.* **1984**, *27*, 310-315.
49. Mokotoff, M.; Mocarski, Y. M.; Gentsch, B. L.; Miller, M. R.; Zhou, J. H.; Chen, J.; Ball, E. D. *J. Pept. Res.* **2001**, *57*, 383-389.
50. Christie, R. J.; Miyata, K.; Matsumoto, Y.; Nomoto, T.; Menasco, D.; Lai, T. C.; Pennisi, M.; Osada, K.; Fukushima, S.; Nishiyama, N.; Yamasaki, Y.; Kataoka, K. *Biomacromolecules* **2011**, *12*, 3174-3185.
51. Hunter, M. J.; Ludwig, M. L. *J. Am. Chem. Soc.* **1962**, *84*, 3491-3504.
52. Charulatha, V.; Rajaram, A. *J. Biomed. Mater. Res.* **2001**, *54*, 122-128.
53. Yi, X.; Batrakova, E.; Banks, W. A.; Vinogradov, S.; Kabanov, A. V. *Bioconjugate Chem.* **2008**, *19*, 1071-1077.

54. Ghodke, S.; Nielsen, S. B.; Christiansen, G.; Hjuler, H. A.; Flink, J.; Otzen, D. *FEBS J.* **2012**, *279*, 752-765.
55. Castle, J. R.; El Youssef, J.; Branigan, D.; Newswanger, B.; Strange, P.; Cummins, M.; Shi, L.; Prestrelski, S. *J. Diabetes Sci. Technol.* **2016**, *10*, 1101-1107.
56. Moens, K.; Heimberg, H.; Flamez, D.; Huypens, P.; Quartier, E.; Ling, Z. D.; Pipeleers, D.; Gremlich, S.; Thorens, B.; Schuit, F. *Diabetes* **1996**, *45*, 257-261.
57. Montero, D.; Tachibana, C.; Winther, J. R.; Appenzeller-Herzog, C. *Redox Biol* **2013**, *1*, 508-513.
58. Koth, C. M.; Murray, J. M.; Mukund, S.; Madjidi, A.; Minn, A.; Clarke, H. J.; Wong, T.; Chiang, V.; Luis, E.; Estevez, A.; Rondon, J.; Zhang, Y. N.; Hotzel, I.; Allan, B. B. *Proc. Natl. Acad. Sci. U. S. A.* **2012**, *109*, 14393-14398.
59. Oh, N.; Park, J. H. *Int. J. Nanomedicine* **2014**, *9*, 51-63.

Chapter 5

Design of Modular Dual-Enzyme Responsive

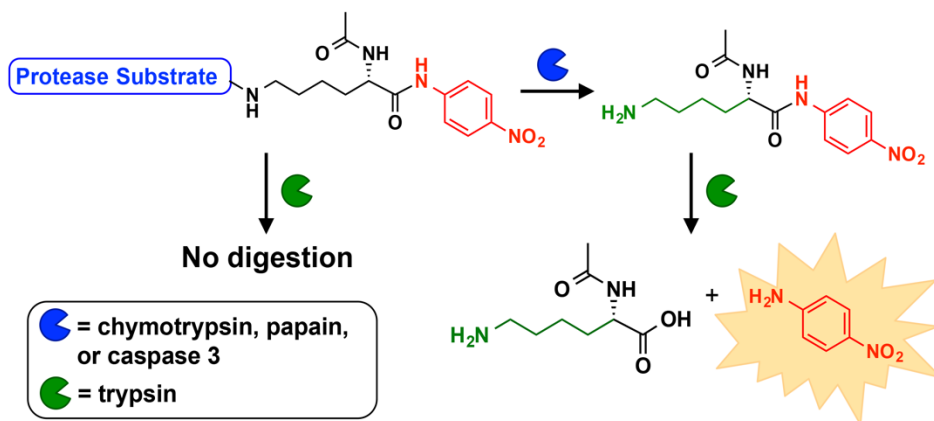
Peptides[†]

5. 1. Introduction

Due to their high selectivity and specificity, enzyme responsive systems are commonly used for diagnostic and drug delivery applications.¹⁻² Though many single enzyme-responsive systems show promise in specific targeting, response to more than one enzyme allows for greater target selectivity and indirect enzyme detection, and provides information about cellular environments.³⁻⁷ For example, caspase-sensitive reporters, which respond to peroxide production or to cancer-related matrix metalloproteinases, have been designed to detect cell injury⁸ as well as to monitor reactivation of the apoptotic pathway after anti-cancer therapy delivery, respectively.^{3,9} Small molecule and protein-based probes have also been designed to monitor enzyme cascades, though these often require very specific enzymes, limiting their modularity.¹⁰⁻¹¹

Enzyme responsive systems can also enable selective biodegradation of materials for biomedical applications. By incorporating multiple enzyme cleavage sites, materials will only degrade and release drugs at specific locations *in vivo*. Many of these systems are responsive to the serine protease trypsin due to its widespread presence throughout the body, including in the digestive tract, and its association with various cancers.¹²⁻¹⁶ For example, trypsin-sensitive sequences have been grafted into enhanced green fluorescent protein to monitor trypsinogen activation in pancreatic cancer cells.¹⁷ Additionally, trypsin responsive sequences have been incorporated into abuse-deterrent opioid formulations, which allow drug release only in the digestive tract of patients.¹⁸ However, degradation of such formulations could be better controlled if sequences that required digestion by multiple enzymes were installed. To this end, we have designed a dual enzyme-responsive

peptide system that requires sequential digestion by two enzymes for cargo release from the C-terminus. In this system, the peptide is first cleaved by an enzyme that unmask the recognition site for a second enzyme allowing for digestion and release of a colorimetric compound (Scheme 5.1).



Scheme 5.1. Dual enzyme responsive systems were designed with a protease substrate coupled to the ϵ -amino group of lysine. When the protease substrate is cleaved off by one of three model enzymes, the lysine is unmasked, allowing for subsequent trypsin digestion. Upon digestion, a colorimetric compound, nitroaniline, is released. The release of nitroaniline does not occur if only one enzyme is present.

5. 2. Results and Discussion

Trypsin is a serine protease that cleaves the C-terminus of positively charged amino acids such as lysine¹⁹ but does not cleave if the ϵ -amine of lysine is acetylated, or masked.²⁰ Previously, trypsin has been used to indirectly measure histone deacetylase (HDAC) activity by monitoring trypsin digestion of lysine after deacetylation by HDAC.^{5, 21} We

designed our system to be dual enzyme-responsive by modifying the ϵ -amine of lysine with substrates for four different proteases: chymotrypsin, papain, and caspases 3 and 8 (Figure 5.1). We chose these substrates to demonstrate that lysine modification can be used to analyze the activity of a broad range of enzymes.

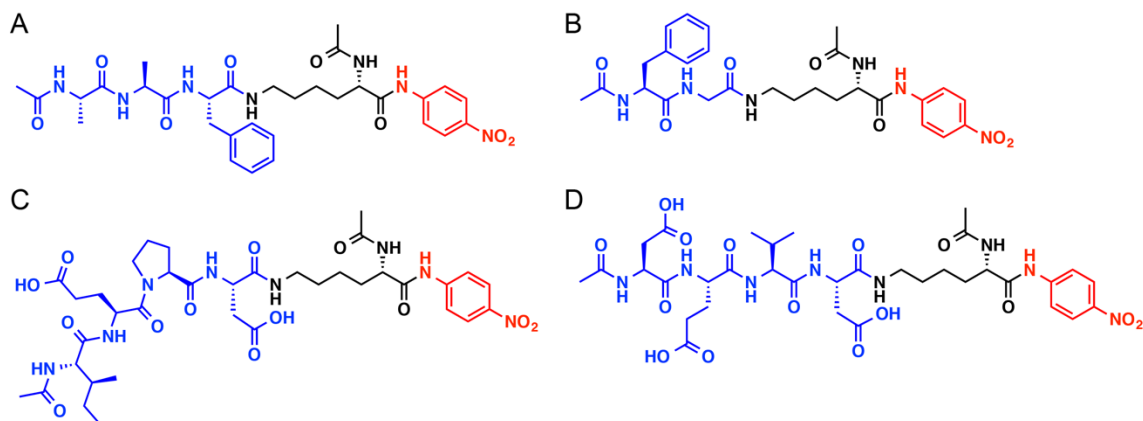


Figure 5.1. Structures of dual-enzyme responsive peptides. Structures of chymotrypsin/trypsin sensitive peptide (AcAAF)K-pNA (A), papain/trypsin sensitive peptide (AcFG)K-pNA (B), caspase 8/trypsin sensitive peptide (AcIEPD)K-pNA (C), and caspase 3/trypsin sensitive peptide (AcDEVD)K-pNA (D).

Enzyme substrates chosen for chymotrypsin, papain, and caspases 3 and 8 were AcAAF, AcFG, AcDEVD, and AcIEPD, respectively. Peptides were synthesized using standard Fmoc solid phase chemistry.²² Initially, the side chain of *N*₂-acetyl-*L*-lysine was modified with various protease substrates on resin before coupling the peptide to *p*-nitroaniline (pNA) in solution phase after cleavage from the resin (Scheme 5.2).²³ This approach proved to be challenging to purify on a larger scale due to the large excess of reagents required to drive the reaction to completion. Therefore, a more modular solution

phase approach was subsequently used in which protease substrates were coupled to a lysine nitroanilide using solution phase conditions (Scheme 2). Peptide identity and purity were confirmed by LC-MS. The synthesized peptides were also analyzed using UV-vis spectroscopy, and the resulting spectra were compared to pNA (Figure 5.14). The absorbance maxima of the peptides occurred near 310 nm, and no peaks were observed around 405 nm, the wavelength used to monitor pNA release. Trypsin and chymotrypsin were chosen as initial model enzymes because they each require only a single amino acid for recognition and cleavage. The peptide sequence chosen for chymotrypsin/trypsin detection, (Ac-AAF)K-pNA, was designed with phenylalanine at the ϵ -amine of lysine nitroanilide to install chymotrypsin sensitivity since chymotrypsin recognizes and cleaves at the C-terminal side of bulky, aromatic amino acids.²⁴

To test the enzyme responsiveness of (AcAAAF)K-pNA, the peptide was first incubated with both chymotrypsin and trypsin, and the absorbance at 405 nm, corresponding to pNA release, was monitored over time. A standard curve was then used to convert absorbance values to pNA concentration (Figure 5.15). A significant absorbance increase was observed, suggesting that both enzymes are required for complete substrate cleavage. Incubation of 50 μ M (AcAAAF)K-pNA with the enzymes showed an absorbance/concentration increase that leveled out at 0.039 ± 0.003 AU after five hours. A two-fold absorbance increase to 0.070 ± 0.002 AU was observed for 100 μ M substrate, and a four-fold absorbance increase to 0.147 ± 0.002 AU was observed for 200 μ M substrate, indicating that release of pNA is substrate concentration dependent as expected (Figure 5.2). When 100 μ M peptide was incubated with only chymotrypsin, no change in

absorbance was observed. However, a minimal absorbance increase (0.016 ± 0.002 AU) was observed when $100 \mu\text{M}$ peptide was incubated with trypsin only. This minimal absorbance increase can be explained: it is known that commercial trypsin contains residual chymotrypsin activity, and thus the second enzyme is present at a low concentration.²⁵ Further, our other dual enzyme substrates (*vide infra*) did not show any absorbance increase when incubated with trypsin alone since they do not contain any chymotrypsin sensitive residues adjacent to lysine, further suggesting residual chymotrypsin activity is the source of the observed slight absorbance increase.

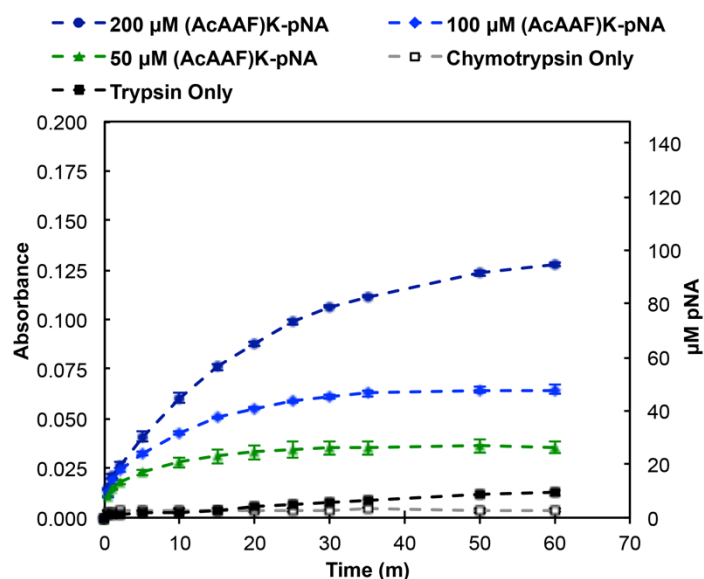


Figure 5.2. (Ac-AAF)K-pNA digestion with trypsin and chymotrypsin resulted in an absorbance increase, corresponding to pNA release. Digestion with trypsin or chymotrypsin only did not result in a significant absorbance increase. Absorbance measurements were taken for first 60 minutes and at the five-hour mark to confirm absorbance values had reached their maxima. Average and standard deviation of three repeats are shown.

The second substrate, (AcFG)K-pNA, was incubated with papain and trypsin. Papain, a cysteine protease, cleaves the C terminal side one amino acid after an aromatic residue.²⁶ In the presence of papain and trypsin, pNA release from the substrate was observed to be substrate dependent, similar to what we had observed for (AcAAF)K-pNA digestion (Figure 5.3). Again, no absorbance/pNA concentration increase was observed when the substrate was incubated with each enzyme separately. It is interesting to note that papain digestion of basic amino acids, such as lysine, has been reported; however, cleavage rates are drastically lower than those observed for Phe-Gly, which is evidenced by the lack of absorbance increase when papain only was added to the substrate (Figure 5.3).²⁷⁻²⁸

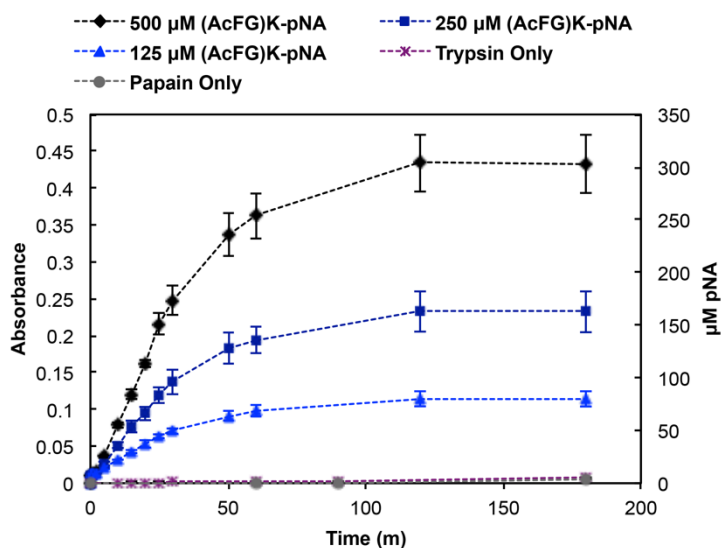


Figure 5.3. Papain and trypsin digestion of (AcFG)K-pNA at varying substrate concentrations released pNA, resulting in proportional absorbance increases. Incubating the substrate with papain or trypsin only resulted in no absorbance increase. Average and standard deviation of three repeats are shown.

To demonstrate the versatility of the design, two other dual-enzyme responsive peptides, (AcDEVD)K-pNA and (AcIEPD)K-pNA, were synthesized by modifying lysine with substrates of two clinically relevant enzymes: caspases 3 and 8, respectively.²⁹ Caspases 3 and 8 are key proteases in apoptotic pathways that are down regulated in certain cancer cells,³⁰⁻³¹ and caspase 3 is found at elevated levels after myocardial infarctions.³² Caspase activity assays are commonly used to monitor delivery of anti-cancer agents since activation of the apoptotic pathway can indicate successful cancer treatment.³³

Initial experiments with (AcIEPD)K-pNA revealed little to no absorbance increase in the presence of caspase 8 and trypsin (Figure 5.16). To ensure the enzyme itself was still active, the activity was confirmed using commercially available single enzyme substrates AcIEPD-pNA and AcDEVD-pNA (Figure 5.17), which cleaved as expected. These results led us to hypothesize that caspase 8 is not able to efficiently digest our substrate because peptide amide bonds are much less labile than the acyl-nitroanilide in commercial substrates. Further, caspases are sensitive to the structure of the amino acid in the P1' position which is adjacent to the substrate cleavage site, and the presence of an ϵ -amide as P1' may negatively affect enzyme digestion.³⁴ Notably, K_{cat}/K_m values for caspase 8 are reduced approximately 50 times on average when compared to caspase 3, prompting us to design a dual enzyme substrate sensitive to caspase 3 and trypsin.³⁴

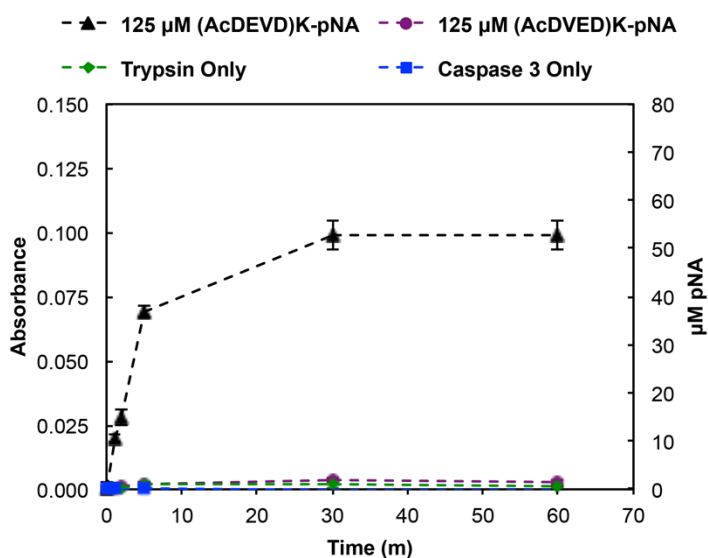


Figure 5.4. Digestion of (AcDEVD)K-pNA with trypsin and caspase 3 results in p-nitroaniline release. No release is observed when only trypsin or caspase 3 is used or when the caspase 3 recognition sequence was scrambled. Average and standard deviation of four repeats are shown.

Enzyme sensitivity of (AcDEVD)K-pNA was assessed after incubating 125 μM of substrate first with caspase-3 then with trypsin, which resulted in an absorbance increase of 0.1 ± 0.006 AU over 60 minutes (Figure 5.4). This indicated that caspase 3 was able to digest the substrate in contrast to our findings for caspase 8. In the presence of trypsin or caspase 3 only, no absorbance increase was observed as expected. A scrambled version of the caspase 3 substrate, (AcDVED)K-pNA was also synthesized, for which no enzyme digestion was anticipated. As hypothesized, no pNA release occurred when (AcDVED)K-pNA was incubated with trypsin and caspase 3 (Figure 5.4). Because of the difference in caspase 8 cleavage rates of (AcIEPD)K-pNA and AcIEPD-pNA, we wanted to compare

caspase 3 digestion of (AcDEVVD)K-pNA to its commercial substrate, AcDEVVD-pNA. We found that pNA release from our substrate corresponded to 83% of the release from the commercial substrate, indicating both substrates are digested efficiently by caspase 3 and that our peptide system may be useful for enzyme activity screening assays (Figure 5.18).

Additionally, these dual-enzyme responsive probes can be used to indirectly measure cleavage rates of peptide bonds, which are difficult to detect through single enzyme assays because these typically require an easily detectable analyte to be released instead of an amino acid. A proof-of-concept kinetics experiment using (AcFG)K-pNA was carried out to determine kinetic parameters of papain. K_{cat} values for papain hydrolysis of comparable substrates range from 1.3 (AcPheGly-pNA) to 5.4 (AcPheGly-OMe) s^{-1} , and K_{cat} of trypsin hydrolysis of a lysine nitroanilide is 44 s^{-1} .^{26, 35} Therefore, we anticipated papain being the rate limiting enzyme, meaning that the rate of pNA release is dependent on papain activity and not trypsin.^{26, 35} Initially, various concentrations of substrate were incubated with both enzymes and the resulting pNA release was monitored via UV-vis. Non-linear regression of substrate concentration versus absorbance increase was carried out to determine K_m (Table 5.1, Entry 1). However, adding enzymes both at once can give lower cleavage rates for the substrate since the enzymes can digest each other in a competitive reaction.

Thus, the experiment was repeated, this time incubating (AcFG)K-pNA first with papain, then adding trypsin at predetermined time points. The resulting K_m was lower than the first experiment whereas K_{cat}/K_m increased twofold (Table 5.1, Entry 2). We reasoned that this approach gave a more accurate result since it allowed digestion by the first enzyme

to occur without interference by the second. Our determined values fall between the values for two similar papain substrates, indicating the hydrolysis rate of (AcFG)K-pNA lies between that of comparable nitroanilides and methyl esters. Similar trends have been observed by others, leading us to believe this strategy may be a useful tool for indirect enzyme kinetic analysis.³⁶ Alternatively, the cleavage rate of each dual-enzyme substrate could be monitored using additional characterization methods, such as LC-MS. This would allow for the monitoring of each enzyme digestion step individually.

Table 5.1. Kinetic parameters of Phe-Gly substrates.

Substrate	Enzyme	K_m (μM)	K_{cat}/K_m (M⁻¹s⁻¹)
(AcFG)K-pNA	Papain + Trypsin	256±29	6.5±0.5x10 ³
(AcFG)K-pNA	Papain then Trypsin	127±48	1.4±0.5x10 ⁴
AcFG-pNA ²⁶	Papain	880±100	1.5±0.2x10 ³
AcFG-OMe ²⁶	Papain	32±1	1.7±0.15x10 ⁵

Due to the modular design of the dual-enzyme responsive peptides, a wide range of protease substrates could be coupled to the lysine side chain. This could be useful for multi-enzyme screening applications as well as for creating selectively degradable materials for drug delivery. For instance, our system allows for the indirect determination of amide hydrolysis kinetics which are not possible with traditional single enzyme assay substrates. While we have not yet explored using other proteases in place of trypsin, doing so would broaden the scope of our system even further. Our data also show that the cleavage rates

of each enzyme must be taken into account when designing further dual enzyme responsive peptides in this manner, providing important information for successful design.

5.3. Conclusions

In summary, we have designed and synthesized a series of multi-enzyme responsive peptides by modifying the ϵ -amine of lysine with substrates of three different proteases: chymotrypsin, papain, and caspase 3. It was shown that dual protease activity is required for nitroaniline release to occur. Due to the modular design, we envision that these peptides could be used for selective drug delivery, for fundamental studies on dual enzyme activity, as well as for diagnostic enzyme screening.

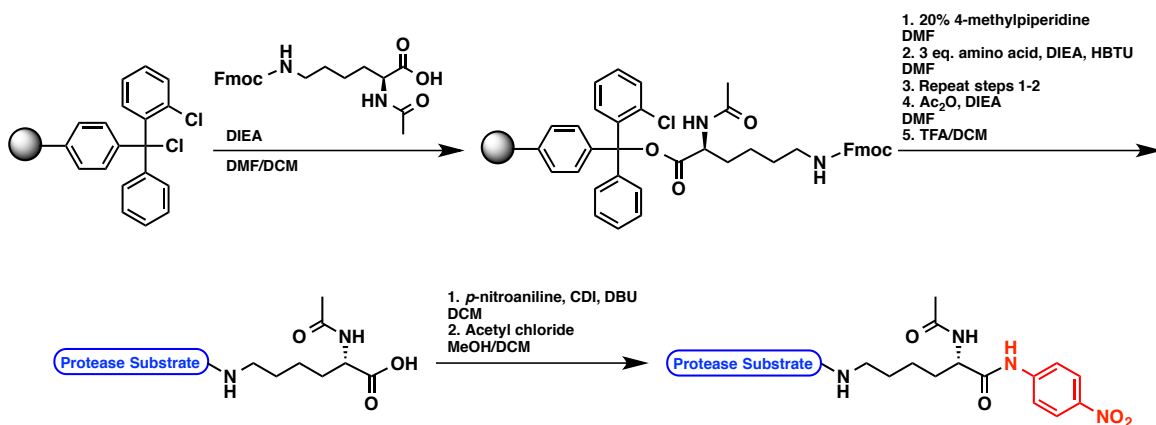
5.4. Experimental

5.4.1. Materials and Analytical Techniques

Fmoc-protected amino acids were purchased from Chem Impex. Chymotrypsin (64.8 units/mg) was purchased from Sigma Aldrich. Trypsin (225 units/mg), papain (30.3 units/mg), and caspases 3 (100 units/ μ L) and 8 (0.2 mg/mL) were purchased from Fisher Scientific. All other chemicals were purchased from Sigma Aldrich. ^1H NMR and ^{13}C NMR spectra were obtained on an Avance DRX 400 MHz instrument. ESI mass spectra were obtained using a Waters Acquity LCT Premier XE. Assay measurements were carried out on a Bio-Tek ELx 800 Microplate Reader.

5.4.2. Methods

Synthesis and Characterization of Peptides

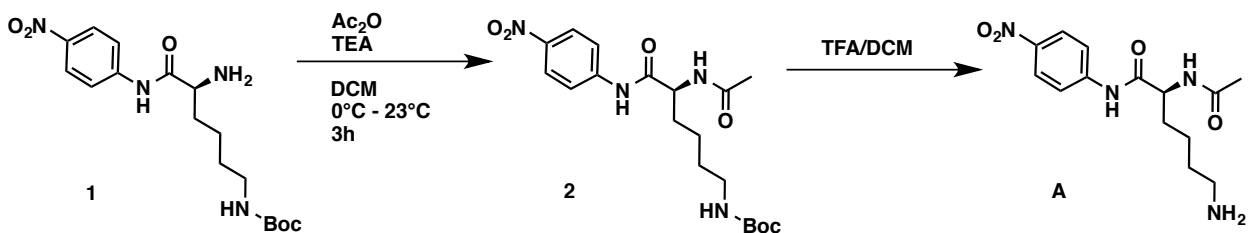


Scheme 5.2. Synthesis of nitroanilide peptides using method 1.

Peptide Synthesis: Initial Method

Peptides were synthesized using standard fmoc solid-phase chemistry with a 2-chlorotrityl chloride resin (0.4 mmol/g substitution). N-termini were acetylated prior to cleavage from the resin using 50 eq. acetic anhydride and diisopropylethylamine (DIEA) in dimethylformamide (DMF) for 30 min. Peptides were cleaved from the resin using 95:2.5:2.5 trifluoroacetic acid (TFA)/triisopropylsilane (TIPS)/H₂O. For peptides containing t-butyl protecting groups, 0.5% TFA in dichloromethane (DCM) was used to cleave from the resin, thereby keeping any protecting groups intact. Peptides were modified with *p*-nitroaniline using a previously reported procedure.²³ Peptides were purified by preparative reverse-phase HPLC equipped with a C18 column using a linear gradient from 95:5 to 5:95 H₂O/acetonitrile with 0.1% TFA at a flow rate of 20 mL/min. ESI-MS was used to confirm the molecular masses of the desired products.

Peptide Synthesis: Modular Method



Scheme 5.3. Synthesis of (*S*)-2-acetomido-6-amino-*N*-(4-nitrophenyl)hexanamide.

Synthesis of (*S*)-2-acetamido-6-amino-*N*-(4-nitrophenyl)hexanamide

Lys(Boc)-pNA **1** (2.0g, 5.46 mmol) was dissolved in dichloromethane (10 mL). Triethylamine (3.4 mL, 24.6 mmol) was added before cooling the solution to 0 °C using an ice bath. Acetic anhydride (2.3 mL, 24.6 mmol) was added drop wise and the reaction stirred for 3 hours. During the reaction, a precipitate formed, and a beige color developed. Dichloromethane was removed under vacuum, and solids were re-dissolved in ethyl acetate (~20 mL) before washing with 2x NaHCO₃, 2x sat. NH₄Cl, and 1x brine. The organic layer was dried over MgSO₄ before reducing volume under vacuum. Product was re-crystallized two times from ethyl acetate to yield a beige solid **2** (1.6g, 72%). Calc. [M+1]: 409.2009 Da; Obs. [M+1]: 409.2072 Da. ¹H NMR of **2** (400 MHz, (CD₃)₂SO) δ 10.68-10.55 (s, 1H), 8.25-8.10 (m, 3H), 7.88-7.77 (dt, 2H, *J* = 10.2, 2.5 Hz), 6.78-6.65 (t, 1H, *J* = 5.5 Hz), 4.38-4.23 (m, 1H), 2.92-2.77 (q, 2H, *J* = 6.4 Hz), 1.87-1.78 (s, 3H), 1.71-1.48 (m, 2H), 1.39-1.16 (m, 13H) ppm. ¹³C NMR of **2** (400 MHz, (CD₃)₂SO) δ 172.6, 170.0, 156.0, 145.6, 142.7, 125.4, 119.4, 77.7, 54.2, 31.9, 29.7, 28.7, 23.3, 22.8 ppm. Carbon 10 not observed due to solvent overlap. **2** was dissolved in 1:1 TFA/DCM (4 mL) and stirred for 1 hour before removing solvent under vacuum to give **A** as a beige solid in quantitative yield. Calc. [M+1]: 309.1485 Da; Obs. [M+1]: 309.1616 Da. ¹H NMR of **A** (400 MHz,

(CD₃)₂SO) δ 10.72-10.63 (s, 1H), 8.29-8.15 (m, 3H), 7.88-7.78 (dt, 2H, *J* = 10.2, 2.5 Hz), 7.78-7.61 (broad s, 3H), 4.42-4.26 (m, 1H), 2.84-2.66 (m, 2H), 1.90-1.78 (s, 3H), 1.75-1.17 (m, 6H) ppm. ¹³C NMR of **A** (400 MHz, (CD₃)₂SO) δ 174.4, 170.1, 159.0, 158.7, 145.6, 142.8, 125.4, 119.4, 54.1, 31.6, 27.1, 23.0, 22.8 ppm. Carbon 8 not observed due to solvent overlap.

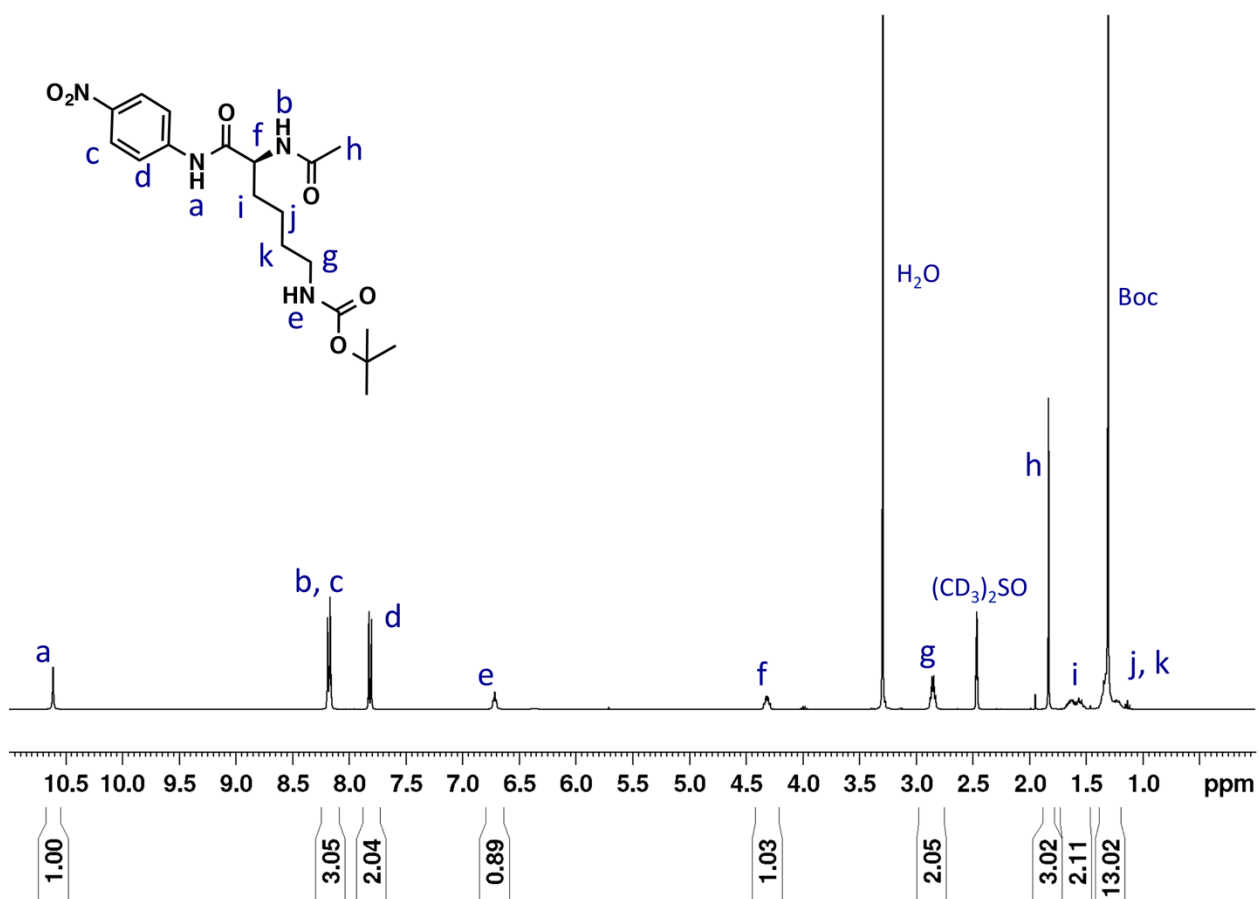


Figure 5.5. ¹H NMR spectrum of t-butyl (S)-(5-acetamido-6-((4-nitrophenyl)amino)-6-oxohexyl)carbamate (**2**) in (CD₃)₂SO.

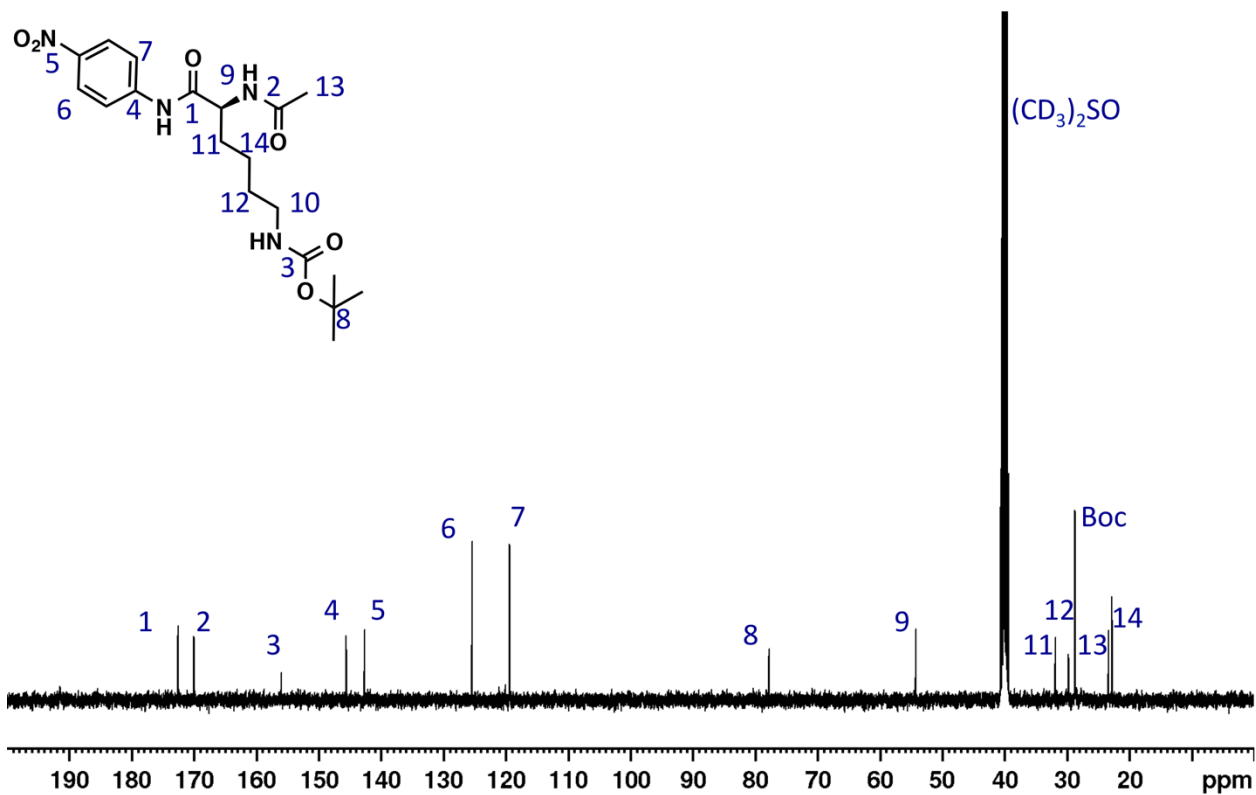


Figure 5.6. ¹³C NMR spectrum of *t*-butyl (*S*)-(5-acetamido-6-((4-nitrophenyl)amino)-6-oxohexyl)carbamate (**2**) in (CD₃)₂SO.

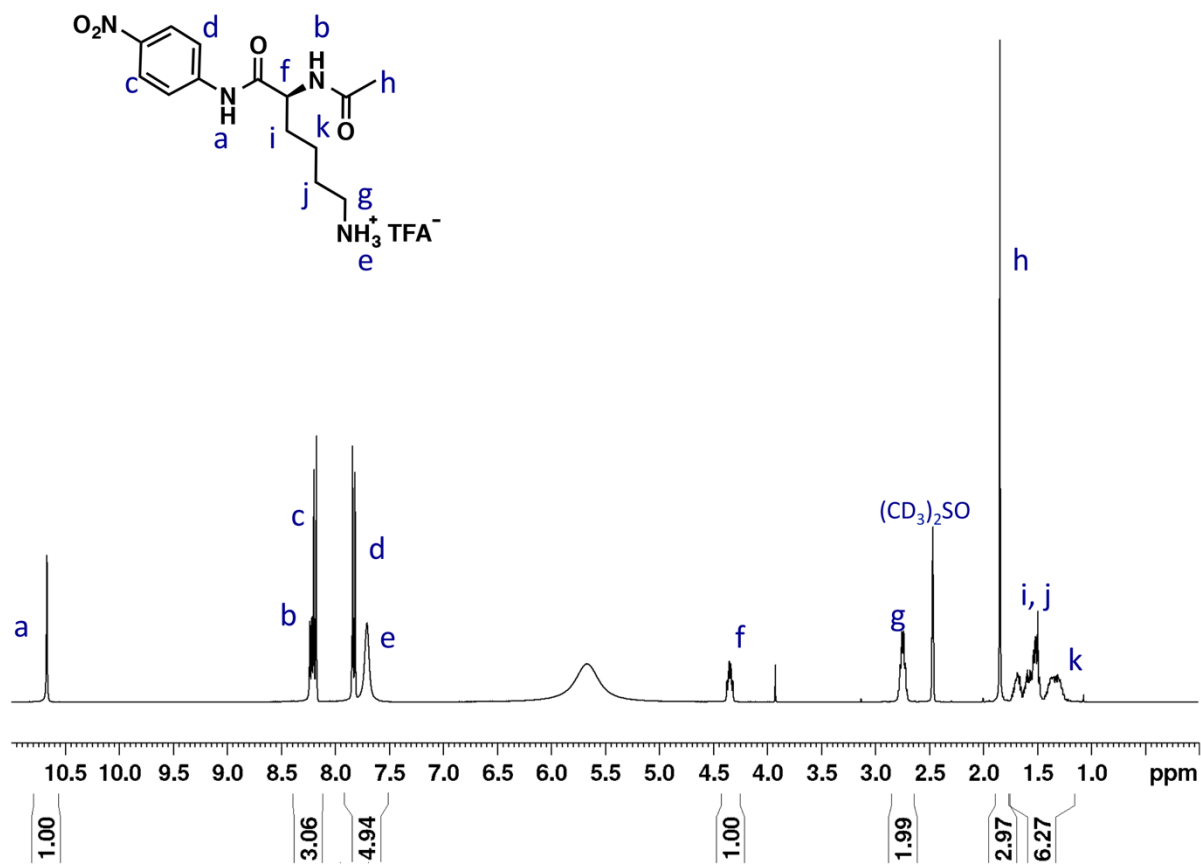


Figure 5.7. ¹H NMR spectrum of (*S*)-2-acetamido-6-amino-*N*-(4-nitrophenyl)hexanamide (A) as the TFA salt in (CD₃)₂SO.

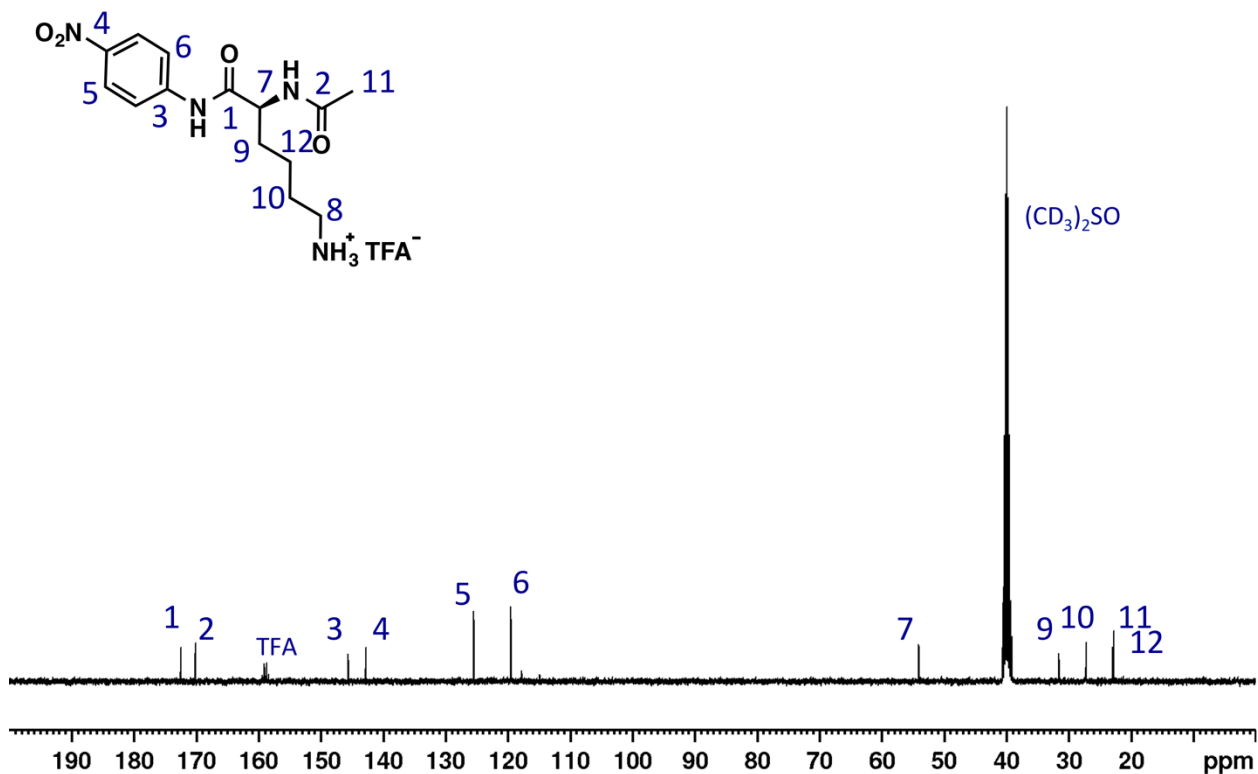


Figure 5.8. ¹³C NMR spectrum of (*S*)-2-acetamido-6-amino-*N*-(4-nitrophenyl)hexanamide

(A) as the TFA salt in (CD₃)₂SO.

Protease substrates (Ac-FG, Ac-DEVD, Ac-DVED, Ac-IEPD) were synthesized using standard fmoc solid-phase chemistry with 2-chlorotrityl chloride resin (0.4 or 1.2 mmol/g substitution). 0.1M HOBt in 20% 4-methylpiperidine in DMF was used for Fmoc deprotection to reduce aspartimide formation.³⁷ N-termini were acetylated prior to cleavage from resin using 50 eq. acetic anhydride and DIEA in DMF for 30 min. Peptides were cleaved from the resin using 0.5% TFA in DCM. Reverse coupling to A was carried out in DMF using 3 eq. HBTU and 6 eq. DIEA. Nitroanilide peptides were purified either by dissolving in ethyl acetate and washing with saturated NaHCO₃, NH₄Cl, and brine, or by

preparative reverse-phase HPLC equipped with a C18 column using a linear gradient from 95:5 to 5:95 H₂O/acetonitrile with 0.1% TFA at a flow rate of 20 mL/min. ESI-MS was used to confirm the molecular masses of the desired products.

Synthesis of Protease Substrates

(AcAAF)K-pNA:

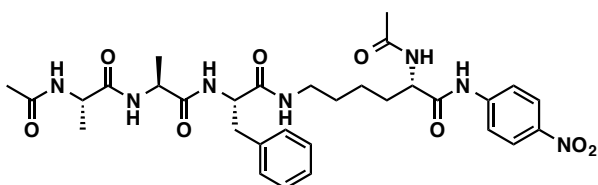


Figure 5.9. Structure of (AcAAF)K-pNA.

Calc. [M+TFA]: 752.2873 Da; Obs. [M+TFA]: 752.3518 Da

Analytical HPLC conditions:

0-0.5 min: 10% ACN with 0.1% TFA

0.5-12.5 min: 10-100% ACN with 0.1% TFA

12.5-15 min: 100% ACN with 0.1% TFA

Peptide eluted at 8.3 min.

HPLC purity: 71.2%

(AcFG)K-pNA:

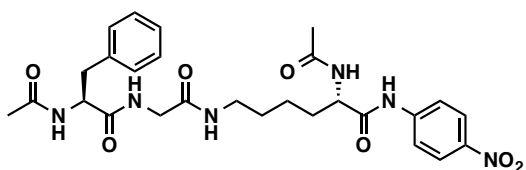


Figure 5.10. Structure of (AcFG)K-pNA.

Calc. [M+Na]: 577.2381 Da; Obs. [M+Na]: 577.2471 Da

Analytical HPLC conditions:

0-0.5 min: 10% ACN with 0.1% TFA

0.5-12.5 min: 10-100% ACN with 0.1% TFA

12.5-15 min: 100% ACN with 0.1% TFA

Peptide eluted at 8.3 min.

HPLC Purity: 96.7%

(AcDEVD)K-pNA:

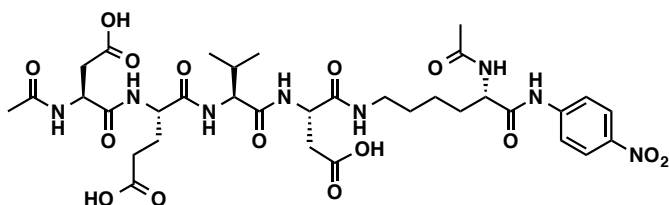


Figure 5.11. Structure of (AcDEVD)K-pNA.

Calc. [M-H]: 807.3240 Da; Obs. [M-H]: 807.3092 Da

Analytical HPLC conditions:

0-0.5 min: 10% ACN with 0.1% TFA

0.5-12.5 min: 10-100% ACN with 0.1% TFA

12.5-15 min: 100% ACN with 0.1% TFA

Peptide eluted at 7.0 min.

HPLC Purity: 84.7%

(AcDVED)K-pNA:

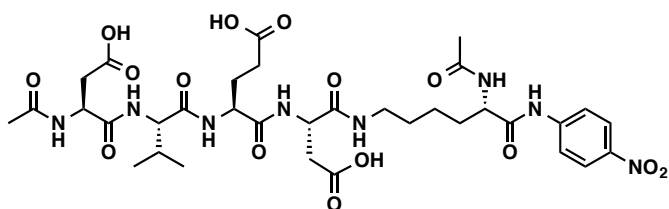


Figure 5.12. Structure of (AcDVED)K-pNA.

Calc. [M-H]: 807.3240 Da; Obs. [M-H]: 807.3287 Da

Analytical HPLC conditions:

0-0.5 min: 10% ACN with 0.1% TFA

0.5-12.5 min: 10-100% ACN with 0.1% TFA

12.5-15 min: 100% ACN with 0.1% TFA

Peptide eluted at 7.0 min.

HPLC Purity: 99.2%

(AcIEPD)K-pNA:

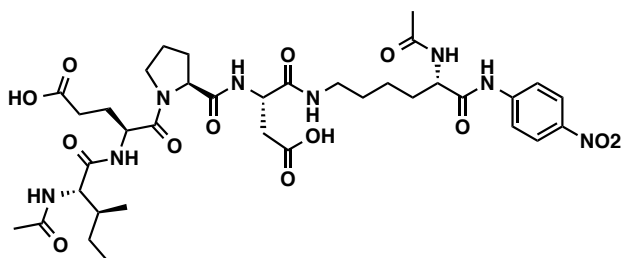


Figure 5.13. Structure of (AcIEPD)K-pNA.

Calc. [M-H]: 803.3654 Da; Obs. [M-H]: 803.3658 Da

Analytical HPLC conditions:

0-0.5 min: 10% ACN with 0.1% TFA

0.5-12.5 min: 10-100% ACN with 0.1% TFA

12.5-15 min: 100% ACN with 0.1% TFA

Peptide eluted at 7.6 min.

Purity by HPLC: 96.2%

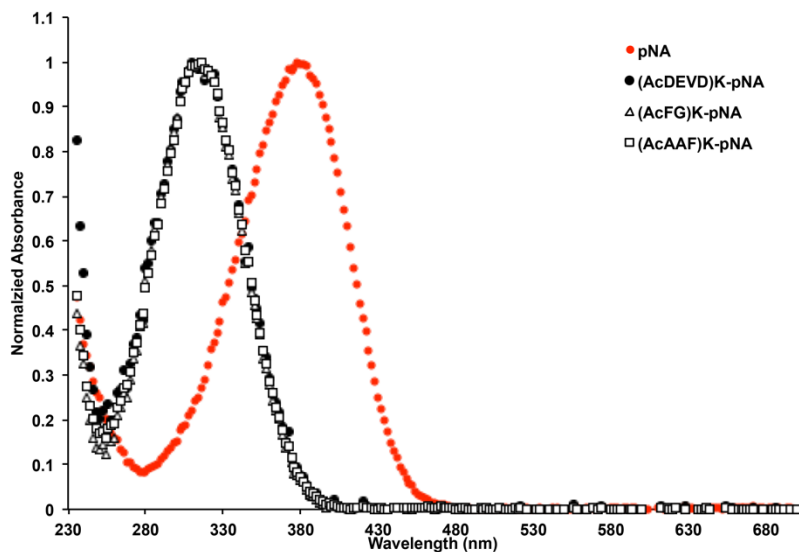


Figure 5.14. UV absorption spectra of dual-enzyme responsive peptides before digestion and of the colorimetric compound *p*-nitroaniline that is released after enzyme digestion of the peptides.

Assays

Trypsin + Chymotrypsin Assay

Stock solutions of enzymes were prepared by dissolving trypsin (60 mg/mL) in 1 mM HCl and chymotrypsin (60 mg/mL) in pH 7.4 0.035M HEPES + 0.1M NaCl. The peptide substrate, (Ac-AAF)K-pNA, was dissolved in DMSO to make a 1 mM stock solution. To wells in a 96-well plate, 87.5 μ L pH 7.4 0.035M HEPES + 0.1M NaCl and 2.5 μ L peptide substrate were added. Absorbance was measured using a plate reader at 405 nm. Then, 5 μ L trypsin and 5 μ L chymotrypsin were added to the wells, and absorbance was measured at pre-determined time points. Absorbance values were subtracted from initial reading of

only buffer and peptide. When testing only one enzyme, 5 μ L buffer were added to keep total volume per well at 100 μ L. All conditions were measured in triplicate.

Papain + Trypsin Assay

Papain was reconstituted in deionized water at a concentration of 1 mg/mL. A stock solution of trypsin was prepared by dissolving the enzyme (10 mg/mL) in 1 mM HCl. The peptide substrate, (AcFG)K-pNA was dissolved in DMSO to make a 5 mM solution. Separately, 3M NaCl and 20 mM EDTA + 50 mM cysteine (pH 6.2) solutions were prepared with deionized water. In a 96-well plate, 5 μ L substrate were mixed with 45 μ L NaCl and 40 μ L EDTA + cysteine solutions. Absorbance was measured at 405 nm to serve as a blank. Then, 5 μ L of both enzyme solutions were added, and absorbance measurements were taken at pre-determined time points. All conditions were prepared and measured in quadruplicate.

Papain + Trypsin Kinetics

Absorbance measurements were carried out using Tecan M1000 plate reader. K_m , K_{cat} , and V_{max} were determined by measuring the absorbance generated by pNA release from enzymatic cleavage of 31.25-1000 μ M (AcFG)K-pNA using previously described assay conditions. For trypsin time points, (AcFG)K-pNA was incubated with papain for 5, 15, and 30 minutes before adding trypsin. Absorbance values were plotted against time for the first fifteen minutes after trypsin addition, during which the slope remained constant, and analyzed using non-linear regression. Absorbance values were recorded against a blank (buffer + substrate). All experiments carried out in triplicate.

Caspase 3/8 + Trypsin Assay

Caspase 3 was taken directly from stock solution containing 1000U/ μ L. A stock solution of trypsin was prepared by dissolving the enzyme (5 mg/mL) in 1 mM HCl. The peptide substrates were dissolved in DMSO to make 10 mM solutions. These were then diluted to 2.5 mM with pH 7.5 0.1 M HEPES containing 10 mM DTT, 2 mM EDTA, and 10% v/v glycerol. In a 96-well plate, 84 μ L of buffer and 5 μ L peptide were mixed together before measuring the absorbance at 405 nm to serve as a blank. 1 μ L caspase-3 was added, and the plate was incubated at 23°C for 12-24 hours and absorbance was measured again. Then, 5 μ L trypsin were added to the well and absorbance measurements were taken at pre-determined time points. All conditions prepared and measured in triplicate. The same protocol was used for caspase 8 assays, adjusting peptide substrate concentration as needed.

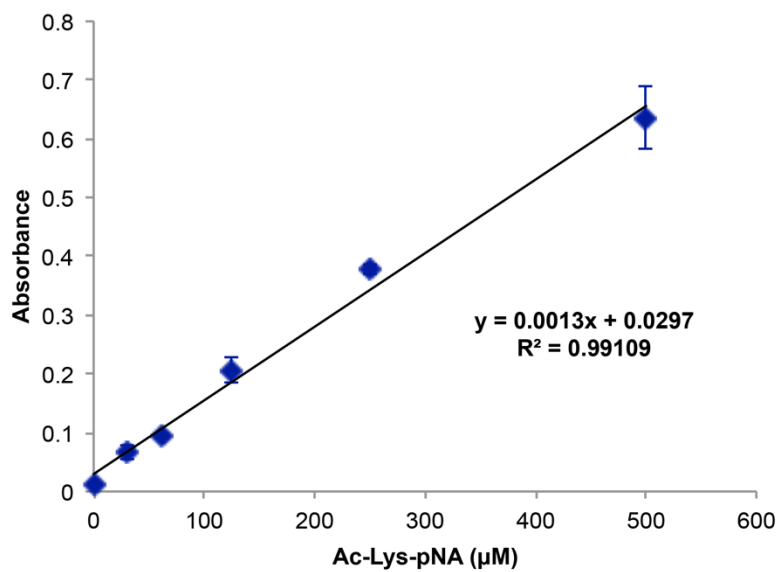


Figure 5.15. Standard curve of trypsin digestion of **A**. Each measurement was carried out in triplicate, and a linear trend line was generated from average absorbance values plotted against concentration.

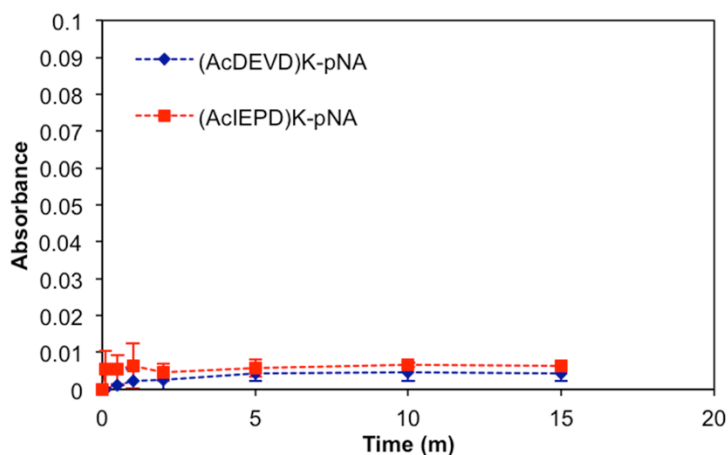


Figure 5.16. 500 μ M (AcDEVD)K-pNA and (AcIEPD)K-pNA was incubated with caspase 8 for 24 hours before adding trypsin, which did not result in a significant absorbance increase. Average and standard deviation of three repeats are shown.

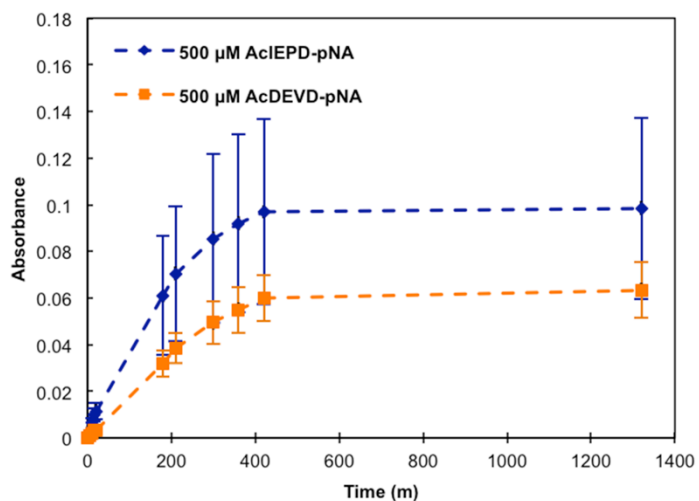


Figure 5.17. Incubating caspase 8 with commercially available AcDEVD-pNA and AcIEPD-pNA resulted in a significant absorbance increase over time. Average and standard deviation of three repeats are shown.

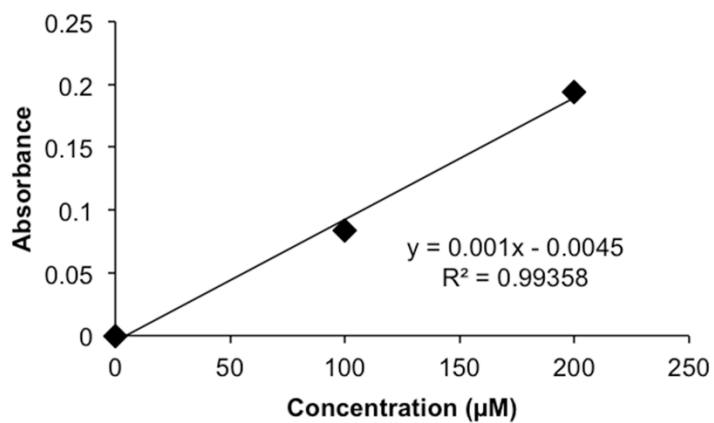


Figure 5.18. Caspase 3 digestion of commercial Ac-DEVD-pNA. Each measurement was carried out in triplicate, and a linear trend line was generated from average absorbance values plotted against concentration.

5.5. References

‡ Chapter 5 has been published as: Boehnke, N.; Maynard, H. D. *Peptide Science*, **2017**, DOI: 10.1002/bip.23035

1. Rautio, J.; Kumpulainen, H.; Heimbach, T.; Oliyai, R.; Oh, D.; Jarvinen, T.; Savolainen, J. *Nat. Rev. Drug Discov.* **2008**, *7*, 255-270.
2. Hu, J. M.; Zhang, G. Q.; Liu, S. Y. *Chem. Soc. Rev.* **2012**, *41*, 5933-5949.
3. Tian, X.; Baek, K. H.; Shin, I. *Chem. Sci.* **2013**, *4*, 947-956.
4. Tucking, K. S.; Grutzner, V.; Unger, R. E.; Schonherr, H. *Macromol. Rapid Commun.* **2015**, *36*, 1248-1254.
5. Wegener, D.; Wirsching, F.; Riestler, D.; Schwienhorst, A. *Chem. Biol.* **2003**, *10*, 61-68.
6. Huang, R.; Wang, X. J.; Wang, D. L.; Liu, F.; Mei, B.; Tang, A. M.; Jiang, J.; Liang, G. L. *Anal. Chem.* **2013**, *85*, 6203-6207.
7. Kimura, Y.; Komatsu, T.; Yanagi, K.; Hanaoka, K.; Ueno, T.; Terai, T.; Kojima, H.; Okabe, T.; Nagano, T.; Urano, Y. *Angew. Chem. Int. Ed. Engl.* **2017**, *56*, 153-157.
8. Van de Bittner, G. C.; Bertozzi, C. R.; Chang, C. J. *J. Am. Chem. Soc.* **2013**, *135*, 1783-1795.
9. Li, S. Y.; Liu, L. H.; Cheng, H.; Li, B.; Qiu, W. X.; Zhang, X. Z. *Chem. Commun.* **2015**, *51*, 14520-14523.

10. Mulder, M. P. C.; Witting, K.; Berlin, I.; Pruneda, J. N.; Wu, K. P.; Chang, J. G.; Merkx, R.; Bialas, J.; Groettrup, M.; Vertegaal, A. C. O.; Schulman, B. A.; Komander, D.; Neefjes, J.; El Oualid, F.; Ovaa, H. *Nat. Chem. Biol.* **2016**, *12*, 523-533.
11. Peters, R. J. R. W.; Marguet, M.; Marais, S.; Fraaije, M. W.; van Hest, J. C. M.; Lecommandoux, S. *Angew. Chem. Int. Ed.* **2014**, *53*, 146-150.
12. Ohta, T.; Terada, T.; Nagakawa, T.; Tajima, H.; Itoh, H.; Fonseca, L.; Miyazaki, I. *Br. J. Cancer* **1994**, *69*, 152-156.
13. Vilen, S. T.; Suojanen, J.; Salas, F.; Risteli, J.; Ylipalosaari, M.; Itkonen, O.; Koistinen, H.; Baumann, M.; Stenman, U. H.; Sorsa, T.; Salo, T.; Nyberg, P. *Cancer Invest.* **2012**, *30*, 583-592.
14. Koivunen, E.; Itkonen, O.; Halila, H.; Stenman, U. H. *Cancer Res.* **1990**, *50*, 2375-2378.
15. Radhakrishnan, K.; Tripathy, J.; Gnanadhas, D. P.; Chakravorty, D.; Raichur, A. M. *RSC Adv.* **2014**, *4*, 45961-45968.
16. van Dijk, M.; Nollet, M. L.; Weijers, P.; Dechesne, A. C.; van Nostrum, C. F.; Hennink, W. E.; Rijkers, D. T. S.; Liskamp, R. M. J. *Biomacromolecules* **2008**, *9*, 2834-2843.
17. Chen, N.; Zou, J.; Wang, S. M.; Ye, Y. M.; Huang, Y.; Gadda, G.; Yang, J. J. *Biochemistry* **2009**, *48*, 3519-3526.
18. Moorman-Li, R.; Motycka, C. A.; Inge, L. D.; Congdon, J. M.; Hobson, S.; Pokropski, B. *P & T* **2012**, *37*, 412-418.
19. Olsen, J. V.; Ong, S. E.; Mann, M. *Mol. Cell. Proteomics* **2004**, *3*, 608-614.

20. Zee, B. M.; Garcia, B. A. *Essays Biochem.* **2012**, *52*, 147-163.
21. Roessler, C.; Tuting, C.; Meleshin, M.; Steegborn, C.; Schutkowski, M. *J. Med. Chem.* **2015**, *58*, 7217-7223.
22. Merrifield, R. B. *J. Am. Chem. Soc.* **1963**, *85*, 2149-2154.
23. Gorske, B. C.; Bastian, B. L.; Geske, G. D.; Blackwell, H. E. *J. Am. Chem. Soc.* **2007**, *129*, 8928-8929.
24. Appel, W. *Clin. Biochem.* **1986**, *19*, 317-322.
25. Groleau, P. E.; Gauthier, S. F.; Pouliot, Y. *Int. Dairy J.* **2003**, *13*, 887-895.
26. Lowe, G.; Yuthavong, Y. *Biochem. J.* **1971**, *124*, 107-115.
27. Tesser, G. I.; Gruber, M.; Nivard, R. J. F. *Biochim. Biophys. Acta* **1964**, *89*, 303-308.
28. Mackenzie, N. E.; Malthouse, J. P. G.; Scott, A. I. *Biochem. J.* **1985**, *226*, 601-606.
29. Stennicke, H. R.; Salvesan, G. S. *J. Biol. Chem.* **1997**, *272*, 25719-25723.
30. Devarajan, E.; Sahin, A. A.; Chen, J. S.; Krishnamurthy, R. R.; Aggarwal, N.; Brun, A. M.; Sapino, A.; Zhang, F.; Sharma, D.; Yang, X. H.; Tora, A. D.; Mehta, K. *Oncogene* **2002**, *21*, 8843-8851.
31. Fulda, S. *Cancer Lett.* **2009**, *281*, 128-133.
32. Agosto, M.; Azrin, M.; Singh, K.; Jaffe, A. S.; Liang, B. T. *J. Am. Coll. Cardiol.* **2011**, *57*, 220-221.
33. Olsson, M.; Zhivotovsky, B. *Cell Death Differ.* **2011**, *18*, 1441-9.
34. Stennicke, H. R.; Renatus, M.; Meldal, M.; Salvesen, G. S. *Biochem. J.* **2000**, *350*, 563-568.

35. Briand, L.; Chobert, J. M.; Tauzin, J.; Declerck, N.; Leonil, J.; Molle, D.; Tran, V.; Haertle, T. *Protein Eng.* **1997**, *10*, 551-560.
36. Smith, E. L.; Parker, M. J. *J. Biol. Chem.* **1958**, *233*, 1387-1391.
37. Lauer, J. L.; Fields, C. G.; Fields, G. B. *Lett. Pept. Sci.* **1994**, *1*, 197-205.